DEVELOPMENT OF AN ULTRA WIDE BAND (UWB) ARRAY ANTENNA

A THESIS SUBMITTED TO
THE GRADUATE SCHOOL OF NATURAL AND APPLIED SCIENCES
OF
MIDDLE EAST TECHNICAL UNIVERSITY

BY

HASAN AKIN CEYLAN

IN PARTIAL FULFILLMENT OF THE REQUIREMENTS
FOR
THE DEGREE OF MASTER OF SCIENCE
IN
ELECTRICAL AND ELECTRONICS ENGINEERING

APRIL 2022

Approval of the thesis:

DEVELOPMENT OF AN ULTRA WIDE BAND (UWB) ARRAY ANTENNA

submitted by **HASAN AKIN CEYLAN** in partial fulfillment of the requirements for the degree of **Master of Science in Electrical and Electronics Engineering Department, Middle East Technical University** by,

Prof. Dr. Halil Kalıpçılar
Dean, Graduate School of **Natural and Applied Sciences** _____

Prof. Dr. İlkay Ulusoy
Head of Department, **Electrical and Electronics Engineering** _____

Prof. Dr. Özlem Aydın Çivi
Supervisor, **Electrical And Electronics Engineering** _____

Examining Committee Members:

Prof. Dr. Gülbin Dural
Electrical And Electronics Engineering, METU _____

Prof. Dr. Özlem Aydın Çivi
Electrical And Electronics Engineering, METU _____

Prof. Dr. Sencer Koç
Electrical And Electronics Engineering, METU _____

Prof. Dr. Birsen Saka
Electrical and Electronics Engineering, Hacettepe University _____

Assoc. Prof. Dr. Lale Alatan
Electrical and Electronics Engineering, METU _____

Date: 25.04.2022

I hereby declare that all information in this document has been obtained and presented in accordance with academic rules and ethical conduct. I also declare that, as required by these rules and conduct, I have fully cited and referenced all material and results that are not original to this work.

Name, Surname: Hasan Akın Ceylan

Signature :

ABSTRACT

DEVELOPMENT OF AN ULTRA WIDE BAND (UWB) ARRAY ANTENNA

Ceylan, Hasan Akın
M.S., Department of Electrical and Electronics Engineering
Supervisor: Prof. Dr. Özlem Aydın Çivi

April 2022, 82 pages

Demand for ultrawideband antenna arrays in telecommunications, space and airborne platforms, RADAR applications and MIMO systems, etc. is rising consistantly. A modern approach to develop an ultrawideband array is to utilize the mutual coupling between array elements. Even though individual elements are of narrowband characteristic in isolated form, they gain ultrawideband performance in array configuration under strong mutual coupling. In this work, an ultrawideband tightly coupled dipole array antenna is designed, fabricated and measured. Overlapping dipole arms is utilized as the tight coupling scheme. Infinite array of proposed TCDA has the bandwidth from 0.9 GHz to 6.8 GHz for VSWR<3.1 condition. For the unit cell of the infinite TCDA, gain varies from -11.1 dBi to 12.8 dBi with respect to frequency. The Klopfenstein tapered line balun and impedance transformer are inserted to feed the infinite array, yielding BW from 1.28 to 6.12 GHz for VSWR<3.1 condition, while having several extremely narrowband common mode VSWR spikes occuring in the band. In order to prove the concept, the TCDA is fabricated with 5×5 configuration, on RO4350b with 0.762 mm thickness with 0.035 mm copper. The ground plane is fabricated with FR4 core material of 1.5 mm thickness. The fabricated TCDA is measured with left-open elements, i.e. active element measurements with unterminated

elements. As the measurement results, the center element of the array has a bandwidth from 2.67 GHz to 6.8 GHz for VSWR<3.1 excluding small peak at VSWR in 3.15 to 3.3 GHz. 5×5 array has a secondary operational BW from 7.73 GHz to 20 GHz for VSWR<3.1. The measured gain of center element varies from -3.75 dBi to 8.36 dBi in 3 to 12 GHz measurement in unechoic chamber. 9 elements of the 25 total are measured, array patterns are synthesized via MATLAB using the 9 measured elements.

Keywords: dipole array, ultra wideband, tightly coupled array, overlapping dipole

ÖZ

ÇOK GENİŞ BANDLI DİZİ ANTEN GELİŞTİRİLMESİ

Ceylan, Hasan Akın
Yüksek Lisans, Elektrik ve Elektronik Mühendisliği Bölümü
Tez Yöneticisi: Prof. Dr. Özlem Aydın Çivi

Nisan 2022 , 82 sayfa

Telekomünikasyon, uzay ve havacılık, RADAR uygulamaları ve MIMO sistemleri gibi birçok alanda çok geniş bantlı anten dizilerine talep sürekli artmaktadır. Çok geniş bantlı dizi geliştirmelerinde modern bir yaklaşım olarak dizi elemanları arasındaki ortak etkileşim öne çıkmaktadır. Dizi elemanları tekil halde dar bantlı bir karakteristiğe sahip olsa da, dizi konfigürasyonu içerisinde güçlü ortak etkileşim sebebiyle geniş bantlı özellik kazanmaktadır. Bu çalışmada, çok geniş bantlı sıkı akupleli dipol dizi anten tasarlanmış, üretilmiş ve ölçümlenmiştir. Sıkı akuple özelliği, üst üste binen dipol kolları kullanılarak kazandırılmıştır. Sonsuz TCDA dizisi, 0.9 GHz'den 6.8 GHz'ye VSWR<3.1 koşulunu sağlayan bant genişliğine sahiptir. Sonsuz dizi eleman kazancı ise frekansa bağlı olarak, -11.1 dBi ile 12.8 dBi arasında değişmektedir. Klopfenstein konikleştirilmiş hatlı balun ve empedans dönüştürücü eklenmiş sonsuz dizi ise 1.28 GHz'den 6.12 GHz'ye kadar VSWR<3.1 koşulunu sağlarken birkaç aşırı dar bantlı eş mod VSWR zıplamalarına sahiptir. Sonlu TCDA, kavramı ispat etmek için, 5×5 konfigürasyonunda, 0.762 mm kalınlıklı 0.035 bakır kaplı RO4350b malzemesi üzerine üretilmiştir. Toprak levhası 1.5 mm kalınlıklı FR4 öz malzemesi kullanılarak üretilmiştir. Üretilen TCDA, açık uçlu elemanlar ile yani sonlandırılmamış

aktif eleman ölçümü ile ölçümlenmiştir. Ölçüm sonuçları olarak, merkez eleman 2.67 GHz'den 6.8 GHz'ye VSWR<3.1 koşullu bant genişliğine sahiptir, 3.15 GHz ile 3.3 GHz aralığında küçük tepe göz ardı edilmiştir. 5×5 dizi, 7.73 GHz'den 20 GHz'ye VSWR<3.1 koşullu ikincil bir çalışma bandına sahiptir. Ölçülen kazanç değeri, merkez eleman için -3.75 dBi ile 8.36 dBi arasında 3'den 12 GHz'ye kadar değişmektedir. Toplam 25 elemanın 9 tanesi ölçülmüş, dizi ışıma örüntüsü MATLAB üzerinde sentezlenmiştir.

Anahtar Kelimeler: dipol dizisi, ultra geniş bant, sıkıca bağlı dizi, örtüşen dipol

to my beloved wife and precious parents

ACKNOWLEDGMENTS

The author wishes to express his deepest gratitude to his supervisor Prof. Dr. Özlem Aydın Çivi for her guidance, advice, criticism, encouragements, and insight throughout the research

The author would also like to thank his team and managers at his workplace for their understanding and encouragements about the research.

TABLE OF CONTENTS

LIST OF TABLES

TABLES

LIST OF FIGURES

FIGURES

LIST OF ABBREVIATIONS

TCDA	Tightly Coupled Dipole Array
CSA	Current Sheet Array
UWB	Ultra Wideband
VSWR	Voltage Standing Wave Ratio
SLL	Side Lobe Level
PUMA	Planar Ultrawideband Modular Array
MIMO	Multiple Input Multiple Output
FSS	Frequency Selective Surface
CPW	Coplanar Waveguide
TL	Transmission Line
BW	Bandwidth

CHAPTER 1

INTRODUCTION

Under the scope of this work, a tightly coupled dipole antenna array (TCDA) is designed, fabricated and measured to be of ultrawideband (UWB) performance. Throughout this chapter, UWB antenna arrays are explained first, then the fundamental features of TCDAs namely current sheet array (CSA) is examined.

1.1 Introduction to Ultrawideband Antenna Arrays

Operational frequency band of an antenna, allows the antenna to be categorized as narrowband, wideband or frequency independent, conventionally [1]. Antenna bandwidth can be defined as the frequency range in which at least one of the antenna characteristics, i.e. input impedance, radiation pattern, polarization, side-love level (SLL), gain, efficiency, etc. are within an acceptable value related to the desired design objective. Antennas generally having a few percent bandwidth are designated as narrowband. Antennas having the numerically equal width as the center frequency (i.e. $f_{center} - f_{center}/2$ to $f_{center} + f_{center}/2$) or couple of times of the center frequency generally called as wideband antennas [1]. The term ultrawideband (UWB) antenna array becomes popular after many application areas developed in recent years, in addition to common military and electronic warfare applications. UWB arrays stated by Adamiuk et. al, having at least quarter of the center frequency as bandwidth for high frequencies or at least 500 MHz absolute bandwidth [2]. There are many ultrawideband antenna types, some examples in literature are vivaldi arrays [3], TCDA [4], planar ultrawideband modular array (PUMA) [5], etc.

Ultrawideband antenna arrays are used in communications, weather control radars

[3], flight control and military radars, and many more. Communication systems are widely used in variety of frequencies and applications. Satellite and space communications are the major ones among them. Due to frequency allocations [6], L, S, C and X-bands are allocated for satellite communications. Since, space and functionality are key aspects in satellite communications, having a low profile with a high bandwidth is the optimal combination of satellite communication antennas. Ultrawideband arrays deployed in such systems but conventionally requiring high thickness and wide spacing on the satellite. In order to maintain the ultrawideband performance while decreasing the physical space requirements, TCDA becomes popular. Ultrawideband phased arrays are also commonly used in ground systems as well as military applications. For developing state of the art passive radars, ultrawideband feature is very popular [7]. Also, for some other radar topics like MIMO, UWB features could be used [8]. Moreover, UWB arrays commonly used in high data rate – high speed communication schemes [9]. For detection systems similar to passive radars, ultrawideband antenna arrays are required. Also, for complex platforms having radio communications with different bands (combination of sat-com, data links, etc.) could merge the antennas of such independent systems into a single ultrawideband array [10], hence only using different hardware, of course with a certain frequency or time division algorithm. In result it decreases the surface area usages of the space system, enabling the extra areas to be used for different applications.

1.2 Current Sheet Array

Decades ago, Wheeler proposed a hypothetical infinite structure called infinite current sheet [11]. His main focus back then was, to propose a theoretical bound for impedance matching for varying scan anles, on large phased arrays. He proposed the antenna plane should be a current sheet. In order to form the current sheet arrays, one could use electric dipoles or magnetic dipoles with respect to creating electric or magnetic current sheet. The work mostly focused on electric current sheet. The current sheet was constructed to obtain a purely resistive impedance on the direction of radiation and yields matching to free-space, having constant resistance of R_0, 377 Ω, independent of scan angles. The current sheet structure is a “fine structure [11]” that

is matched to free-space independent of scan angles. For the implementation of such array, one must place very small elements with very small spacing. Which indicates that, using tightly spaced small electric dipole as elements can work when creating a current sheet. Wheeler, actually did not formulize or provide a definition for what is "very small", but after his work many scientists develop the concept further and further. A distinguished one of them is Ben Munk, realizing the Wheeler's design and showing that it is not only for achieving wide-scan angles but also for achieving wide frequency bandwidth [12]. Munk developed the realization of the current sheet by introducing a ground plane backing the tightly spaced small elements. [12].

Ben Munk introduced a wideband array consisting of dipoles. Dipole arrays are often considered as narrowband arrays, this is due to the fact that a single dipole has a rather limited bandwidth, generally 10-20%, unless broadband compensated [13]. To widen the bandwidth of a dipole array, Ben Munk utilized the commonly avoided mutual coupling between elements. Elements under tight mutual coupling and backed by a ground plane enables the array to be able to reach around 4:1 impedance bandwidth [13]. Munk's array opens the way of practical implementations of Wheeler's "current sheet" theory [11]. First demonstration of the concept was named as the current sheet array (CSA). Which is shown in the Figure 1.1 below, the demonstrated array consists of 3x6 elements [14]. This array operates in VHF/UHF bands and named as CSA breadboard designed to be flush-mounted into a cavity [14]. Munk also suggested several methods to further improve the performance of the current sheet array, which are eventually; inspire many works on the concept. Such improvements focus on using dielectric superstrates, magnetic substrates, or lossy absorber layers placed above the ground plane. Also, one could improve the bandwidth of current sheet array via using low-loss dielectric superstrates with the cost of increasing the height of the array [15].

Figure 1.1: Current Sheet Array. [14]

1.3 Development of Tightly Coupled Dipole Arrays

After the introduction of Wheeler's current sheet theory and Munk's realization of it, there have been many researches on how to implement different variations of current sheet array and how to improve its bandwidth. The term, TCDA (tightly coupled dipole array) arises from the direct translation of the array structure. There are several reasons which made TCDA more and more popular during time in the ultrawideband phased array researches. One of them is, TCDA provides wide scan angle with less compromise from the impedance bandwidth. Another major reason is that, TCDA overall thickness is very small compared to many other wideband array structures. Below Figure 1.2 shows a comparison matrix with a popular wideband array element, Vivaldi array [16]. Also, TCDA antennas, have a wide design complexity range. There could be a lot of features added to the array, which makes it very complex but, in the meantime achieving better performance in general. On the other hand, a designer could choose to use simple features and the array becomes easy to design and manufacture, yet still outputting a convenient level of performance. The common features of the TCDA's in the literature are the mutually coupled small dipoles as the elements and a ground plane behind them. Hence, it is seen as the most basic form of TCDA. Such a configuration could be seen in the current sheet array example in Figure 1.1. There are various methods to obtain strong mutual coupling in dipoles, in CSA TCDA strong mutual coupling is made via interdigital capacitive dipole arms,

which could also seen in Figure 1.3 [14]. Details of why capacitive coupling is necessary and other relations will be examined in Chapter 2 of this work.

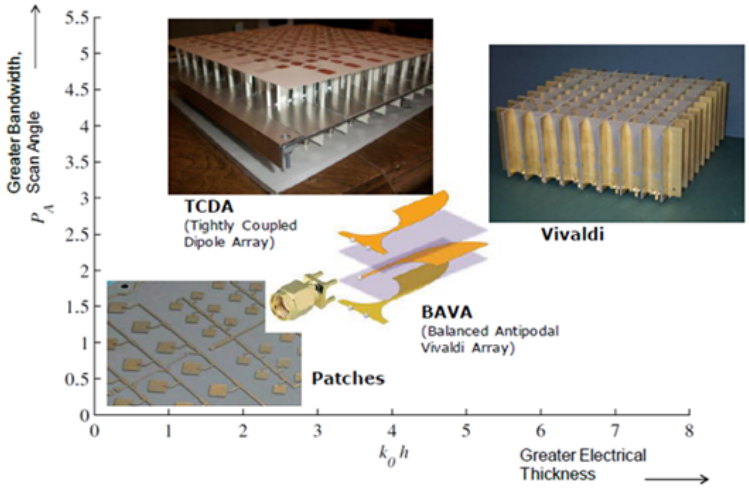

Figure 1.2: Some ultrawideband array topologies comparison [16].

One of the most challenging features of designing a TCDA is to design an equally wideband, tightly spaced baluns. There have been a wide selection of feeding designs in the literature, using different types of baluns, combination of power dividers with baluns to feed dual polarized elements and an example of using a wideband differential feeding network [17].

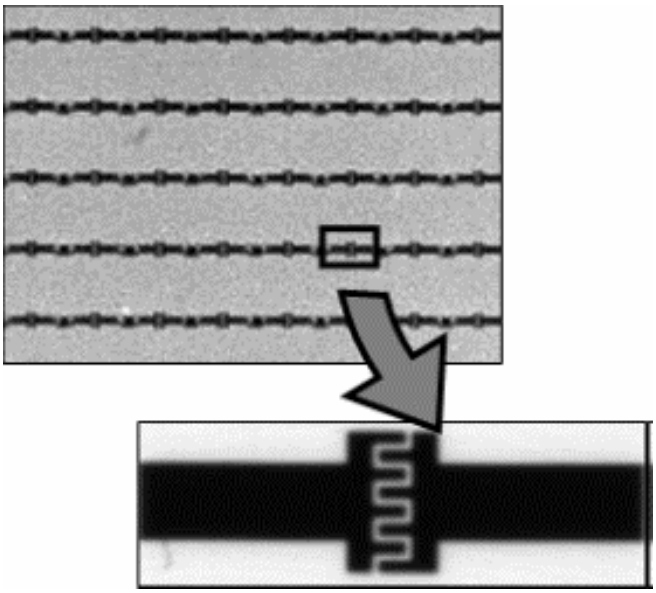

Figure 1.3: Interdigital coupling structure of CSA [14].

The dipole plane and the balun plane could be perpendicular to each other as could be seen in Figure 1.4, or coplanar as could be seen in Figure 1.5. These examples are for integrated balun structures within the TCDA. There are also some other balun examples in the literature, the most widely used ones are Marchand Baluns [18] and exponential tapered or Klopfenstein tapered baluns which could be seen in Figure 1.6.

One of the most common desired achievement is to obtain high scan angles when designing TCDA arrays. As mentioned earlier, loading a superstrate on top of the elements could increase impedance bandwidth as well as scan angle capability, which can be seen on Figure 1.7. FSS surfaces could be used on top of the superstrate in order to further improve the scan angle capability as well as some advantages on the impedance matching [19].

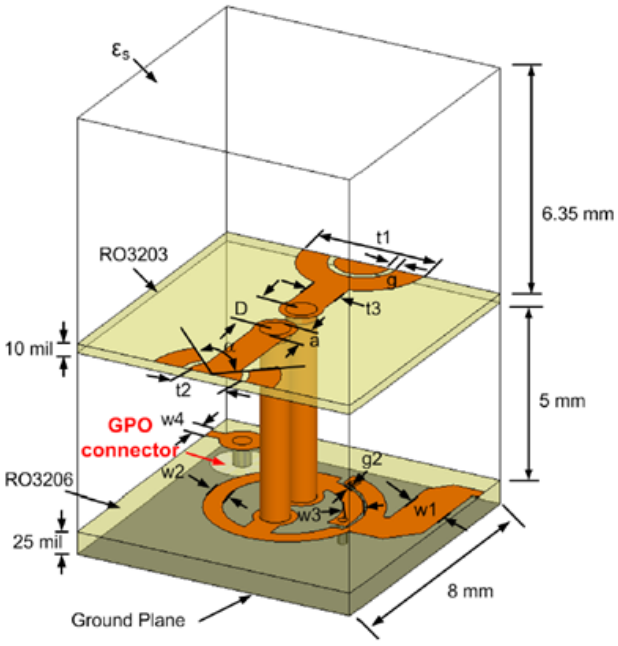

Figure 1.4: Integrated balun structure, perpendicular to dipole plane [20].

Dipole antennas have linear polarization. Which indicates that the array constructed by using dipoles also have linear polarization. In order to cover all polarizations, some TCDAs are constructed in dual polarized forms [21]. Dual polarized unit cell in TCDA requires overlapping dipole arms in perpendicular directions or introducing a junction at the crossing, increasing the complexity of the design. Such a configuration can be seen in Figure 1.7 below.

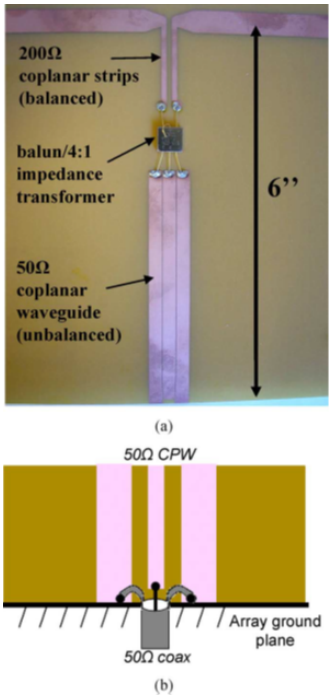

Figure 1.5: A CPW feeding scheme of a coplanar dipole-feed structure [22].

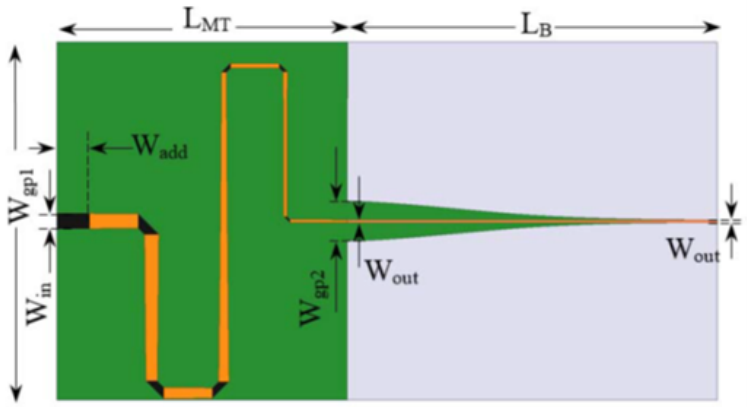

Figure 1.6: A Klopfenstein taper example of a coplanar dipole-feed [19].

For some TCDA designs, in order to improve the impedance bandwidth, some resistive mid-layer in between ground plane and the dipoles are used [23]. Resistive layer increases the bandwidth via mitigating the ground plane caused mismatch at a small portion of the bandwidth, at the cost of power dissipation all over the bandwidth, creating a lower efficiency for TCDA.

State of the art level of complex TCDA design yields all of the features defined above.

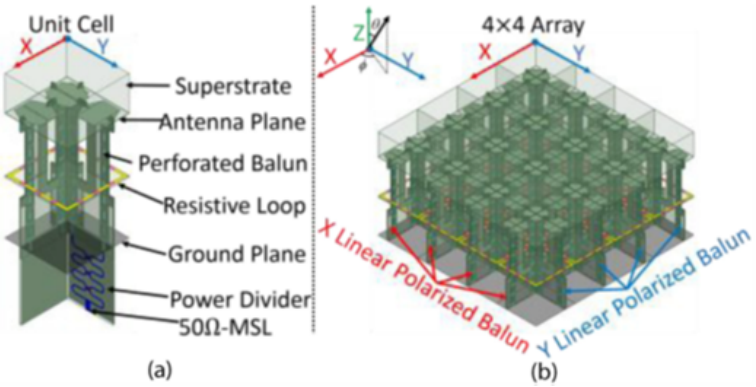

Figure 1.7: Superstrate, power divider, resistive loop, integrated balun and dual polarization features [21].

Meaning a complex structure, delicate design and also expensive manufacturing and material cost. Below Table 1.1 [24] summarizes some of the prominent design and academic works on TCDAs.

Table 1.1: Some prominent designs in TCDA literature [24].

Reference of Design	**Bandwidth**	**HPBW**	**Distinguishing Features**
[25]	10:1 VSWR<2	Not Given	Spiral element
[23]	21:1 VSWR<3	Not Given	UWB Resistive FSS
[26]	1.6:1 VSWR<2	70^o E-plane 60^o H-plane	Integrated balun Shorted edge terminations
[4]	7.35:1 VSWR<2.65	45^o	Integrated balun
[10]	6:1 VSWR<1.8(Boresight) VSWR<2.4(45^o) VSWR<3.1(60^o)	60^o	Dual polarization
[27]	6.1:1 VSWR<3	75^o E-plane 65^o H-Plane	Maximum scan angle FSS superstrate
[28]	13.5:1 VSWR<2.5 (Boresight) 13.1:1 VSWR<3.1 (45^o)	45^o	UWB Substrate loading
[29]	5.24:1 VSWR<3 (Boresight)	Not Given	Four-square
[5]	5:1 VSWR<2.1 (Boresight)	45^o	PUMA
[30]	3:1 VSWR<2.1 (Boresight)	45^o	PUMA Dual polarization
[31]	2.5:1 VSWR<2	60^o	Wide angle steering Substrate loading

1.4 Objective of the Thesis

Traditional phased arrays achieve wideband performance via using wideband elements. Mainly because in most traditional designs, all elements considered, analyzed and measured solely and simply integrated into the array, creating a wideband array out of wideband elements. As a modern and creative approach, there have been some scientists utilizing mutual coupling to create wideband arrays out of narrowband elements. This approach founds the basis of this work. The author's aim is to create an ultrawideband tightly coupled dipole array, having VSWR<3.1 starting from S-Band to K-Band, covering most of the stated bands. Focuses of designing such a TCDA array in this work, are the ease of manufacturing and low-cost application. By concentrate many addible features to the array, a compact and cost-effective solution is achieved. The feeding scheme of the TCDA utilizes a Klopfenstein tapered impedance transformer and again Klopfenstein tapered balun structure. The whole structure of the unit cell, from dipole to the feeding connector, is manufactured on a single substrate hence decreasing the cost and manufacturing requirements of the element. Feeding is done via 50 Ω SMA connector. The structure in [19] taken as basis and the similar approach is directed besides the FSS layer. First, an ultrawideband tightly coupled dipole array unit cell is designed and infinite array analysis is conducted. After analytical design formula applications, unit cell performance is optimized by using Genetic Algorithm. Infinite array analysis being the reference case, a finite array of size 5x5 is designed, analyzed, manufactured and measured. The results are examined and the comments on performance are presented. Manufacturing substrate material is RO4350b of thickness 0.762 mm and 0.035 mm copper thickness. Manufacturing method is laser-cut PCB manufacturing. The analysis and design CAD tool is CST and for implementing the impedance transformer and balun MATLAB software is used. Moreover, return loss measurements are obtained by both Keysight and Rohde & Schwarz analyzers. Finally, the pattern measurements of the finite array are conducted in the anechoic chamber of METU EEE Department. The impedance bandwidth performance is ultrawideband, namely, from 1.28 GHz to 6.1 GHz for infinite array, neglecting the common modes. It is also observed that due to ground plane reflection, around 6 to 8 GHz frequency stop band, the finite version of TCDA obtains another operating frequency band for the higher values on the

spectrum.

1.5 Outline of the Thesis

Chapter 2 of the thesis contains the background theory and circuit modeling of the TCDA array. Formulations, mathematical relations, and some expressions are presented.

Chapter 3 begins with the methodology, then design and analysis of TCDA infinite array are presented. Some typical restrictions and parametric simulations of unit cell parameters are presented. All simulations in this chapter is in CST environment.

Chapter 4 focuses on finite array design and analysis on using CST. After that, fabrication and measurements of the proposed finite array are presented. The measurement results are compared with the simulation results. Finally, ideas of future work are presented.

Chapter 5 contains summary of the study, discussions and conclusions.

CHAPTER 2

OPERATION PRINCIPLES OF TIGHTLY COUPLED DIPOLE ARRAYS

Within this chapter, first of all, theoretical background of the UWB TCDA that is utilizing the mutual coupling is investigated. After that, circuit modelling of a TCDA structure is given so that it shall be clear that which feature yields which effect on the TCDA.

TCDA theory is based on using antenna elements' self-inductance and inductive ground plane impedance, compensating with capacitive loading to achieve resistive impedance along a wide frequency range. To achieve this, utilizing elements that either have inductive impedance or self-inductance is essential [13]. For example, small loop antennas have inductive impedances [32] which are also used in tightly coupled array design, yet the literature started and mainly focused on dipole elements (bow-tie, slanted-edges, wire, etc.) since dipole's self-inductance could be utilized in TCDA arrangement. In order to analyze TCDA, transmission line based equivalent-circuit analysis is utilized. This approach was first demonstrated by Munk in [13]. As can be seen in Figure 2.1, Munk depicted a dipole array with interdigital capacitor as lumped elements and transmission lines combination. Figure 2.2 shows the basic difference mentioned in the previous chapter, that is a TL representation of uncoupled small dipole within an array with TL representation of a tightly coupled dipole within an array. To fully understand the transmission line (TL) based equivalent circuit approach, first let us examine the short dipole and ground plane impedances altogether.

Electrically small dipoles have capacitive input impedances [1] but the capacitive reactance decreases as the electrical length increases, and for lengths larger than $\lambda/4$ dipole has inductive reactance. While at low frequencies (dipole becoming electrically small) ground plane introduces large inductive reactance because of physically

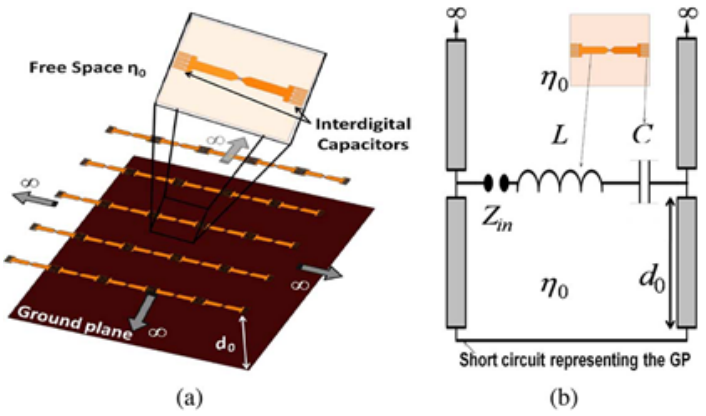

Figure 2.1: (a) Munk's TCDA (CSA), (b) its equivalent circuit [13].

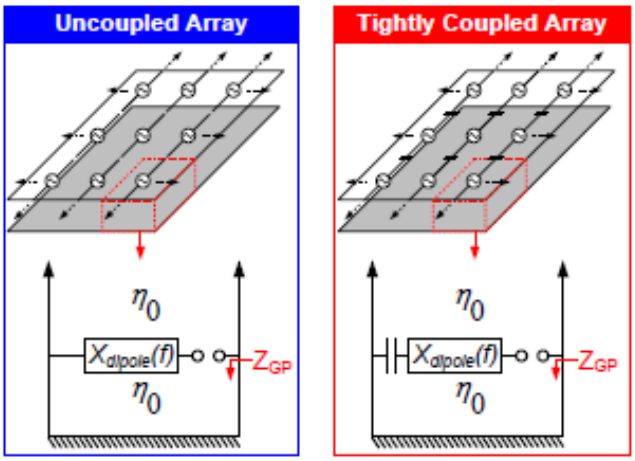

Figure 2.2: A TL representation of uncoupled and tightly coupled array unit cells [16].

constant but electrically small dipole to ground plane height. In order to examine this, below equations are utilized. Eqn. (2.1) shows the reactance of a small, thin dipole antenna.

$$X_{dipole} = \omega L_{dipole} - \frac{1}{\omega C_{dipole}} \approx \frac{\omega \mu_0}{2\pi} \ln \frac{l}{d} - \frac{\ln \frac{l}{d}}{\pi \epsilon_0 \omega l} \tag{2.1}$$

Where l: length of the dipole, d: thickness of the dipole, Then, impedance seen from height "h" from the ground plane which is represented as a shorted TL from the dipole antenna is given as,

$$Z_{GP} = j\eta_0 \tan k_0 h, \ \ where\, \eta_0 = 377\Omega \tag{2.2}$$

Eqn. (2.2) shows a purely reactive impedance value, inductive for $h < \lambda/4$ and $\lambda/2 < h < 3\lambda/2$. Note that, the free-space has an intrinsic impedance, i.e. η_0. The TL to the upwards direction, towards the free-space, and TL to the downwards direction, towards the ground plane are in parallel when looking from the input terminals of the antenna. The configuration can be seen in Figure 2.2. Then, the overall input impedance seen from the terminals of dipole in the unit cell becomes,

$$Z_{in} = R_{dipole} + jX_{dipole} + Z_{GP}//\eta_0 \tag{2.3}$$

In order to simplify this model, Munk only represents the small dipole as a lumped inductance, representing self-inductance and additional capacitance which is introduced via tight coupling [13]. Then, the simplified model impedance becomes,

$$Z_{in} = j\omega L + \frac{1}{j\omega C} + Z_{GP}//\eta_0 \tag{2.4}$$

Where "L" represents the lumped inductive representing dipole, "C" means lumped capacitive impedance that the designer introduce purposefully, that is the concept of tight coupling. The circuit model for this configuration is given in Figure 2.2

Within this model, matching Z_{in} means that the balun and feeding network is matched to input impedance of the antenna. But, in the model, one can see that the free-space impedance η_0 is also modelled. The objective is to match the total structure, that is antenna, balun and feeding network altogether, to free-space so that the fields couple to air and radiate [13] [32].

Note that, Eqn. (2.2) goes to zero when $h(f_H) = \lambda_H/2$ yielding a short circuited behavior. Considering the TL model, the current entering from input terminals, directly flows through the zero impedance seen at the node connection of ground plane TL and free-space TL, hence no radiation occurs. This short circuiting frequency limits the operation of antenna. This corresponding frequency, f_H determines the upper limit of the frequency band in TCDA.

$$for\ h = \frac{\lambda}{2},\ Z_{GP} = j377 \tan \frac{2\pi\lambda}{2\lambda} = 0 \tag{2.5}$$

In order to investigate lower limit, first an important length of quarter-wavelength inserted to impedance equation. Eqn. (2.6) shows the impedance towards the ground plane, Z_{GP}, when the ground plane height becomes quarter wavelength.

$$for\ h = \frac{\lambda}{4},\ Z_{GP} = \frac{2\pi\lambda}{4\lambda} = \infty \tag{2.6}$$

Eqn. (2.6) shows that, for the quarter-wavelength Z_{GP} shows infinite impedance. In the trasmission lines point of view; this indicates that a current flowing from antenna input terminals into the junction of antenna input, ground plane and free space node, is directed to free-space transmission line due to open-circuited ground plane transmission line. Hence, this frequency does not bring limitations to the circuit. As mentioned earlier in this chapter, for the lower frequencies, ground plane impedance becomes dominant. In order to obtain the lower limit, calculating the limit Eqn. (2.2) for the condition of $h \ll \lambda, h \to 0$;

$$\lim_{h \to 0} Z_{GP} = j377 \tan \frac{2\pi 0}{\lambda} = 0 \tag{2.7}$$

This means that, as long as the height gets smaller then $h = \lambda \setminus 4$ ground plane impedance gets smaller (still inductive) yet converges to zero as the limiting case. This means that, after a certain point, the antenna could not be matched at lower frequencies, the lower frequency limiting case is not strict as f_H but could be taken as $h(f_L) \approx \lambda \setminus 10$ for most cases [13]. For exact value where (VSWR>3.1 could be taken as "mismatch beginning condition") full-wave analysis tools might be useful. One could easily calculate the bandwidth that can be obtained with TCDA as,

$$BW = \frac{f_H}{f_L} = \frac{c/\lambda_H}{c/\lambda_L} = \frac{\lambda_L}{\lambda_H} = \frac{h/2}{h/10} \approx 5 \tag{2.8}$$

By this approximate bandwidth calculation based on TL equivalent circuit Munk had managed to achieve 4.5 BW [13]. So, for the input impedance point of view, the

ground plane placement below the array, strictly determines the upper frequency of the operational bandwidth. Also, if the ground plane is too close to the array, it creates "ground plane deterioration [13]", which causes fields to couple to ground plane as the electrical length decreases yielding low efficiency at overall bandwidth and prevent antenna to operate on lower frequencies in comparison to larger ground plane heights. Since then, ground plane placement must be optimized for the array.

The element size and dimensions are also important since it determines the reactance represented in Eqn. (2.1), affecting all the spectrum response. The element dimensions and the ground plane placement distance should be optimized altogether. For a fine tuning of small dipole dimensions and geometry as well as the ground plane distance, variations on input impedance can be decreased drastically over a wide range of frequencies. Since the primary method of obtaining an UWB antenna is to cancel the reactance and obtain a purely resistive impedance over a significant range of frequencies.

CHAPTER 3

DESIGN AND ANALYSIS OF INFINITE ULTRAWIDEBAND TCDA ARRAY

Design process of an UWB TCDA starts with an infinite array configuration. In order to produce an operational TCDA array, one must start with an element, construct it to be a unit cell into infinite array analysis. After the results of the infinite array analysis, then finite version is to be designed, optimized, fabricated and measured. Most of the work in the literature, infinite array designs have bandwidths at low frequencies, i.e. sub-GHz to C-Band. In this study, proposed TCDA design's infinite version is objected to operate from L-band to C-band. First the element, i.e. dipole, is to be designed, the feeding structures and balun shall be integrated into the unit cell. Overall structure is constructed in CST and full-wave analysis is taken place, parametric analysis is performed.

3.1 Element Design and Parameter Effects

As mentioned before, the aim is to design an operational ultrawideband tightly coupled dipole array with the concerns of ease of fabrication and low-cost application. There are two alternatives in selecting the planes of antenna and feed structure, two-plane or single plane. Two-plane means that, e.g. the antenna is at the xy-plane and balun and feed structure is at yz-plane, single plane structure means that both the antenna and the feed network is in xy-plane. In order to accomplish low-cost and easy fabrication, two-plane structures like [23] or [10] are avoided. Though, perpendicular array plane to the feed network plane has its own advantages, the fabrication and integrating these two planes precisely is an overwhelming task. Also, most of the two-plane tightly coupled arrays are constructed to have dual polarization, as in the

aforementioned references. Moreover, in order to produce the antenna dipole arms altogether with the balun and feeding network, via printed circuit board technology, the author decided to use printed dipole and feeding structure topology in single plane design. The most iconic feature of the TCDA is the coupling scheme of the dipole elements. In the proposed design, the coupling scheme is overlapping dipoles.

The TCDA element design is based on the approach of [19], antenna, balun and feed network are on the same plane, xz-plane, the infinite array extends in the xy-plane and radiation direction is z-direction. A dipole shown in Figure 3.1 is constructed by placing arms on both sides of the substrate and fed at the center, bandwidth is starting around L-band and extending to the C-band. The feeding scheme is with a lumped port element, having internal impedance as 170 Ω, the lumped port will be replaced by a proper balun and feed network in the following stages in this study. The parametric demonstration of the dipole element and important parameters are shown in Figure 3.1. The dimensions are shown in Figure 3.2 and the related VSWR is shown in Figure 3.3. The infinite array configuration that is simulated is shown in Figure 3.4. Simulations are held from 0.5 GHz to 10 GHz bandwidth. In the parameter sweep simulations, simulation configuration is a dielectric substrate with ϵ_r=10.2, annealed copper as conductor and lumped port excitation. The further simulations include a COTS dielectric which is RO4350b. The initial unit cell used for parameter sweep simulations are presented in Table 3.1.

Table 3.1: Initial unit cell for parameter sweep simulations dimensions list

Parameter	**Dimension**
h	20 mm
dx	22 mm
dy	18 mm
y1	6 mm
y2	3 mm
y3	2 mm
z1	2 mm
x1	1 mm

In order to observe the parameters's effects on VSWR, unit cell parameters are swept

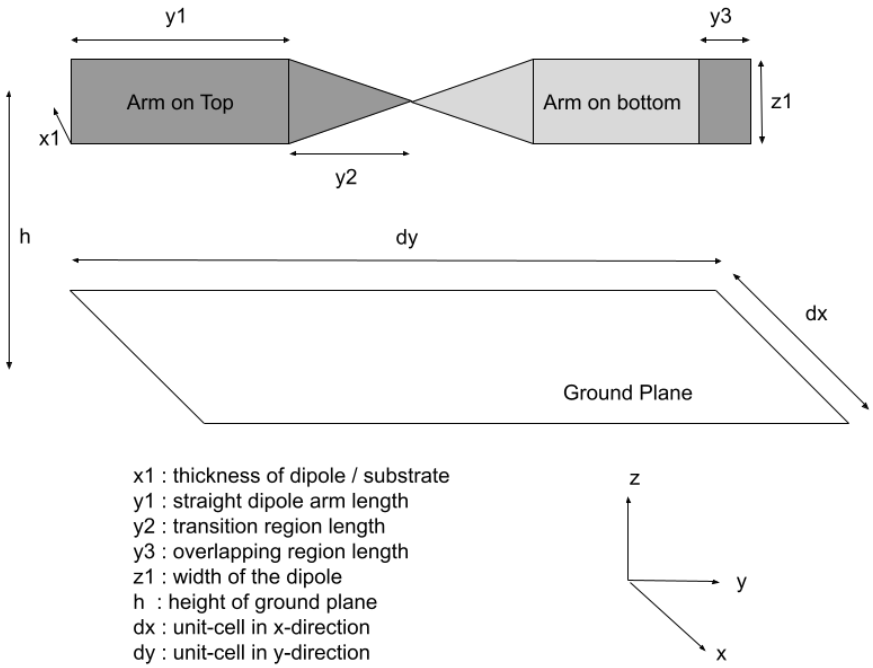

Figure 3.1: Parameters of array unit cell

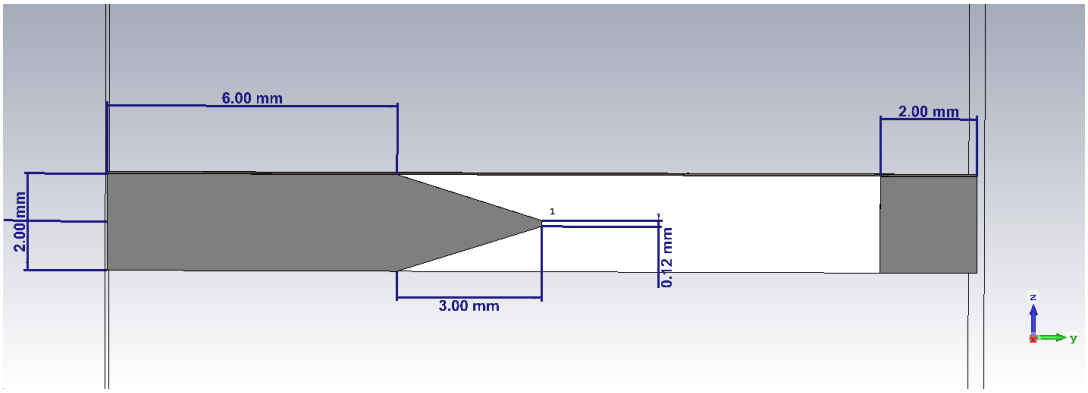

Figure 3.2: Initial dipole element and dimensions

in full-wave analysis. Each parameter is swept while the rest are kept constant as stated values in initial design. The parameters of the unit cell are provided in 3.1. The swept parameters are as follows, ground plane height, H-Plane element distance, dipole element flat arm length, overlapping dipole edge length and dipole element width.

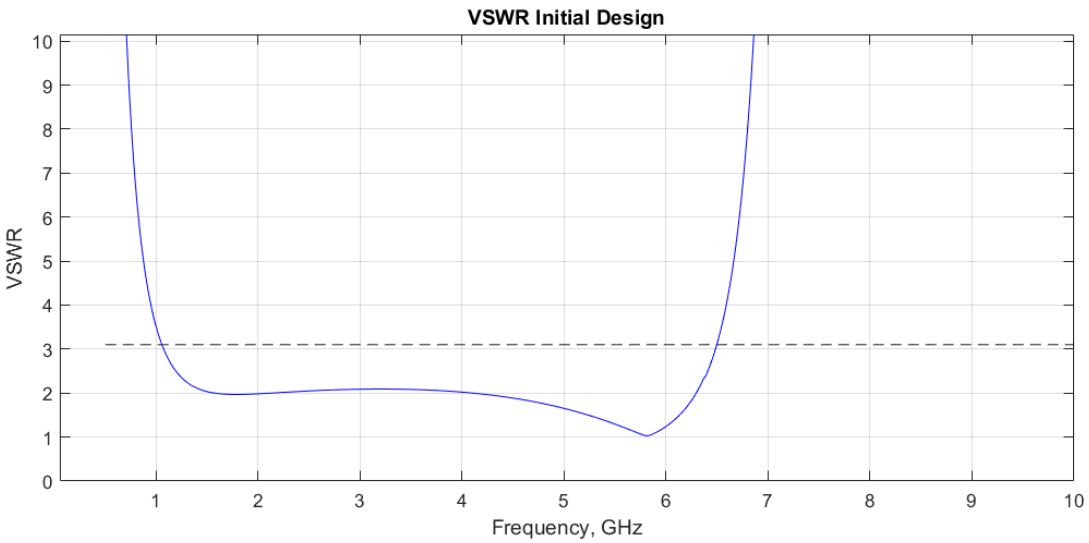

Figure 3.3: VSWR of initial element design.

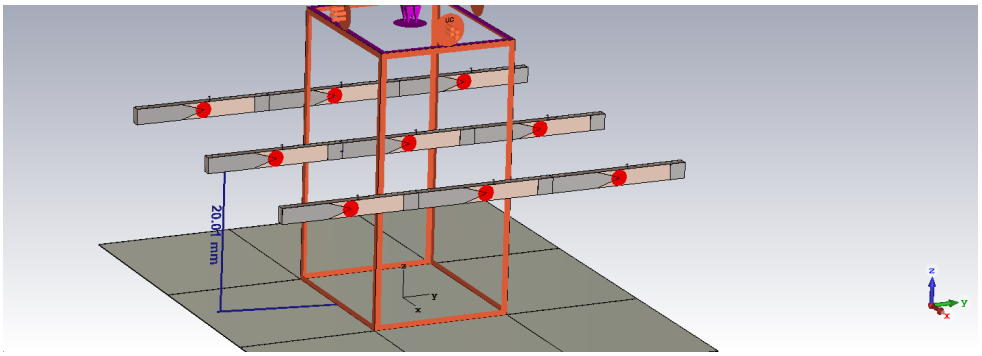

Figure 3.4: Unit-Cell infinite array setup.

3.1.1 Ground Plane Effects

TCDA arrays are the realizable version of the uniform current sheet array [11]. Theoretically, infinite amount of electrically small dipoles should be interconnected to create the uniform current sheet, without a ground plane and totally in free-space. This inherits the impracticality in both the infinite size and without any conductor backing up the array. Since most of the applications the arrays should be shielded from the feeding network or related electronics or confined with a casing [15]. By the works of Munk, TCDA is configured as the tightly coupled dipoles placed above a ground plane. Introducing the ground plane to the array, detoriates the impedance bandwidth significantly, as can be seen in Figure 3.5. The ground plane basically introduces an

inductive impedance over a wide range of frequencies [13], especially large inductive impedance for low frequencies. Interacting with the capacitive impedance caused by the tight coupling between the elements, ground plane inductance is compansated for the total input impedance to be resistive, or to a very low reactance implying matching. Ground plane is modeled as a shorted transmission line in circuit model of TCDA, as explained in Chapter 2. As could be observed by this model, at a certain frequency that is, $h = \lambda/2$ the short (zero impedance) is directly carried to the input of the array, creating a zero impedance seen. This yields all fields to couple to ground plane and prevent the radiation. This is simply expressed as the unmatched case, due to ground plane. So, ground plane determines the upper bound of TCDA impedance bandwidth. The previously mentioned, $h = \lambda/2$ zero impedance is a strong boundary, meaning that unless introducing another impedance parallel with ground plane, ground plane $h = \lambda/2$ frequency always determines the upper bound. To clarify the previous sentence, there has to be another impedance parallel with ground plane to prevent zero impedance seen, in order to accomplish that there is a proposal of using lossy materials in between dipoles and ground plane [23].

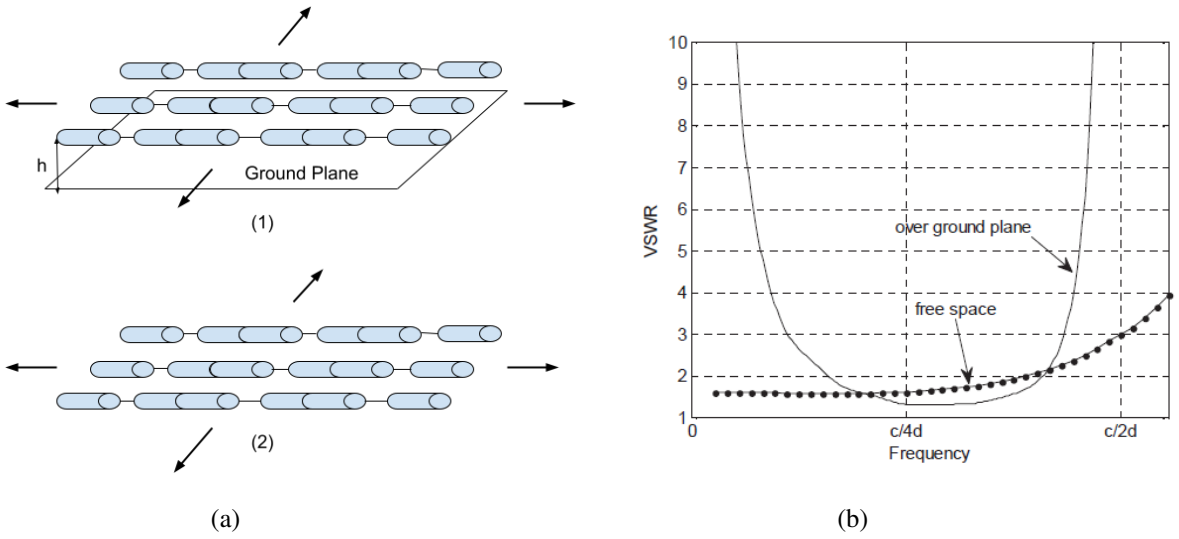

Figure 3.5: (a) An example of dipoles over ground plane(1) and free-space(2), (b) VSWR of such configurations by Tzadinis's work [15]

Ground plane also creates a limit for the lower frequency of impedance bandwidth. Note that, this lower frequency limit is not absolute like $\lambda/2$ condition. Rather it is

due to the h (height of dipoles from ground plane) to be electrically very small, creating another zero impedance effect. The beginning of this effect is estimated to be around $h \approx \lambda/10$ [13]. This detoriation value for lower boundary in bandwidth could be improved via the tight coupling. Note that the idea behind using the strong mutual coupling is to compansate the large inductance introduced by the ground plane. Investigating the frequencies that are close to the upper bound, for those frequencies, ground plane inductance becomes so small that it could be neglected. Hence, tight coupling capacitance which is aimed to compansate the inductance, becomes dominant. Then the input impedance becomes largely capacitive towards the upper bound. For improving the lower limit, coupling capacitance can be increased but in return this decreases the higher bound. Hence, to maximize the bandwidth a fine tuning for the ground plane height is essential. Also note that the introduced capacitance by tight coupling is dependent on the substrate, coupling scheme, geometry, etc. meaning that there is a limited space to manipulate the capacitance. This is another reason to tune the ground plane height rather than merely focusing on the mutual coupling.

Aside from the impedance bandwidth boundaries, ground plane also has significant effects on the radiation pattern of the TCDA. A wide usage purpose of a ground plane behind an array is to confine the radiation to a half-plane, blocking the backside. It increases the directivity compared to the array floating in free-space. Moreover, the ground plane also modeled as a PEC creating images of the dipoles. For TCDA, current flows through the dipoles horizontally, parallel to ground plane. Parallel current vectors over a ground plane which can be considered as horizontal electric dipole has an image of reversed orientation below the ground plane, creating an array behaviour for far-field radiation [1]. In Figure 3.6 radiation pattern of a single horizontal dipole over an infinite ground plane with different electrical height, h, is seen. In TCDA configuration, note that the bandwidth is very large and the ground plane height, h, is varying over a wide range, electrically. For $h > \lambda/2$ radiation pattern of a horizontal dipole (in our case, unit cell of TCDA) has tilted radiation pattern, in order to mitigate this effect ground plane height should not exceed the half wavelength. Also note that, for heights below $\lambda/2$, horizontal dipole over a ground plane has boresight radiation patterns but still the beam shape is affected by ground plane height even though a small variation is observed.

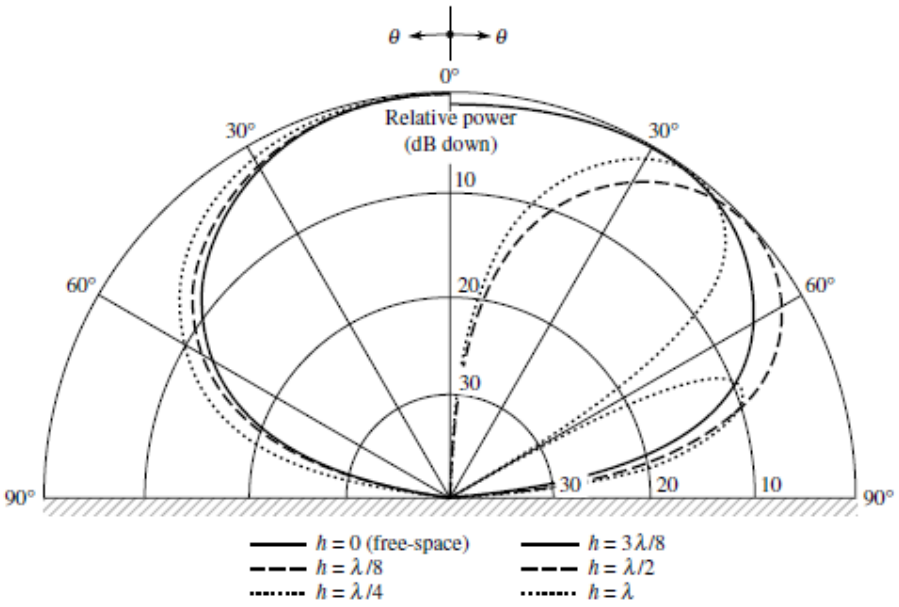

Figure 3.6: Radiation pattern of a horizontal dipole over a ground plane, varying "h" [1]

Based on the theoretical and literature knowledge on ground plane effects on TCDAs, we swept the parameter. "h" value is changed from 12 mm to 28 mm and obtained VSWR results are plotted in Figure 3.7. As can be seen in Figure 3.7, the height decrease yields a shift in higher frequencies. But note that, for the 12mm case, the VSWR values never goes below 3.1 threshold. That is due to the fact that element and overlapping section capacitance values are not sufficient to overcome the higher inductive reactance introduced by decreasing the height. Since the impedance of the element does not change in these simulations, decrease in the height increases the inductive impedance of ground plane. As we examine the 28 mm case, that is the inductance introduced by the ground plane is lower, we see another small VSWR, not close to be considered as operable. Note that the frequency is also shifted below as the ground plane shorting frequency decreased by increasing physical length. Also, it is observed that the ground plane affects the lower cut-off, the higher cut-off and the operational band VSWR. This strong effect shows that the ground plane placement is a crucial parameter in TCDA design.

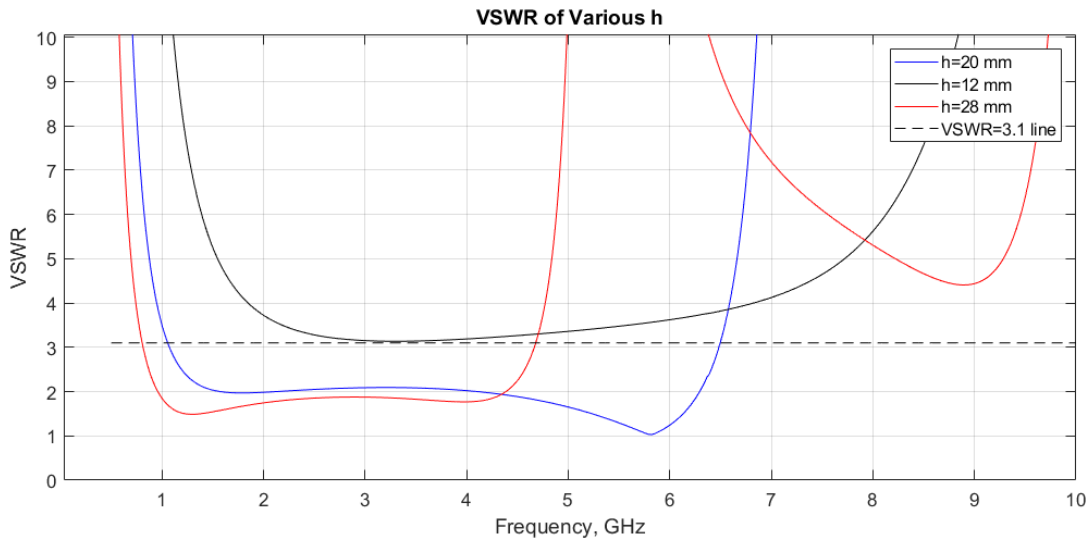

Figure 3.7: VSWR of infinite array with different ground plane heights.

3.1.2 H-Plane Seperation Effects

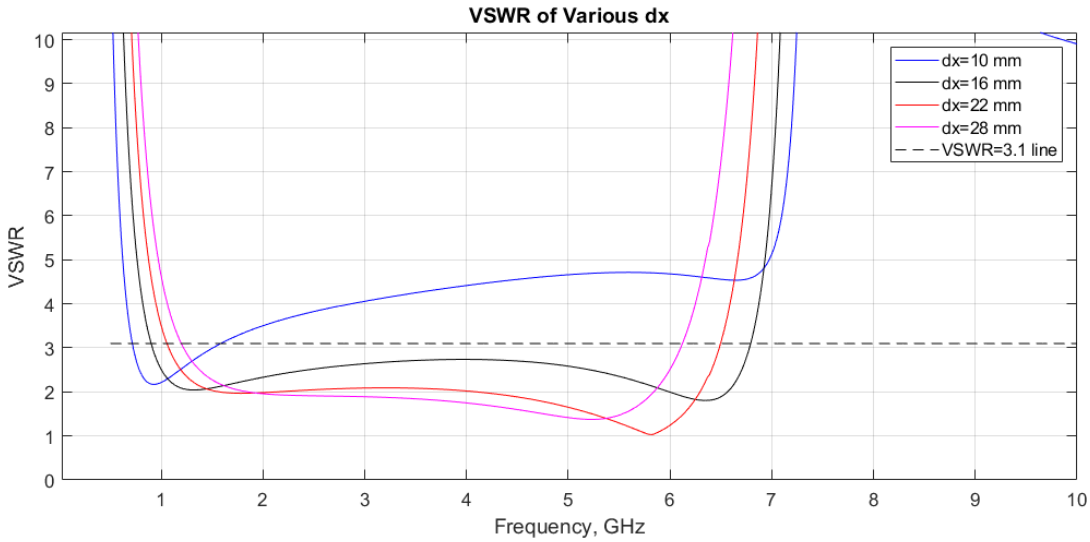

Figure 3.8: VSWR of infinite array with different H-plane distances, dx.

H-plane in the proposed TCDA is the non-overlapping plane which is not tightly coupled plane. The array is simulated for four different H-plane spacings, dx, in order to observe the effects on VSWR. The results are provided in Figure 3.8. The decreased H-plane distance yielding more coupling in the H-plane, shifting the operational band towards higher frequencies, but to a certain extend. Since being too close to the dipole

length, d=10 mm case, is out of acceptable value in VSWR. Note that, tight coupling in the TCDA concept is realized with interdigital capacitor-like structure at the ends of the dipole [14] and can be seen in Figure 1.4, the intentional coupling plane is the E-plane of the dipoles. Due to that, coupling in the H-plane is unwanted though for larger spacing in between the elements, it is observed that the impedance bandwidth (range of frequencies of which VSWR<3.1) is decreased, as seen in Figure 3.8. Both of the cut-off frequencies got closer to each other, decreasing the bandwidth. Increasing H-plane distance makes the VSWR response getting better(lower) meanwhile the BW gets narrower. Hence, the H-plane coupling has to be optimized if TCDA and UWB performance is aimed, as in this study's purpose. For the simulated four values, the optimal value among them is the medium value, 16 mm.

3.1.3 Dipole Arm Length Effects

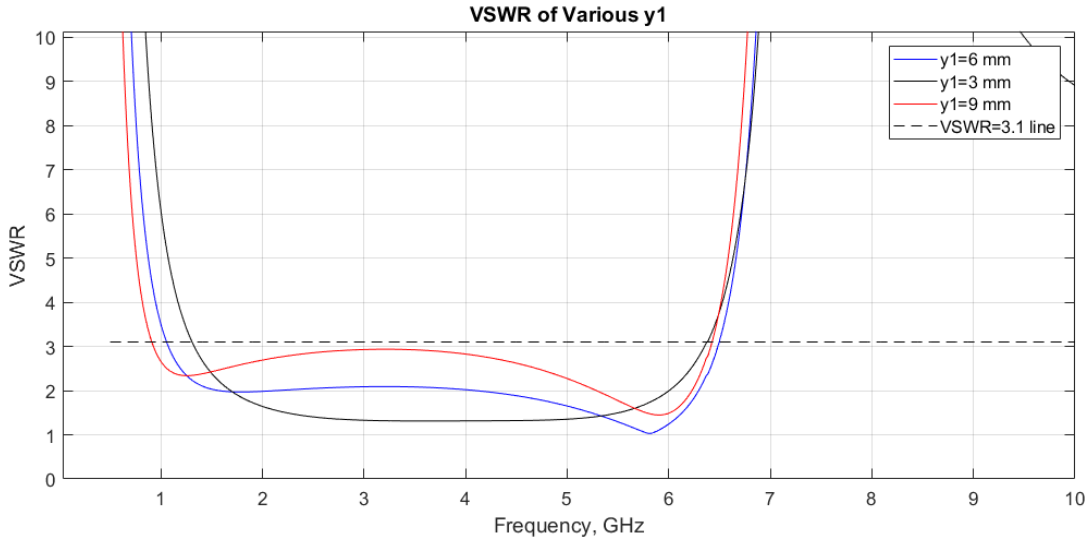

Figure 3.9: VSWR of infinite array with different flat-arm lengths, y1.

The unit cell is designed with three different flat dipole arm lengths, and simulated. The results are presented in the Figure 3.9. Note that at the simulations in Figure 3.9 the transition length of the dipole from feed-point is kept constant at 3 mm. The overlapping dipole size is kept at 2 mm as well. The dipole size getting smaller, meaning electrically small dipole which is a desirable feature in TCDA concept. But, considering the space required for the surface currents to flow after the transition length as

well as the overlap size, may disfunction an element if the flat-arm length gets too small. In the presented simulations, smallest value yields the lowest average VSWR in the operational band in the meantime has the most narrow bandwidth. Largest length has slightly wider bandwidth but considerable worse VSWR performance at the operational band. Which concludes that, even though in theory the dipole size should be as small as possible, the configuration of h, d, and other parameters as well as the dipole geometry demands a fine tuning. Also, for y1=3 mm value, note that the dipole width is very close to dipole length which is an undesired case.

3.1.4 Overlapping Dipole Effects

Tight coupling is introduced with overlapping dipoles in the proposed TCDA. Tightly spaced elements have already high mutual coupling yet, in order to create a high capacitive impedance in between the elements tight spacing is not enough. Overlapping region has a crucial role of lowering the VSWR during whole bandwidth and one of the pillars to obtain ultrawideband performance out of dipoles.

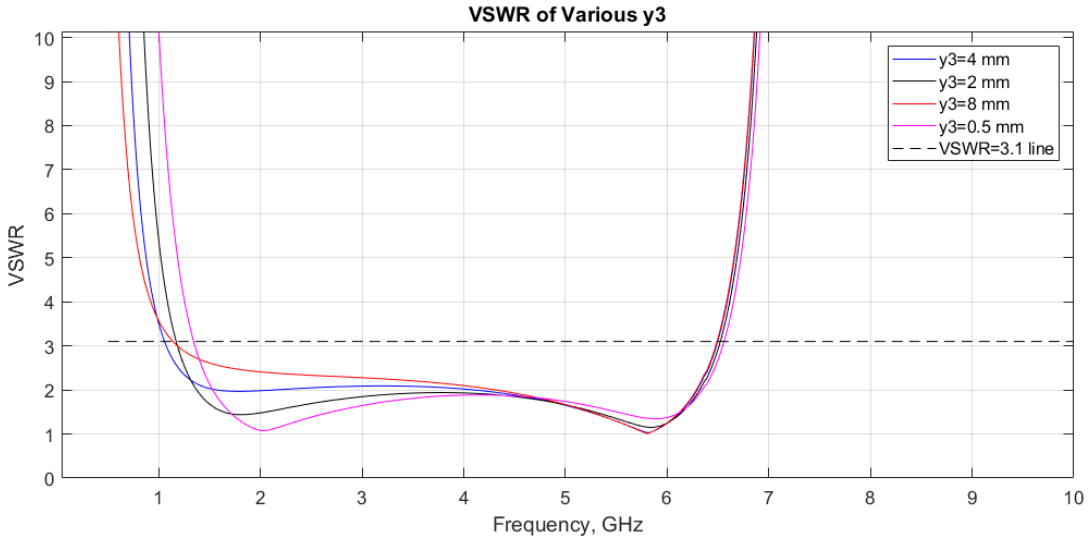

Figure 3.10: VSWR of infinite array with different overlapping dipole lengths, y3.

The overlap region introduces highly capacitive effect at the impedance of the unit cell. The author must notify that the overlap length and the used material permittivity both has crucial role in determining the introduced capacitance. The capacitance gets higher as the overlap region gets longer. Note that the overlap region has almost no

efffects on the upper cut-off frequency, instead it affects the lower frequencies the most since it operates to compansate the highly inductive impedance of the ground plane at the lower frequencies. Even so, larger capacitance introduced negatively affects the operational band VSWR values since the inductance gets smaller as the frequency increases. For the lower capacitance introduction to the array, VSWR performance in the operational band gets better but in return, the lower cut-off increases. As the result of this anlysis, one could conclude that the capacitance should be critically tuned to maximize the bandwidth while still providing low VSWR values. This is expected since the main reason for introducing the intentional tight coupling is to mitigate the inductance from ground plane and self-inductance of the array, generating a resistive impedance at wider spectrum [13].

3.1.5 Dipole Width Effects

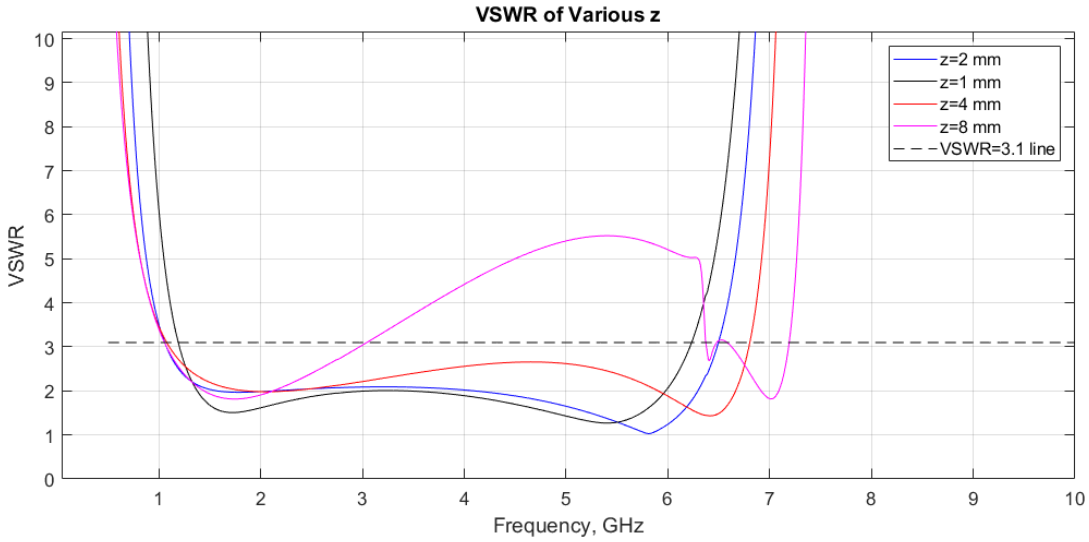

Figure 3.11: VSWR of infinite array with different element widths, z1.

Width of the dipole should be small as explained in Chapter 2. The assumptions by Munk [13] indicates that, very thin and electrically small dipoles should be utilized in TCDA configurations. As the dipole gets thinner, average VSWR gets better as indicated by Munk. But, width of the dipole has an affect in the impedance value of the dipole as l/d ratio. In order to tune the array's impedance, dy/dz ratio is critically important. In the presented simulations, the dy value kept constant while dz is varied.

This results yields also as different dy/dz ratios hence, extremum values are not the best. The mentioned concept of tuning the array impedance with ground plane and the capacitive coupling is dependent upon the element length-to-width ratio.

3.1.6 Edge Element Effects

TCDA concept is developed under the assumptions of infinite array and electrically small dipoles. Transmission line circuit model of TCDA is built under these assumptions. It is impossible to create an infinitely large array, therefore the designer should determine the number of elements in the array. In finite arrays, elements at the edges cannot be considered as tightly coupled, since they only confine a single edge to the array. To clarify that, please refer to Figure 3.12. For these edge elements, the circuit model assumptions and TCDA or CSA concept formulations does not apply since they do not meet the criteria. Having those elements at the edges of the all four directions on the array plane, the VSWR and radiation pattern are affected drastically. First of all, theoretically, the impedance is matched via fine tuning of ground plane impedance and mutual tight coupling, edge elements lack the controlled mutual tight coupling at least in one direction. This discrepancy of edge elements results in significantly different impedance values for that particular elements. Since the design of TCDA starts with infinite array, edge elements have the lowest performance on both VSWR and for radiation pattern. Edge element VSWR and comparison with corporate feed and internal elements are shown in Figure 3.13. For the cases of four corner elements, worsening effects are even higher for the rest of edge elements.

To improve their performance, there are several methods proposed by Tzanidis et. al [22]. These methods are based on terminating the edge elements, either with a resistive load or a shorting pin to the ground. Shorting pin terminated elements are referred as shorted elements further. Tzanidis et. al. terminated the edge elements with a matched resistive load, that is the Z_0 of the system [22] and compared the results with the shorted elements. It is observed that both schemes have different advantages. For comparing with the unterminated array, the effects of edge elements and their terminations are as provided in Table 3.2, in a comparison point of view and generalized. In this proposed design of TCDA, the edge elements are chosen to be

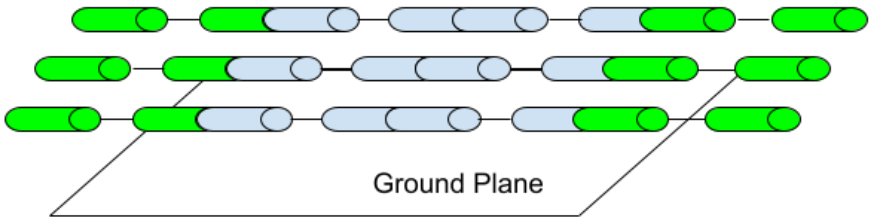

Figure 3.12: Demonstration of edge-elements in a TCDA, green elements are edge elements.

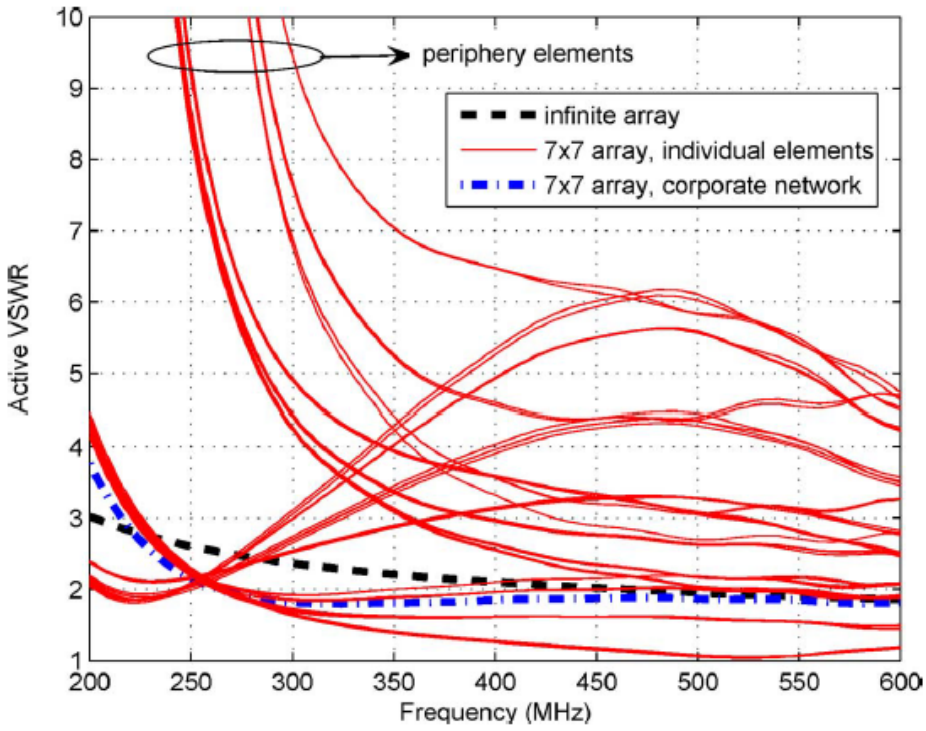

Figure 3.13: VSWR of internal elements and edge elements of design of Tzanidis et. al. [22]

terminated to the ground plane.

Table 3.2: Tabular comparison of several edge terminations of TCDA [22], performances are relativistic.

Type of Edge Element Termination	**VSWR**	**Gain**	**Efficiency**
Unterminated	Worst	Average	Average
Shorted Termination	Average	Best	Best
Resistive Termination	Best	Worst	Worst

The next step, is to change the material of the array into a low-cost and commercially-of-the-shelf product. In the proposed antenna, RO4350b with design permittivity, $\epsilon_r = 3.66$ is used with the thickness of 0.762 mm. As mentioned previously, antenna material has significant effect on the capacitance occuring in the tight coupling region. Hence, in order to change the material, a cycle of optimization with the parameters are done, manually. The process of designing the single plane TCDA infinite array, continued with the arranging the previously mentioned parameters iteratively. The obtained structure and dimensions are shown in Figure 3.14 and the related VSWR is shown in Figure 3.15.After the initialization of infinite array element is done, lumped port should be replaced with a realistic feeding structure.

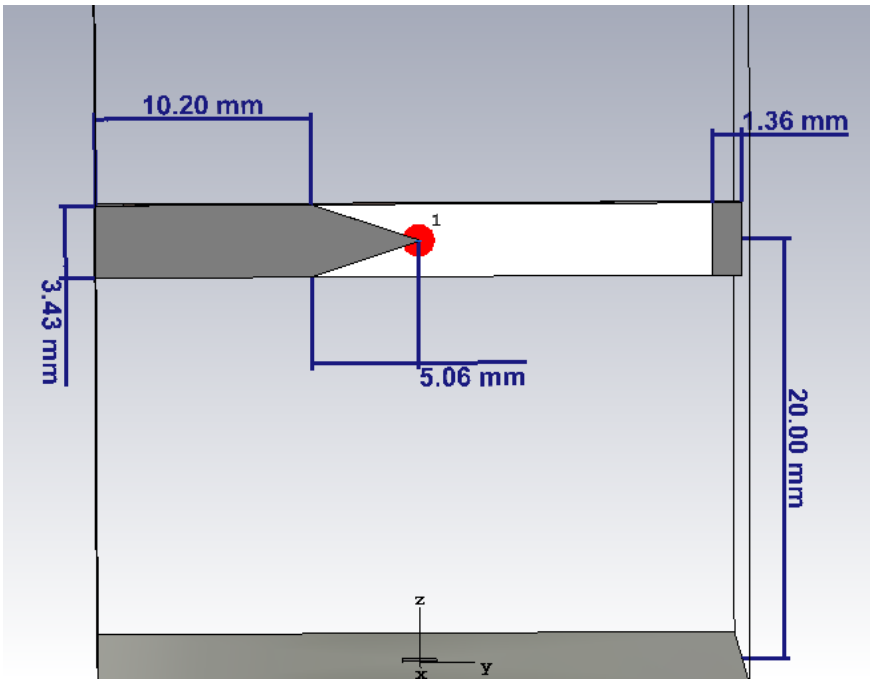

Figure 3.14: Dipole element of unit cell design.

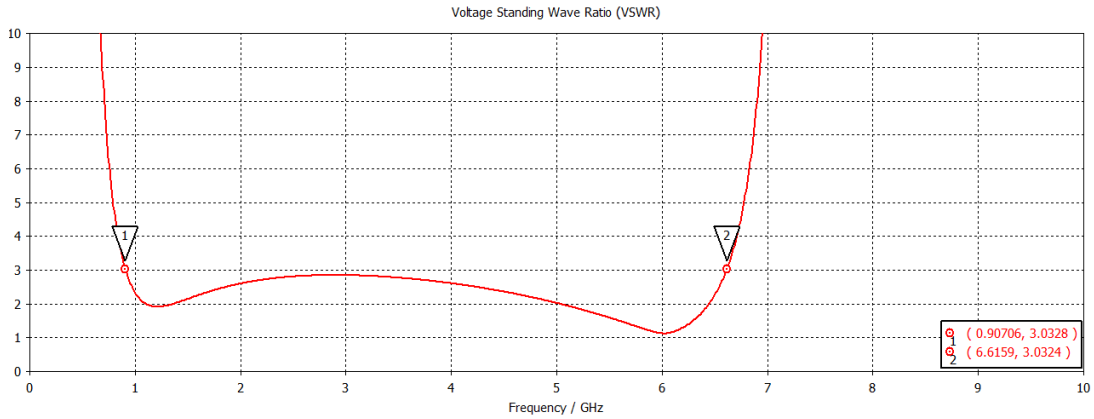

Figure 3.15: VSWR of infinite array simulation of dipole element

3.2 Balun and Impedance Matching Network

For an UWB antenna to be fabricated and used in applications, at least equally wide bandwidth feed network must be designed. Moreover, as in the case of TCDA, using dipoles requires balun structures. Desiging an ultrawideband balun is a challenging task. For a TCDA balun, most distinguishable feature relative to other array baluns is, as the elements are tightly spaced the baluns are also tightly spaced. The number of elements used does not affect the balun performance much, but on the other hand the tight spacing of the baluns causes the fields on the lines to couple to adjacent ones for some specific frequencies. This is named as common modes in TCDA literature [19]. Connecting the baluns to the dipoles, significantly degrades the VSWR in the operation bandwdith. There are two popular balun types used in TCDA, one is Marchand balun [18] and the other is Klopfenstein tapered lines [33]. Marchand balun's are mostly chosen when dipole plane is perpendicular to balun plane [20] (e.g. dipole on xy, balun on yz), and Klopfenstein tapered lines are mostly chosen when the dipole plane is same with balun plane [19].

The feeding network for the proposed TCDA consists of two stages, the balun and the impedance transformer. Since elements used in the TCDA, i.e. dipoles, require differential feeding (or balanced line) and the typical connectors (2.92, SMA or SNP, etc.) are based on unbalanced line transmission, balanced to unbalanced transformation is required. That is the balun structure. Also, as analyzed above, the dipole input resistance is quite high compared to 50 Ω. So that the impedace transformer is

needed. Since it is very hard to convert the high impedance to 50 Ω at a single stage, a tapered line or multi-stage line is required.

In order to feed the TCDAs, Marchand Baluns [18] or some integrated versions of Marchand Baluns [20] are widely used. But, these balun structures are mostly applied on two-plane structures, that is the antena plane being perpendicular to the feeding network plane. Also, they require multi-layer production which is a high-cost and complex production method requiring expensive manufacturing devices. In the proposed TCDA, the author studied on tapered lines, exponential tapers, linear tapers and mostly Klopfenstein tapers [33]. As one of the most efficient ways to construct a wideband balun and wideband impedance transformer, Klopfenstein tapers comes ahead. Klopfenstein tapers could be considered as the optimized version of the Dolph-Tchebycheff's tapering.

The antenna input is modeled with 170 Ω lumped port, we need a similar impedance balanced line (stripline) at that point. In order to obtain that, the similar width is taken as 97 Ω microstrip line having the same width with approximately 170 Ω stripline. This sections was the balun section, since it starts with 97 Ω microstrip line to 170 Ω stripline. The later section simply transforms the 97 Ω to 50 Ω towards the connector input. All the tapering was applied as Klopfenstein taper, the calculations provided at [33] were integrated into the proposed design. The proposed Klopfenstein tapered balun and impedance transformer is shown in Figure 3.16

The balun and impedance transformer sections are separetely analyzed before getting the structure in Figure 3.16. For the Balun, the termination is 170 Ω lumped element at one end and 97 Ω at the other end, for the impedance transformer the termination is 97 Ω lumped element and the other end is the 50 Ω port. The balun structure analysis geometry is presented in Figure 3.17 and the resulting VSWR is presented at Figure 3.18. Simulation results show that balun has VSWR<2 for the 0.5 GHz to 20 GHz simulation interval, demonstrating a promising wideband balun characteristic.

Note that the ground plane is also included in the analysis of balun. The balun and impedance transformer penetrates through the ground plane with gaps. The gap actually affects the impedance at the crossing of balun to transformer so it has been optimized to yield good results. The gap dimensions are presented in Figure 3.19.

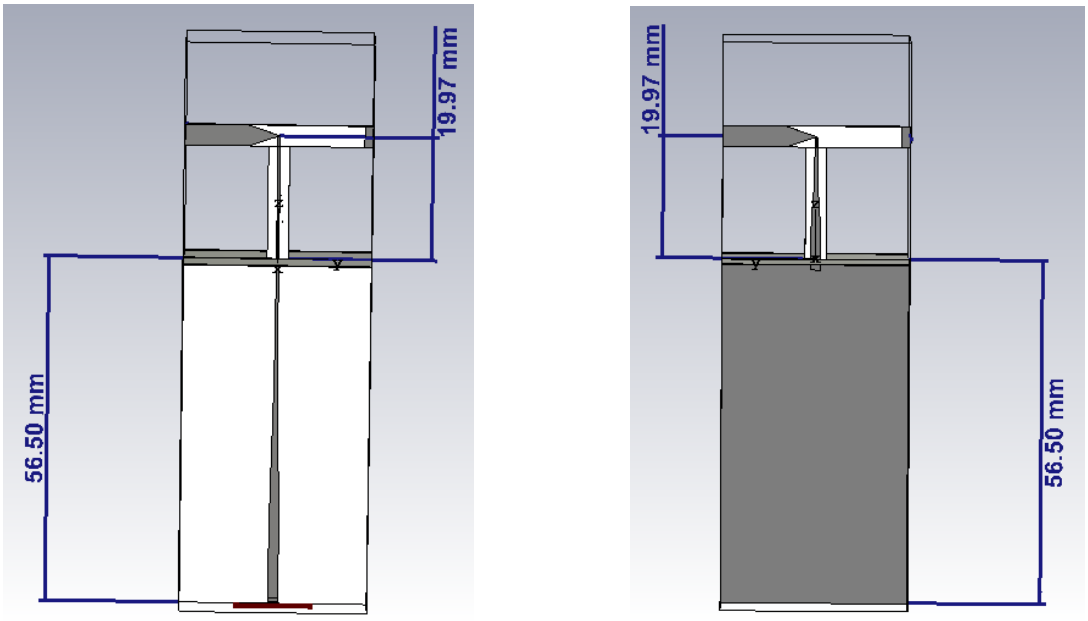

(a) (b)

Figure 3.16: (a) Front view, (b) Back view.

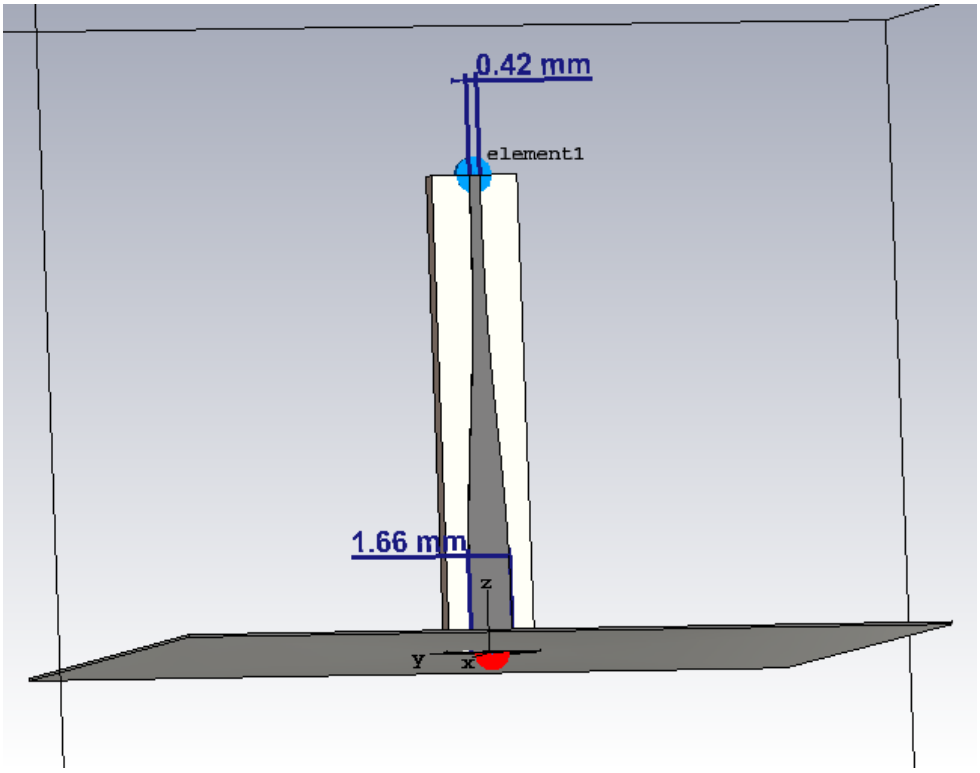

Figure 3.17: Constructed balun structure together with ground plane.

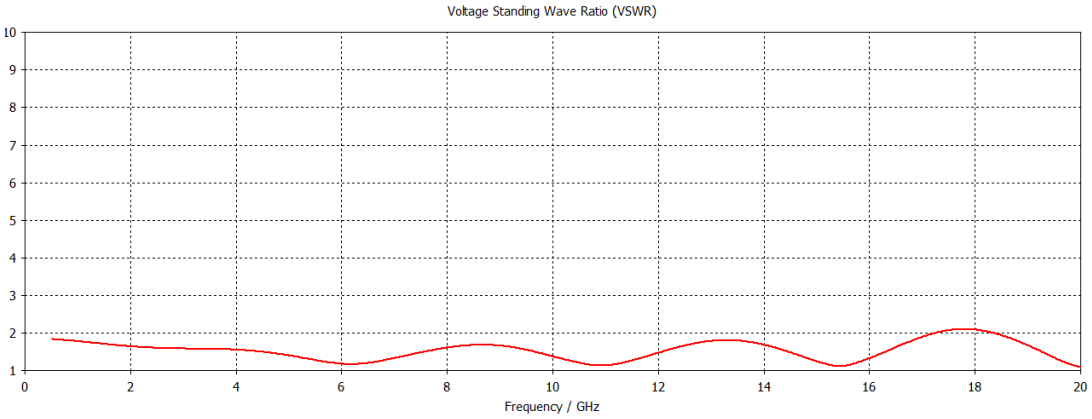

Figure 3.18: Balun structure VSWR, 0.5 to 20 GHz simulation result of isolated placement.

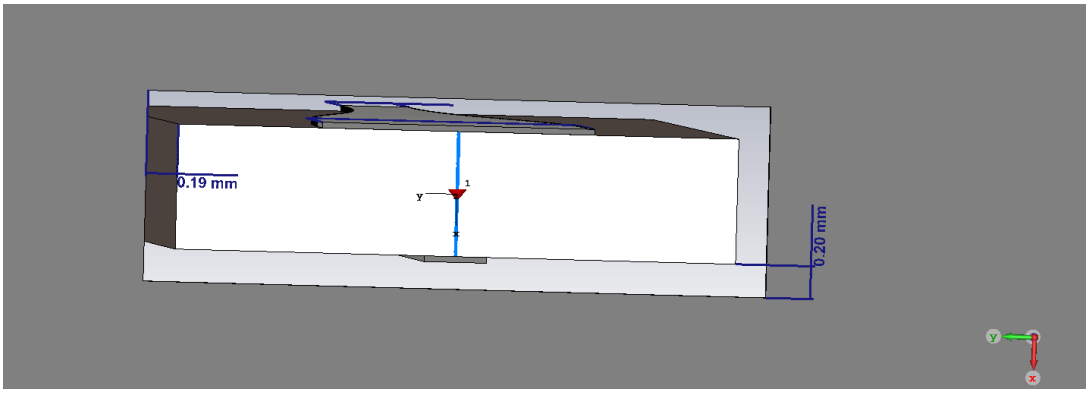

Figure 3.19: Ground plane penetration gap dimensions.

As well as the balun structure, the impedance transformer section is to be designed and simulated. The setup geometry and the resulting VSWR simulation result is provided in Figure 3.20 and Figure 3.21, respectively. Simulation results shows that impedance transformer has VSWR<2 for 0.5 to 20 GHz simulation interval, with the same characteristic as balun structure. Impedance transformer can also be designated as suitablle for wideband use in that interval.

Since aforementioned analysis is done in isolated setup, that is single object under open boundary conditions, it is not exactly similar to the proposed design usage. In the proposed design, these feeding networks also have tight spacing and high interaction with the adjacent elements. Since in the literature, tapered line-fed TCDA structures exhibit common mode currents at some frequencies [19], it is decided to

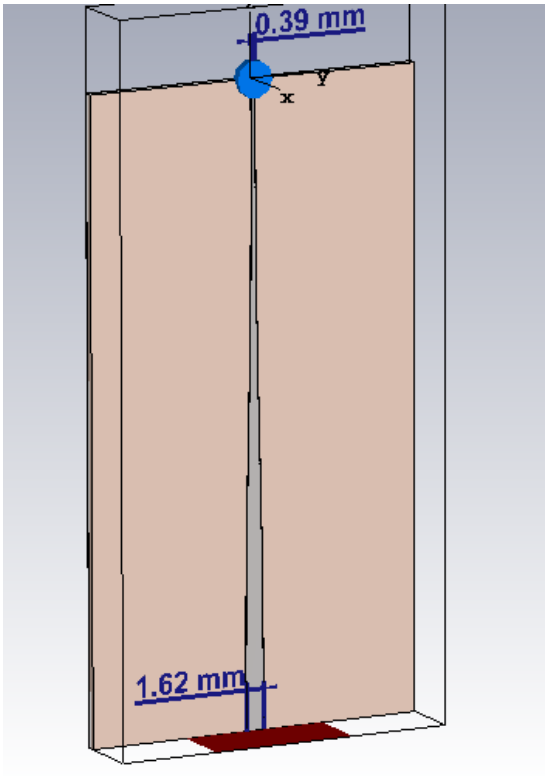

Figure 3.20: Impedance transformer network.

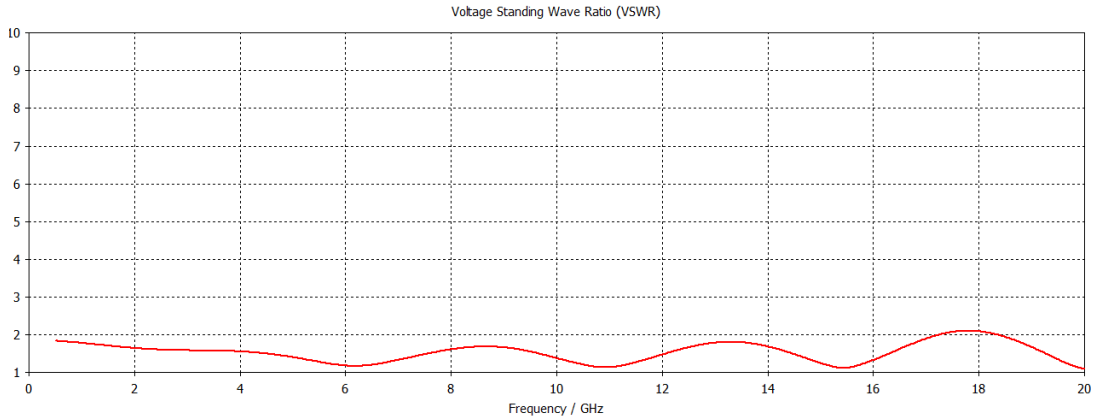

Figure 3.21: Impedance transformer network simulation VSWR result, isolated simulation.

simulate both the balun and the feeding network under infinite array configuration and unit cell boundary conditions in CST. The balun setup and related VSWR as well as feeding network setup and related VSWR are presented in Figure 3.22, Figure 3.23, Figure 3.24 and Figure 3.25, respectively.

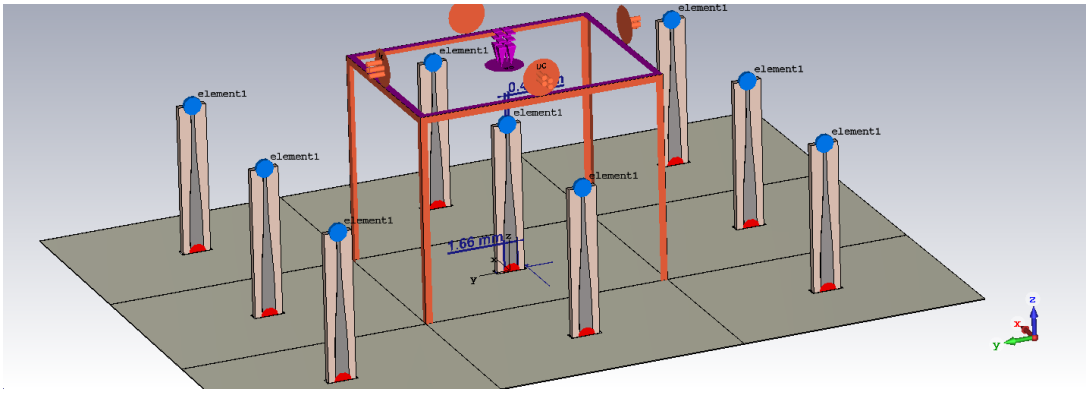

Figure 3.22: Balun structure under unit-cell boundary conditions, infinite array

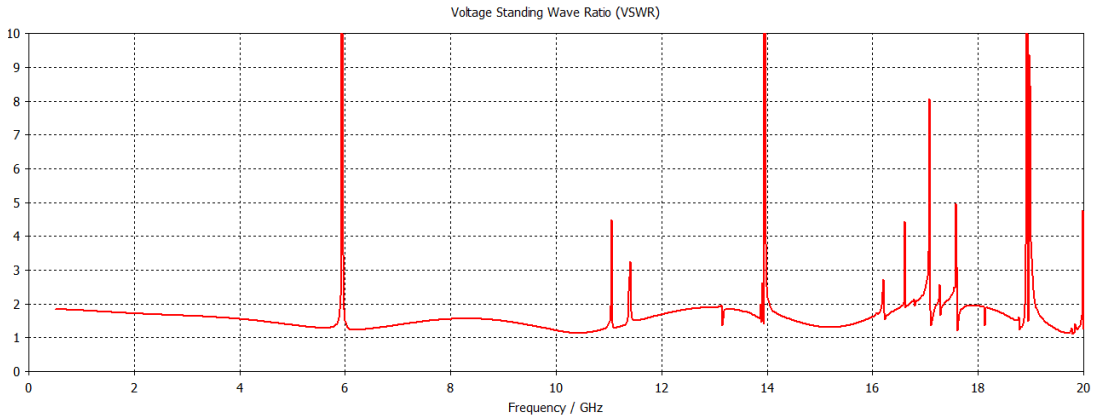

Figure 3.23: VSWR of infinite balun array.

Note that the termination resistances are identical in infinite array and the isolated cases. Also, in order to maintain the fully distributed ground plane effect and the realistic results, the ground plane with penetrating gaps shown in Figure 3.19 is also included. As can be cleary seen in Figure 3.23 and Figure 3.25, there are several spikes in VSWR indicating the existance of common modes in the simulation bandwidth, of 0.5 to 20 GHz. The density of common mode frequencies increase when the operating frequency gets higher. On the other hand still the overall operational bandwidth of the balun and impedance transformer is wider compared to the infinite dipole array with lumped port excitation, it can support the dipole array. After completing the network analysis, the next step is to build a full unit cell with proposed dipole and proposed feeding network.

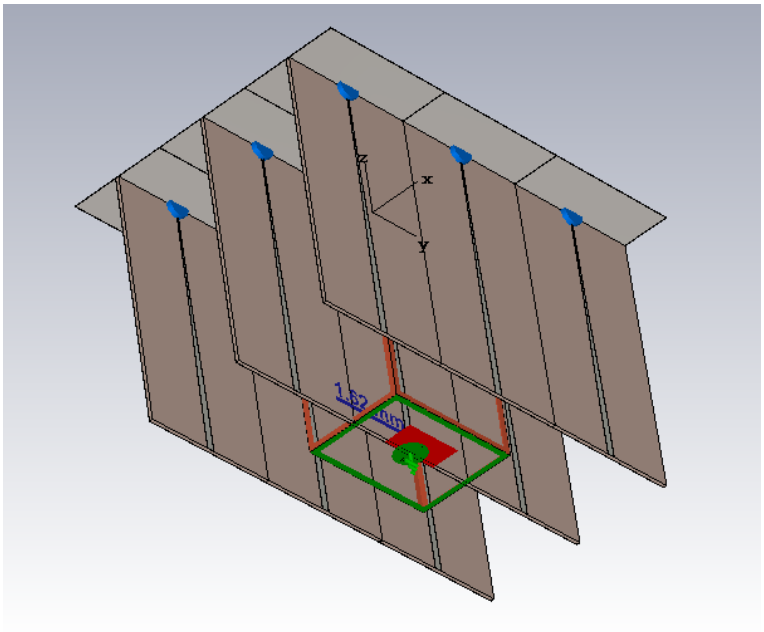

Figure 3.24: Impedance transformer under unit-cell boundary conditions, infinite array

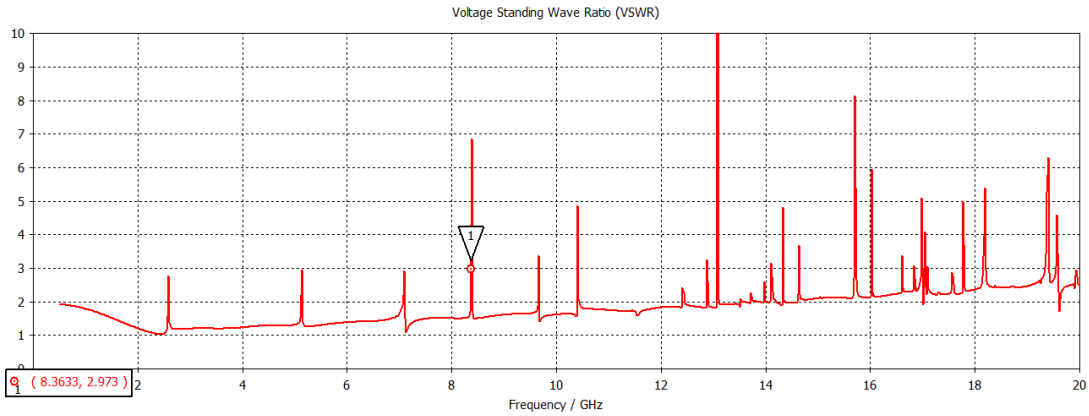

Figure 3.25: VSWR of infinite impedance transformer array.

3.3 Optimization and Final Form of Infinite TCDA

The dipole element is designed and analysed using 170 Ω lumped port. The feeding network is designed and analyzed throughly. Balun and impedance transformer inserted unit cell can be seen in Figure 3.16 and the simulated VSWR result is in Figure 3.26.

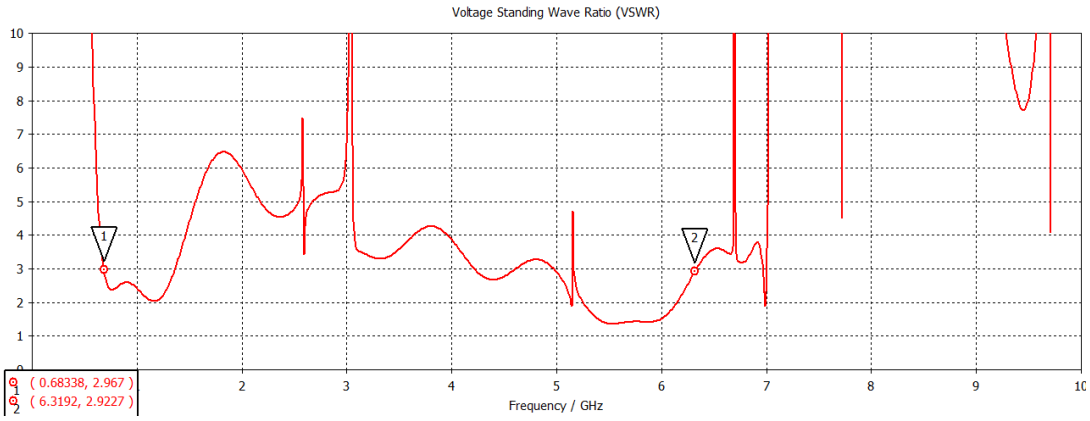

Figure 3.26: VSWR of infinite array of dipole and feeding network.

As can be seen in Figure 3.26 and comparing it with Figure 3.15, it is clear that the feeding network decreased the wideband impedance match of the dipole array. Common modes combined from balun and the impedance transformer increased the VSWR average value. In order to compansate that effect, it is decided to alter and optimize some of the array parameters. After many variations on several parameters, the VSWR is improved but still not good enough, in order to finalize the impedance performance genetic algortihm based optimization is utilized.

After examining the response in Figure 3.26, and literature review upon the subject of suprassing the common mode currents arising in the lines, altering the taper shape comes into mind. But more importantly, shorting the dipole ends is an accepted and proven method to surpass or more specifically shift the common modes out of the desired operational frequency [19]. In order to test these, an altered taper from Klopfenstein into an exponential form (used as th 0.18 constant 'loft' tool on CST) as well as shorting both edges of the dipole are simulated. The simulated geometry and related VSWR are shown in Figure 3.27 and Figure 3.28, respectively. All elements used in this section has same parameters as section 1, except $y_1 = 4.9\ mm$ and $z_1 = 1\ mm$.

Note that the VSWR performance got significantly better compared to the initial case. This is because of the shorting application. In order to determine it, various balun changes are applied with shorting kept intact and all other parameters kept constant. As the second step, balun kept constant while shorting only on a single side or de-

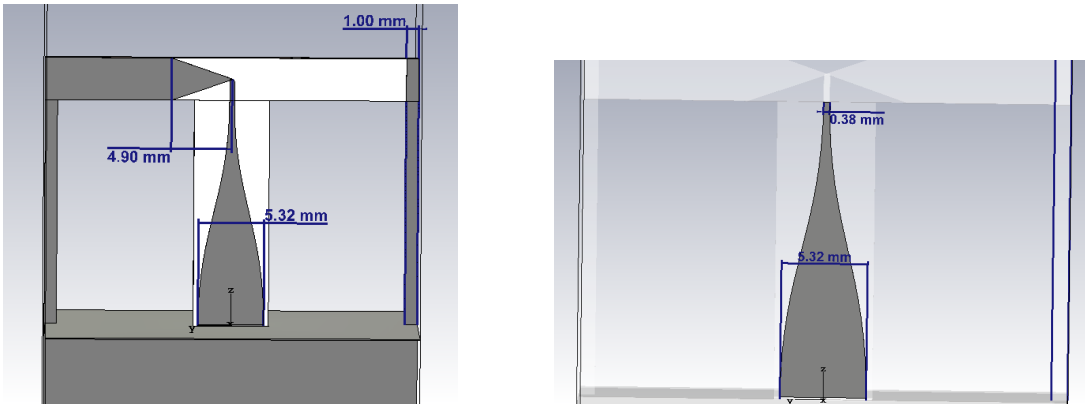

(a) (b)

Figure 3.27: (a) Element and the balun, back view. (b) Balun highlighted.

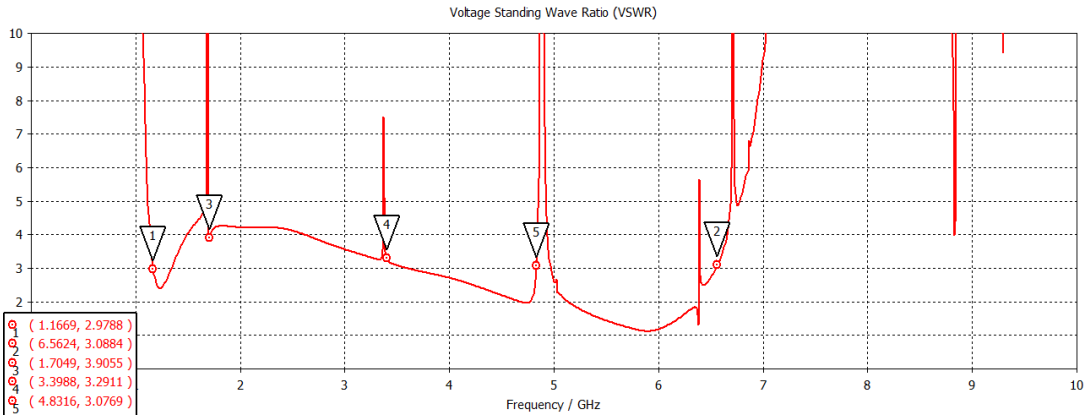

Figure 3.28: VSWR of infinite array of both sides shorted loft tapered example.

creasing the shorting pin size while keeping all dipole parameters constant.

In order to test the shorting side importance, only one side is shorted. The shorted side is the 'active' side, that is the untapered side of the antenna. The structure and the resulting VSWR is provided in Figure 3.29 and Figure 3.30, respectively.

The marker number '2' common mode suprassed below VSWR 3 value and the marker 5 decreased in frequency. Overall changes are small but slightly better. Meaning that shorting only a single side could be more effective, as studied in [19]. After that, many other taper shape changes and even inserting some inset towards the ground plane to increase the balun length while keeping the ground plane height constant, are applied. The results were not different than the previous ones, so the balun

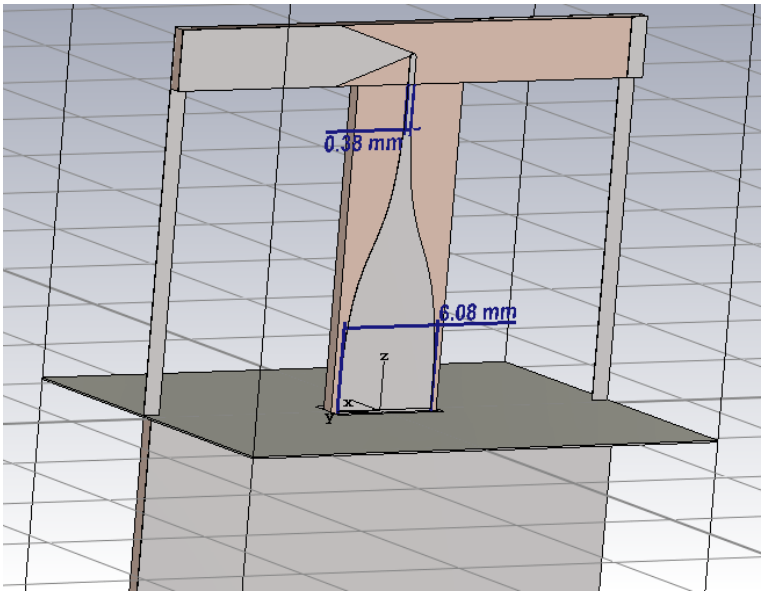

Figure 3.29: Single-side shorted lofted unit cell.

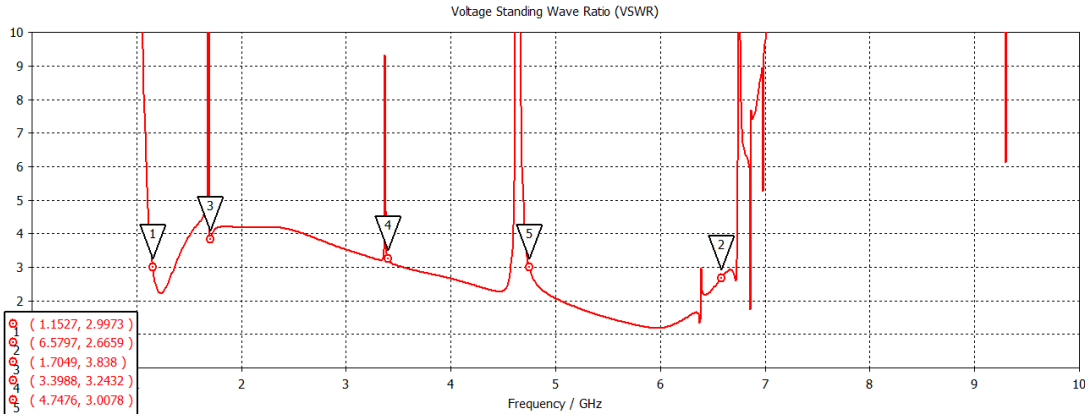

Figure 3.30: VSWR of infinite array of single side shorted built-in loft tapered example.

shape changes have low effect compared to original Klopfenstein taper. But for the Klopfenstein taper, the starting width from the ground plane had significant impact. In order to demonstrate this and compare it with the initial design result in Figure 3.26, the design shown in Figure 3.31 and VSWR shown in Figure 3.32 is obtained.

The comparison of the results in Figure 3.26 and Figure 3.31 shows that, wider starting width (lower starting impedance) in Klopfenstein balun structure yields better results. Note that, Marker 5 has no common mode at all in this configuration, instead

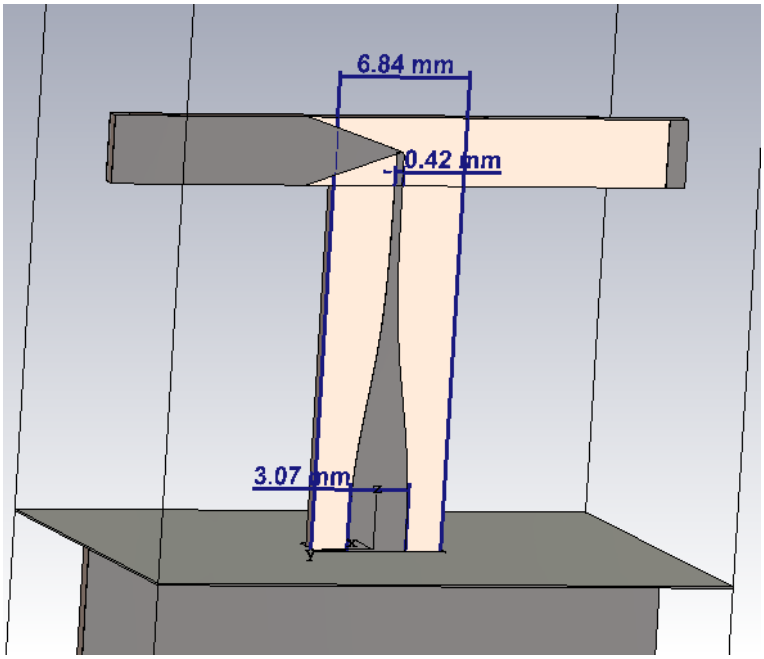

Figure 3.31: Un-shorted wider Klopfenstein tapered balun geometry, back view.

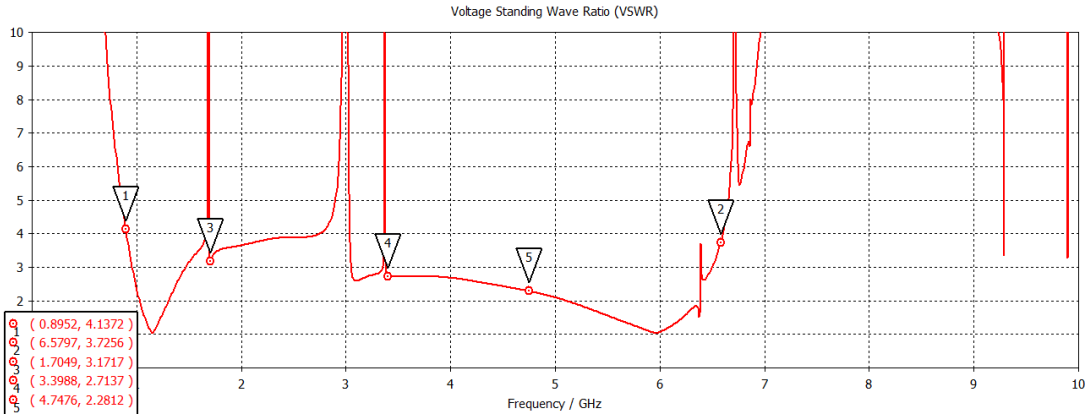

Figure 3.32: VSWR of infinite array of un-shorted Klopfenstein tapered unit-cell.

the common mode rise shifted towards marker 4. In order to optimize this, a shorted version of this wider balun structure is simulated as well.

The shorting application shifts the mid area common mode towards higher frequency, still not out of the operational band but more promising than the previous results. In order to give more realistic analysis, the shorting pins are backed with RO4350b material, as it shall be manufactured in that form. The resulting final form of the infinite array unit cell and the resulting VSWR is shown below in Figure 3.35 and

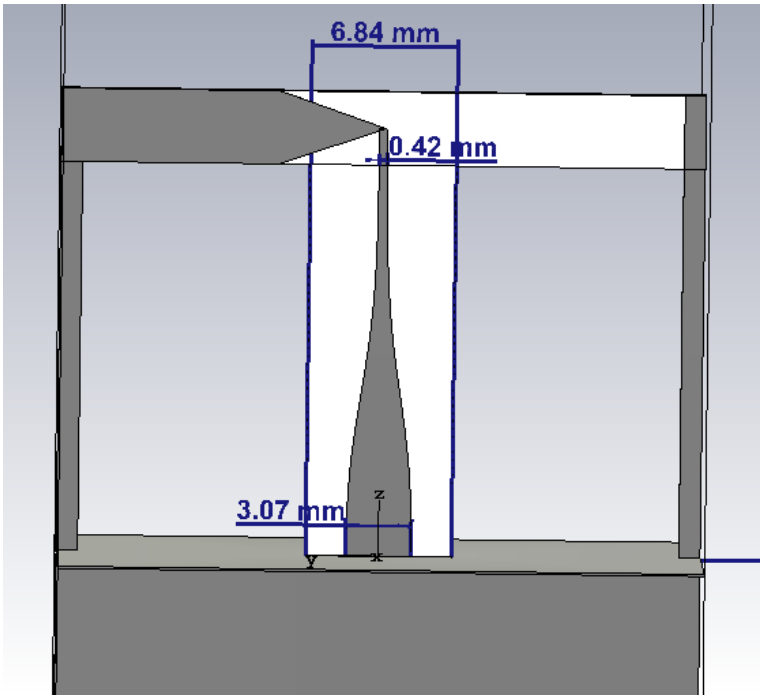

Figure 3.33: Single-side shorted wider Klopfenstein tapered balun geometry, back view.

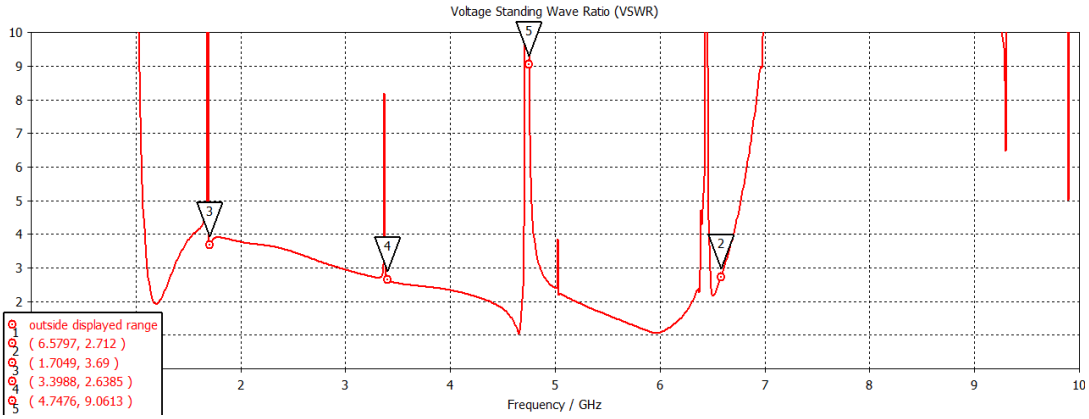

Figure 3.34: VSWR of infinite array of single-side shorted wider Klopfenstein tapered unit-cell.

Figure 3.36, respectively.

In order to optimize the element dimensions, CST's genetic algorithm based optimization tool is utilized. The variable parameters are almost all, the parameters that are not varied in the optimization runs are substrate (thickness and type), ground

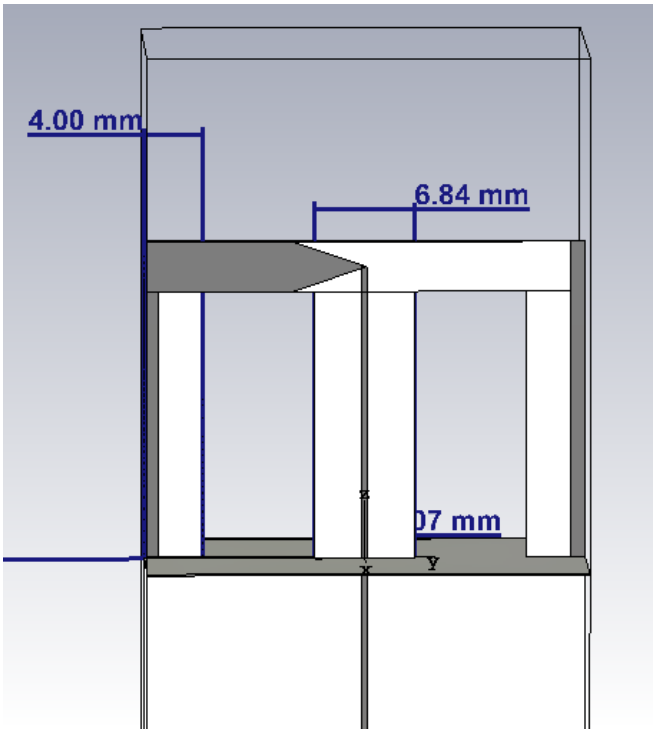

Figure 3.35: Single-side shorted wider Klopfenstein tapered balun geometry with substrate, back view.

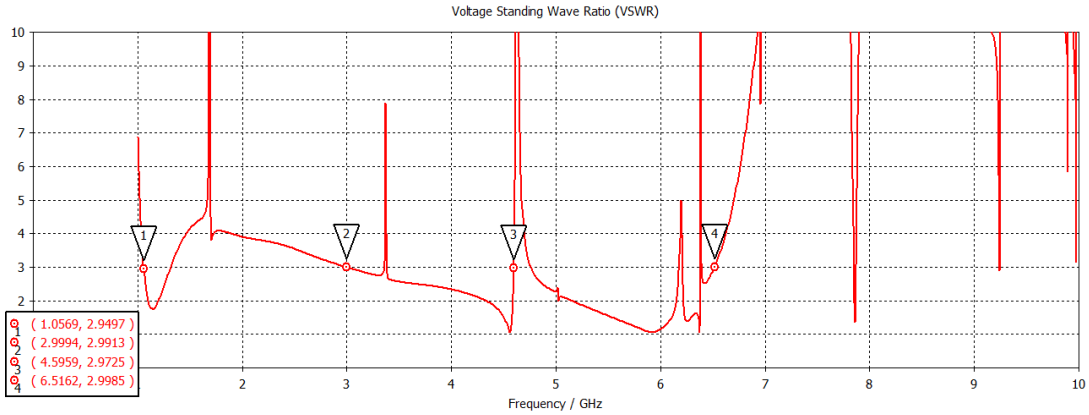

Figure 3.36: VSWR of infinite array of single-side shorted with substrate wider Klopfenstein tapered unit-cell.

plane height, feed width and penetration gaps on ground plane. The goal function is $VSWR < 2.9$ for $1.05 - 6.5$ GHz with maximum difference squared goal norm. The optimization parameter values; best results and optimization ranges are presented in Table 3.3.

Table 3.3: Optimized parameter values

Parameter	**Min**	**Max**	**Best**
dx	21.6	30.2	27.4
Shorting Pin Width	3.2	4.8	3.725
y1	2.23	6.7	2.99
y2	4.5	13.5	6.89
y3	0.5	4.08	2.345
z1	1.5	4.5	1.64

As the result of optimization, the VSWR average performance got better but the common modes still exist. The resulting geometry and related VSWR are presented in Figure 3.37 and Figure 3.38, respectively.

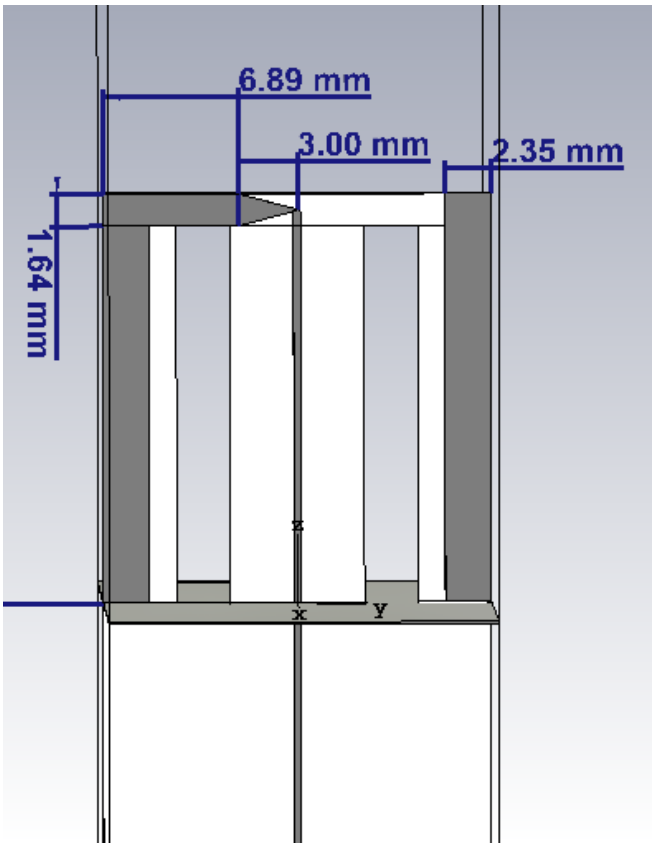

Figure 3.37: Optimization output element geometry.

Even after the optimization process, VSWR has several spikes in the bandwidth. Balun and impedance transformer sections under tight spacing are causing this prob-

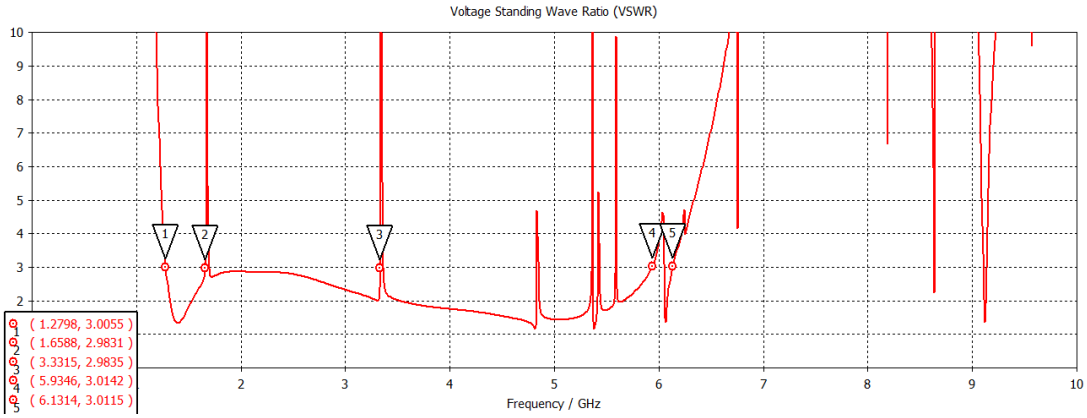

Figure 3.38: VSWR simulation of infinite array after optimization.

lem. Since the spacing cannot be enlarged due to reducing the coupling of the elements, common modes arising in the bandwidth are accepted. This is for the infinite array setup, for finite number of elements we know that the coupling of the feed lines are weaker due to finite number of adjacent lines. It is commented that in finite array configuration, VSWR spikes at the lower frequencies may result in higher f_{low} and vanish, for VSWR spikes at the higher frequencies (around 6 GHz) may decrease f_{high} and vanish. In order to observe this, a finite version is simulated and fabricated. After the optimization process is concluded, the infinite array is then converted to a finite array of size 5×5.

CHAPTER 4

DESIGN, ANALYSIS AND MEASUREMENT OF FINITE TCDA

As the element of the infinite array is designed and analyzed thoroughly in the previous chapter, it is the input of the design process of this chapter. To validate the TCDA concept, 5×5 finite array is designed and fabricated. The analysis of the finite array is conducted under various meshing, solvers and iterative steps on CST. After the simulation results of the finite design is verified, the production process began. Produced array is connectorized, mounted on an interface unit and measured. The results are compared with the simulation results and with the literature.

4.1 Design and Analysis of the 5×5 Finite Array

Theory of TCDA and mathematical expressions and transmission line modeling of the concept are all based on an infinite array structure. For the proof of concept demonstration we fabricated a 5×5 array.

For finite array configurations, there are several limitations on performance, which could be seen in Chapter 3 in detail. Since the infinite array elements are shorted at the edges, edge-element truncation method is already utilized in the proposed array. 5×5 array geometry is constructed and all elements are excited with a waveguide port in CST and simulated from 2 to 20 GHz bandwidth. The configuration of the finite array can be seen in Figure 4.1, Figure 4.2 and Figure 4.3

In the simulation set-up, VSWR of all 25 elements are investigated, far-field radiation patterns of all 25 elements are examined. All elements are terminated with a waveguide port and excited seperately. All metal structures are annealed copper with

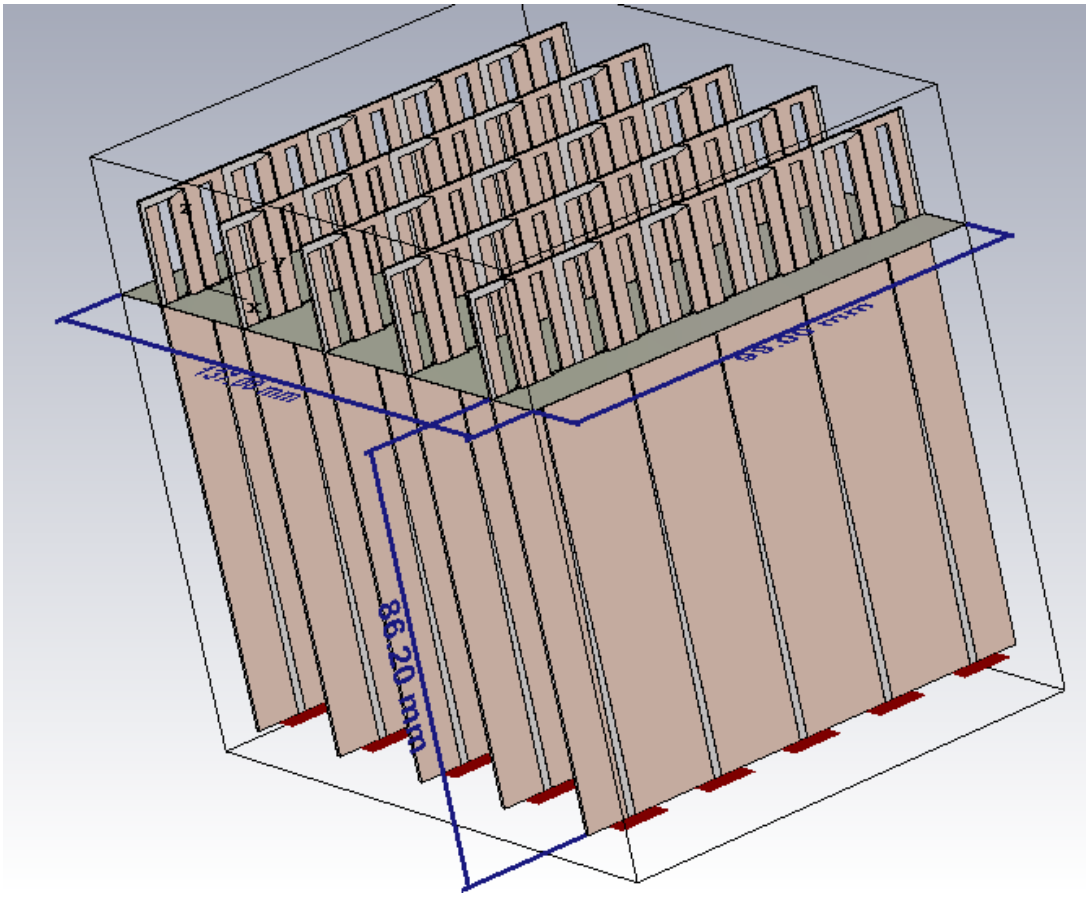

Figure 4.1: Perspective view of the 5×5 array.

substrate of RO4350b with all dielectric losses included. Two different solvers are utilized, F-Solver of CST which is frequency domain solver and T-Solver which is the time domain solver of CST. At both solvers and all simulations, mesh refinement of CST is enabled. F-Solver is the recommended unit-cell boundary condition simulation solver used for infinite array, and T-Solver is utilized for the 5×5 array in this work. In order to compare infinite and finite arrays fairly, the array is first simulated in F-Solver and then T-Solver. After observing that F-Solver and T-Solver results in similar VSWR and patterns, T-Solver is chosen for further analysis because of solving time efficiency. To show an example of F and T solver VSWR results, please refer to Figure 4.5 and Figure 4.14, respectively. All displayed pattern results in this chapter is simulated with T-Solver.

For tightly coupled arrays, internal elements tend to have similar performance to center element. Edge elements and corner elements are the worst performing elements

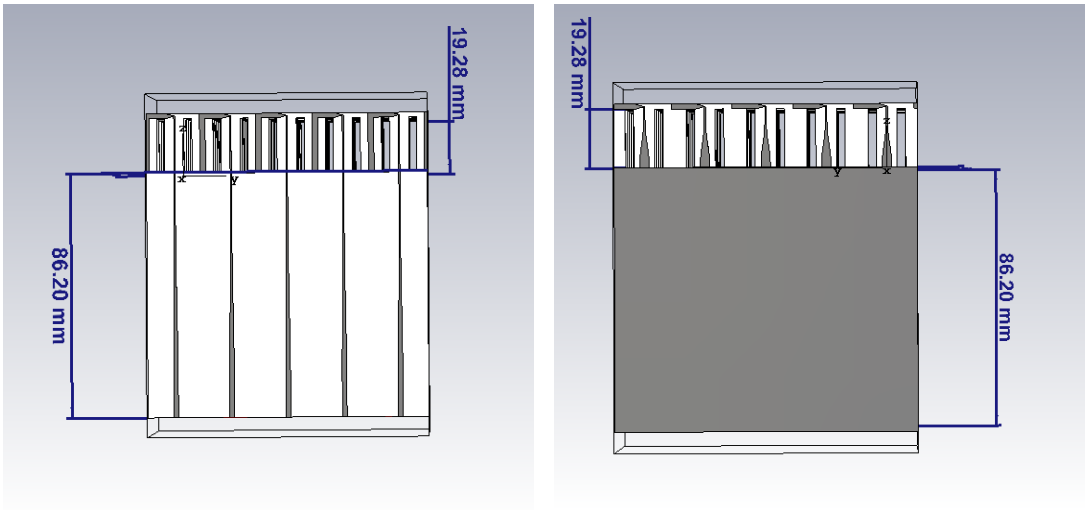

(a) (b)

Figure 4.2: (a) Front view 5×5 array, (b) Back view 5×5 array.

in terms of VSWR and radiation pattern. Due to that reason, they can be called as distinguishable elements in the proposed TCDA. By examining all 25 elements in the proposed array, edge and corner elements are indeed have discrepancies. Four elements are chosen to be distinguishable elements, which are top left corner element (one of the four corners), center element of the E-Plane Edge, center element of the H-Plane Edge and finally the element at the array center. In order to clarify the definitions, visualization of the selected elements are presented in Figure 4.4.

Due to avoiding overcrowding the thesis paper, only the aforementioned elements, "Element Corner", "Element EEC", "Element HEC" and "Element Center" are presented with the results. The VSWR result of the simulated with F-Solver, 5×5 array is provided in Figure 4.5 and in Figure 4.6 seperately for 2-10 GHz and 10-20 GHz simulation bandwidths. The simulation bandwidth seperation is needed since the computer could not compute the 2-20 GHz simulation at the single setup due to insufficient hardware. For the results in Figure 4.6, all elements are below VSWR=3.1 value, meaning that all the elements are matched to the 50 Ω port. They are even below VSWR=2 value for the most of the bandwidth. But, for the simulation in 2 to 10 GHz case, in Figure 4.5, all elements show similar characteristics but slightly different frequencies for VSWR=3.1 value. Note that in VSWR response, corner el-

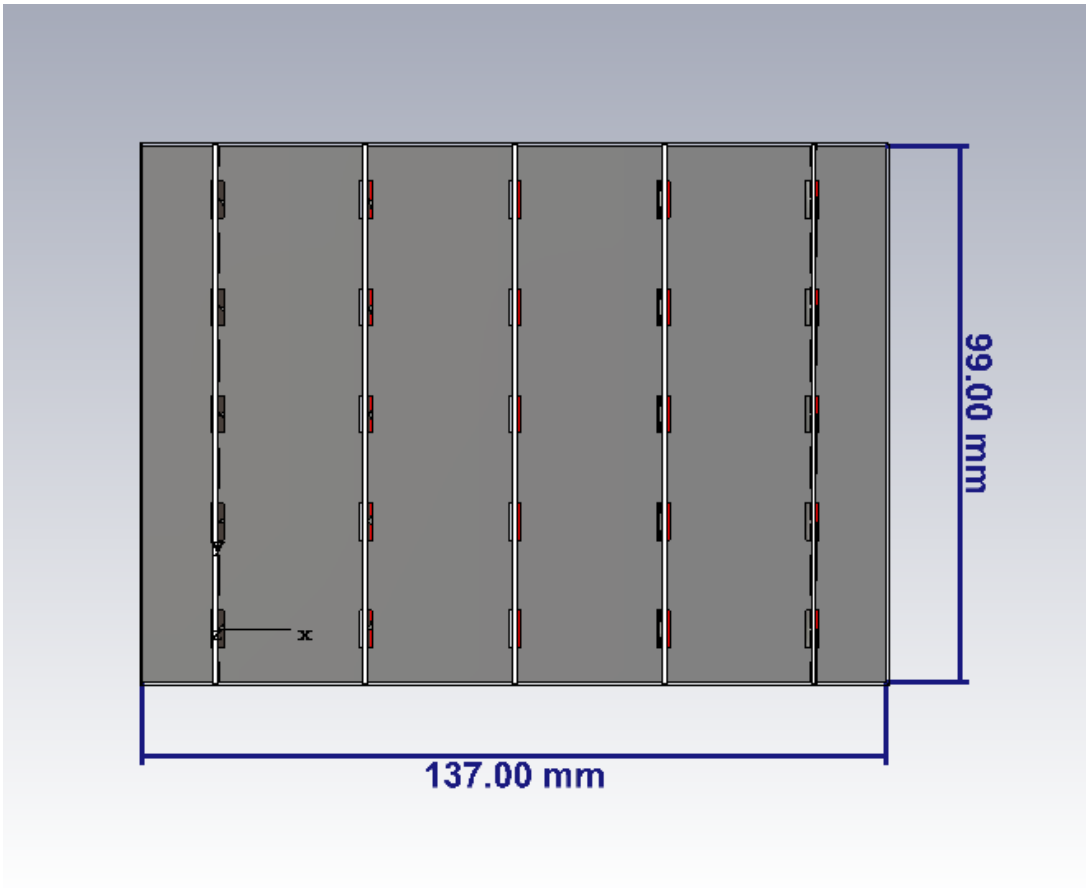

Figure 4.3: Top view of the 5×5 array.

ement and HEC element are of similar characteristics and EEC and center element have similar characteristics. The similar VSWR characteristic elements are at the same H-plane coordinate, that is they both are the end elements at E-plane, meaning that the tight coupling at the E-plane (the overlapping dipoles) yields a strong effect on the VSWR response, which corner and HEC elements lack of. On the other hand, EEC and center element has wider bandwidth (slightly), due to having both dipole arms covered with overlapping dipoles and tight coupling. This shows that the elements that are at the end of E-plane on each antenna card, have worse performance comparing to other edge or inside elements.

For all of the elements compared with the infinite array analysis results, can be seen in Figure 4.5, 5×5 array has higher lower frequency. This is due to the finite configuration. Because the wider bandwidth, i.e. UWB phoenomena, is dependent upon infinite number of tightly coupled dipoles over a ground plane in TCDA. Since we

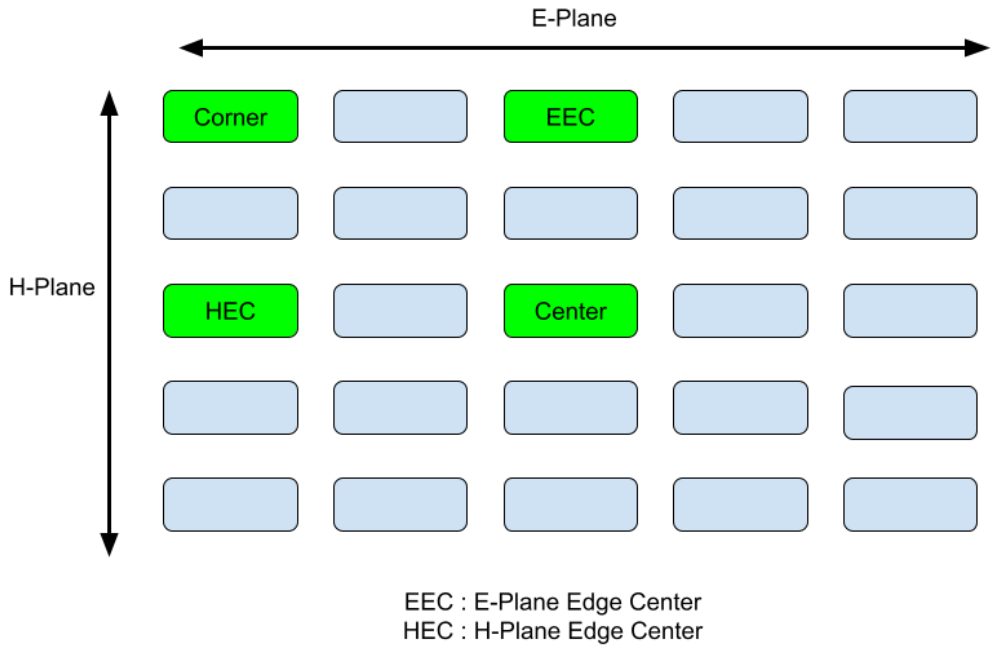

Figure 4.4: Selected elements to be demonstrated, green ones are selected.

limit the number of elements, in our case to 25, the tight coupling repetition is decreased. On the other hand, the upper frequency is significantly increased. The half-wave cut-off frequency stop-band still exists in between 6 to 8.5 GHz, the higher frequencies are also matched, can be seen in Figure 4.6. Remembering that, in the infinite array design frequencies larger than 6 GHz are unmatched, i.e. they have high VSWR. Considering the 5×5 array, now those frequencies have significantly lower VSWR and can be accepted as matched. The reason behind this is hidden in the balun and feed network common modes, explained in Chapter 4 Section 2. Note that the balun structure has UWB performance in isolated analysis but have many (densely on higher frequencies) singular frequencies have rapid increase in VSWR. The amount of coupling in the feed network drastically decreases the continuity in VSWR of the feed networks. Since in finite array we have finite amount of elements adjacent to each other and 25 elements in total, the amount of common modes arising in the feed network is compansated. TCDA could operate at both below and above the half-wave cut-off frequency as, this behaviour is could be seen in the works by Volakis and his team [23].

VSWR response is considered as sufficient for the design purposes considering the

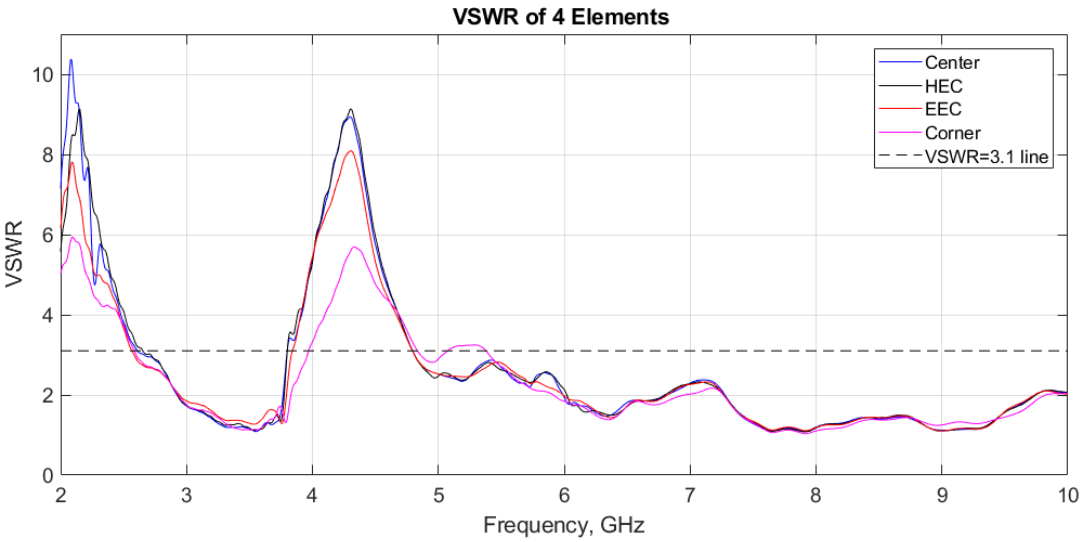

Figure 4.5: 5×5 array VSWR at 2 to 10 GHz.

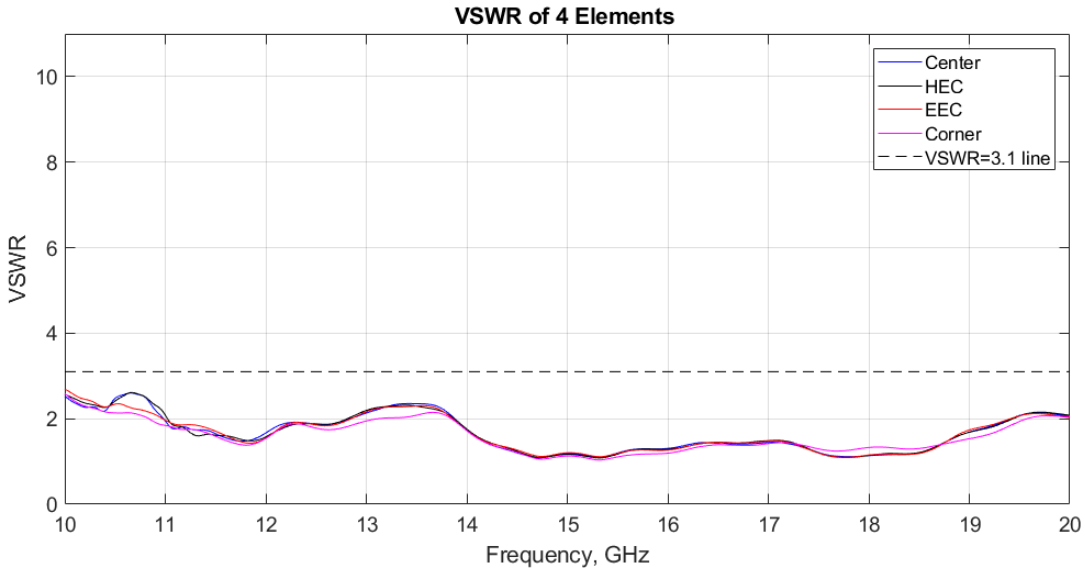

Figure 4.6: 5×5 array VSWR at 10 to 20 GHz.

Figures 4.5 and 4.6. Now, for examining how the radiation occurs and how is the gain pattern in the 5×5 TCDA array, the radiation patterns of the aforementioned four elements are obtained in various frequencies. The realized gain graphs of the CST simulations are provided in the figures starting from Figure 4.7 to Figure 4.10.

TCDA radiation pattern performance should also be evaluated by considering the corporate feed case of 5×5 array. The corporate feed result is modeled with the

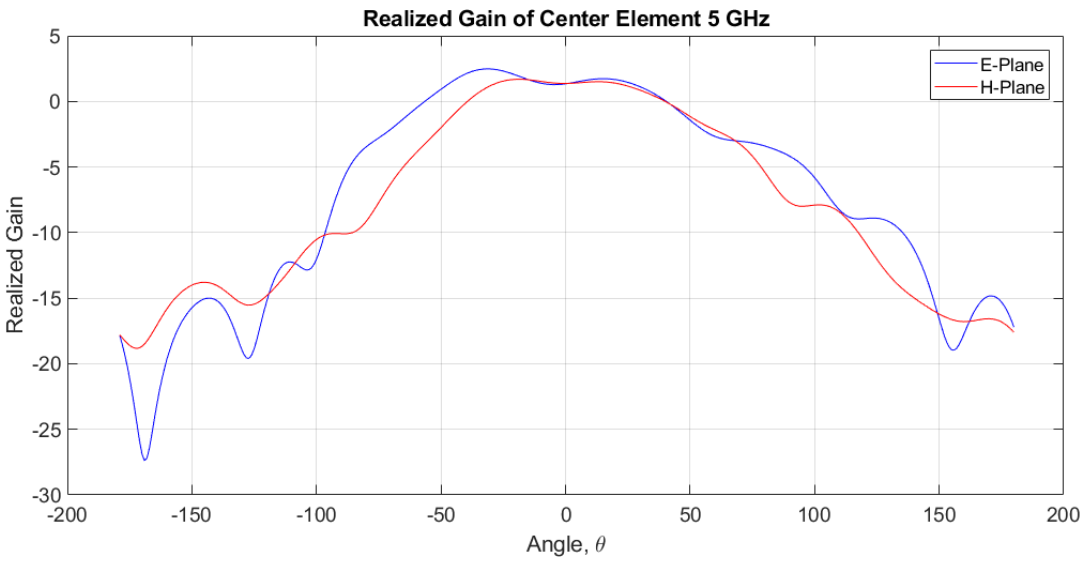

Figure 4.7: Center Element simulation gain pattern at 5 GHz.

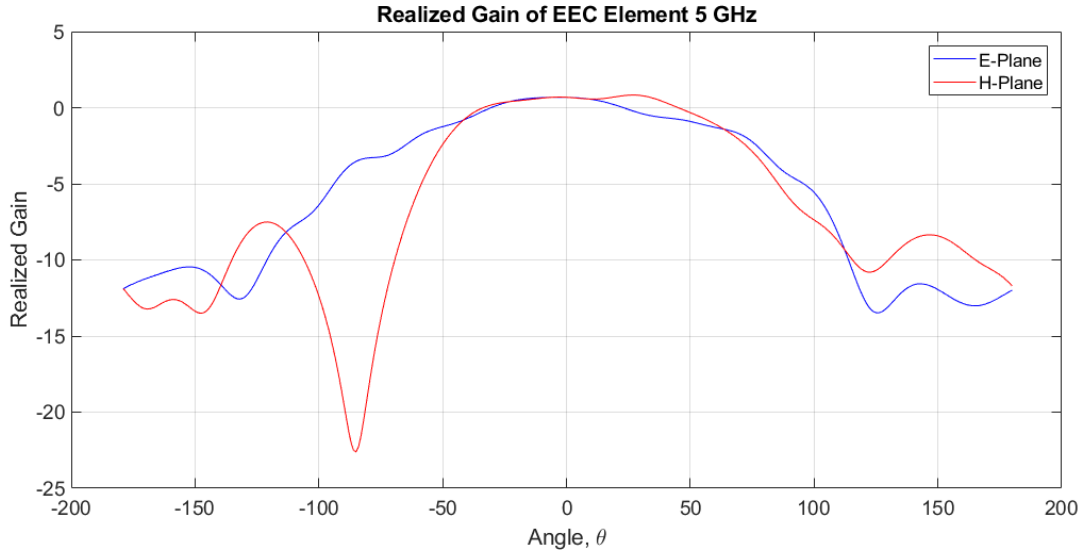

Figure 4.8: EEC Element simulation gain pattern at 5 GHz.

summation of all elements without a phase difference, that is the boresight radiation of the TCDA. The total 5×5 array gain pattern is obtained in two frequencies, one example from below the half-wave cut-off frequency, 5 GHz, another example from above the half-wave cut-off frequency, 11 GHz. The patterns are presented in the figures, from Figure 4.11 to Figure 4.12.

Evaluating the demonstrated gain patterns of the whole array in Figure 4.11 and to

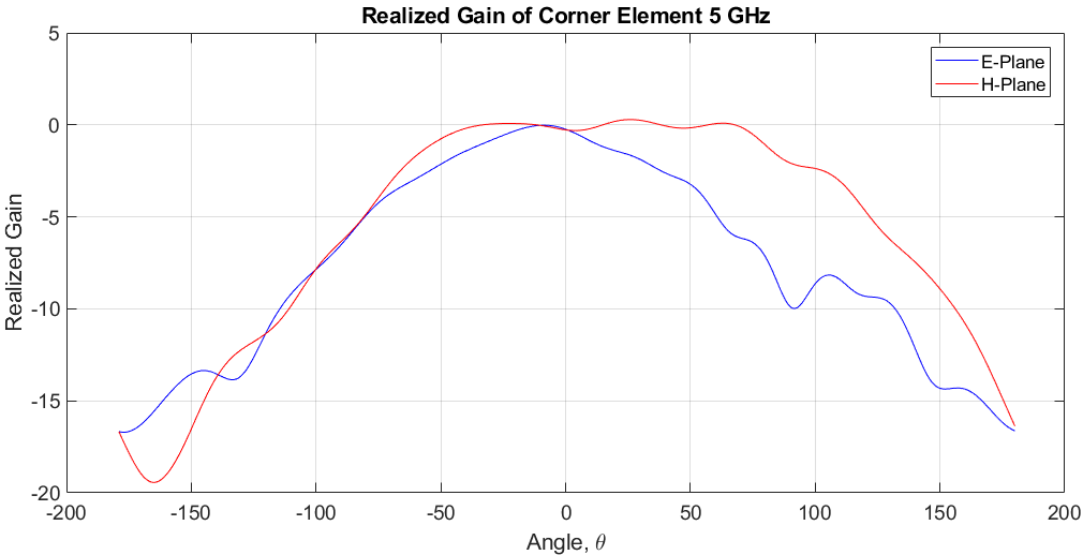

Figure 4.9: Corner Element simulation gain pattern at 5 GHz.

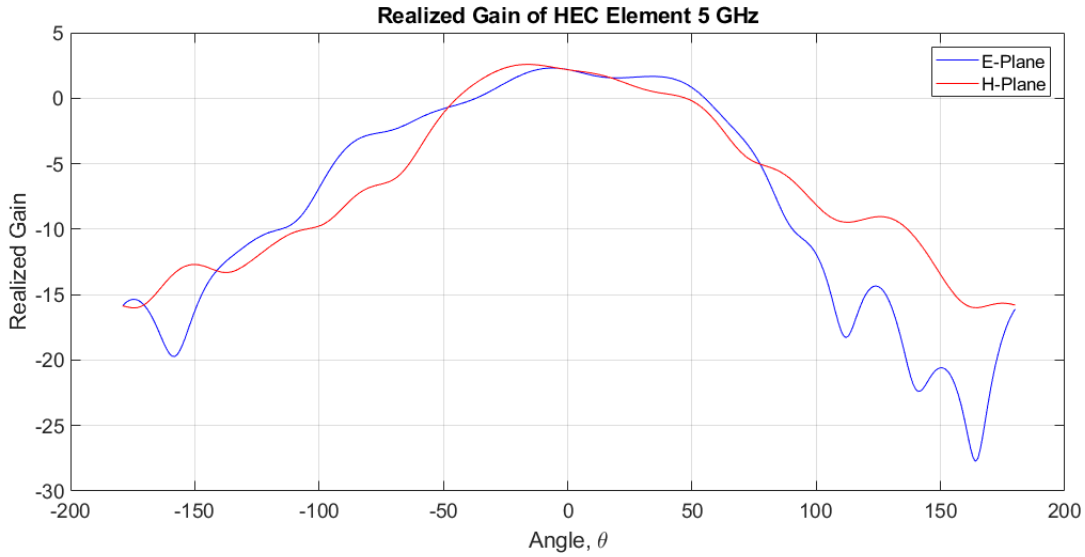

Figure 4.10: HEC Element simulation gain pattern at 5 GHz.

Figure 4.12, sidelobe levels (SLL) are significantly low at 5 GHz comparing with 11 GHz. As the frequency increases, TCDA shows higher gain, as expected, and also grating lobes are introduced. Note that the E-plane pattern at Figure 4.12 has a lot smaller sidelobes comparing with the H-plane result. The low SLL pattern is in the E-plane where the tight coupling is introduced. Note that, seperation in H-plane, dx, is actually larger than seperation in E-plane, dy, indicating that the grating lobes in the

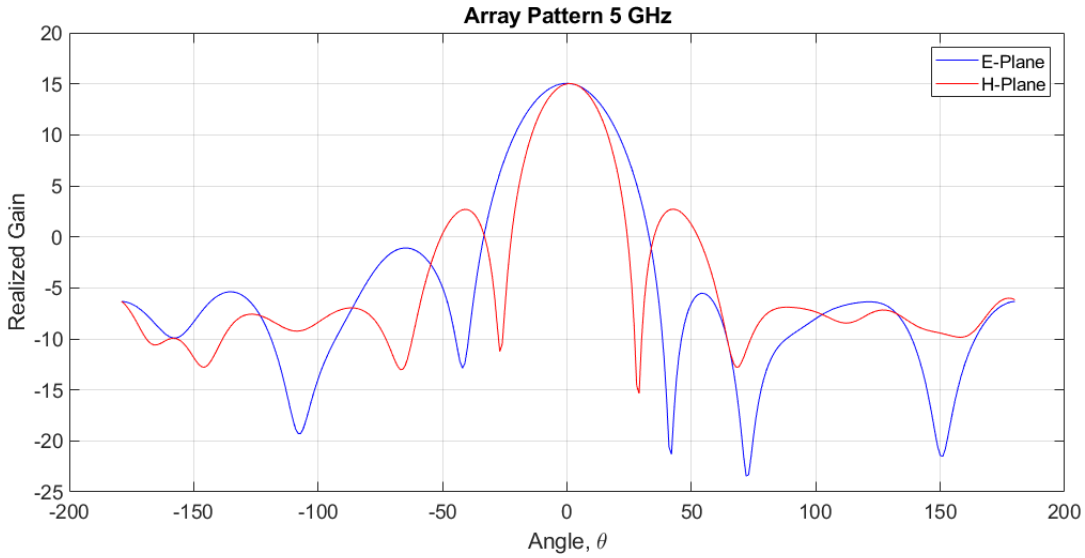

Figure 4.11: Array Pattern simulation at 5 GHz.

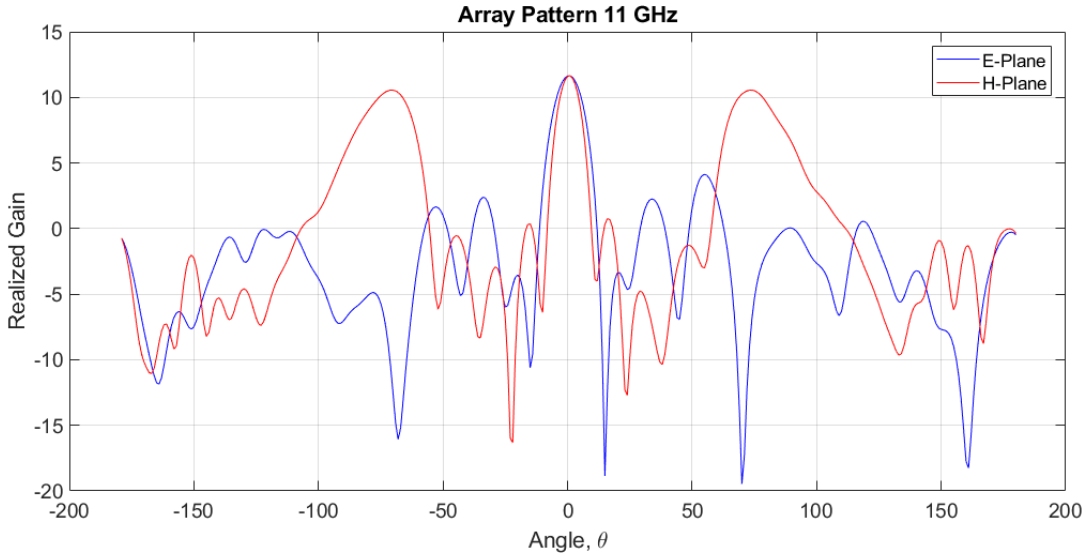

Figure 4.12: Array Pattern simulation at 11 GHz.

H-plane could not be occured by smaller seperations. Instead, having tight coupling in the E-plane yields better gain pattern performance comparing to H-plane. Note that, back lobes are same in both E-plane and H-plane for both of the frequencies, and are quite large. Since the ground plane is penetrated for the feed network to pass through, the fields from the backside also passes through, creating higher backlobe.

4.2 Fabrication of the 5×5 Array

The 5×5 TCDA is fabricated and measured. Ground plane is extended in a small amount in order TCDA to be connected to a support unit, while mounting on the measurement setup. The extended ground-plane version, fabrication version of TCDA is presented in Figure 4.13.

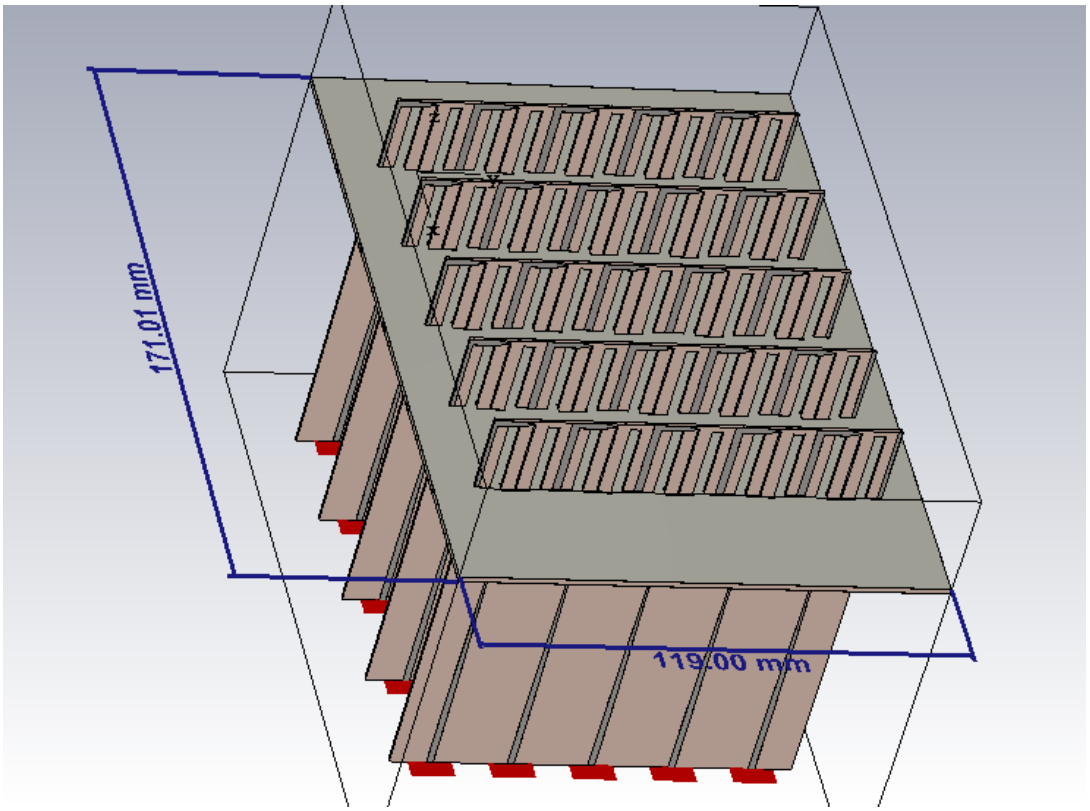

Figure 4.13: Extended ground plane, fabrication version of 5×5 array.

The other change at the fabrication version is the ground plane itself. Note that, the ground plane needs to be flat, so that the assumptions and calculations made could hold for TCDA. In order to guarantee that, it is decided to use an FR4 core material with 1.5 mm thickness, coated with 0.035 mm copper on both sides. The FR4 core material is soldered at the edges to connect both sides of the substrate. The fabrication version, excluding the 3D printed support unit, of the 5×5 TCDA is also simulated in CST and the resulting VSWR of the aforementioned four elements is presented in Figure 4.14.

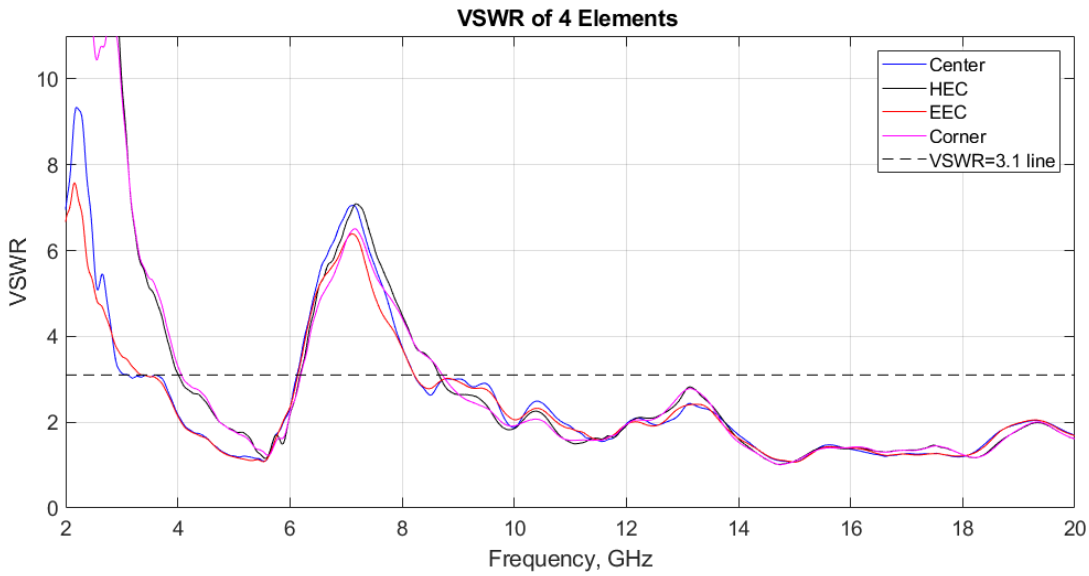

Figure 4.14: VSWR of fabrication version

Dipole, balun and impedance transformer are fabricated on the same substrate. TCDA is fabricated as 5 substrate sheets (namely antenna cards), each containing 5 dipoles with 5 baluns and 5 impedance transformers. The photographs of the fabricated antenna card are given in Figure 4.15. Fabrication of antenna cards are done on LPKF U3 laser-cut technology PCB fabrication device. Then, in order antenna cards to be placed, ground plane needs to be divided into smaller parts which can be soldered later to obtain a continuous ground plane. Ground plane is fabricated out of FR4 substrate as smaller pieces (could be seen in Figure 4.16) on LPKF S103 PCB fabrication device. The antenna cards are passed through two ground-plane parts and then two ground plane parts are soldered. After the soldering process, the TCDA fabrication is finished. For the measurement setup and holding the array in a secure level, an interface is needed to be designed. Antenna casing and measurement interface connection is produced in a 3D printer with ABS plastic material. The overall fabricated array and the casing can be seen in from Figure 4.17 to Figure 4.19. The fabricated array required 25 connectors for each element. Unfortunately, due to lack of connectors supplied in the time schedule of this study, we only connectorized 9 elements of the total array. The connectorized and measured elements are demonstrated in Figure 4.20.

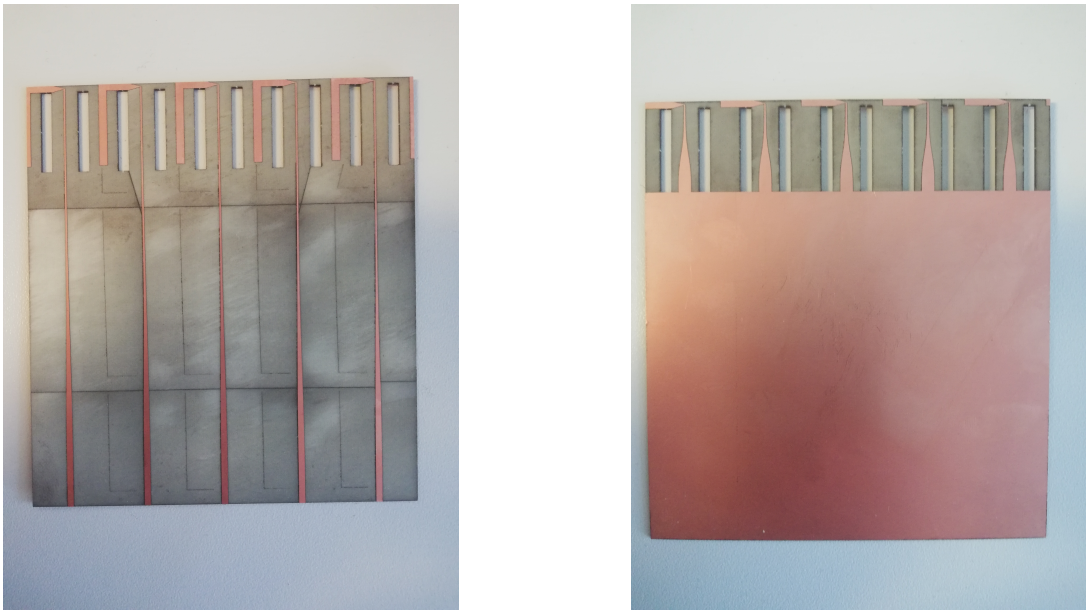

(a) (b)

Figure 4.15: (a) Front view of fabricated antenna card, (b) Back view of fabricated antenna card.

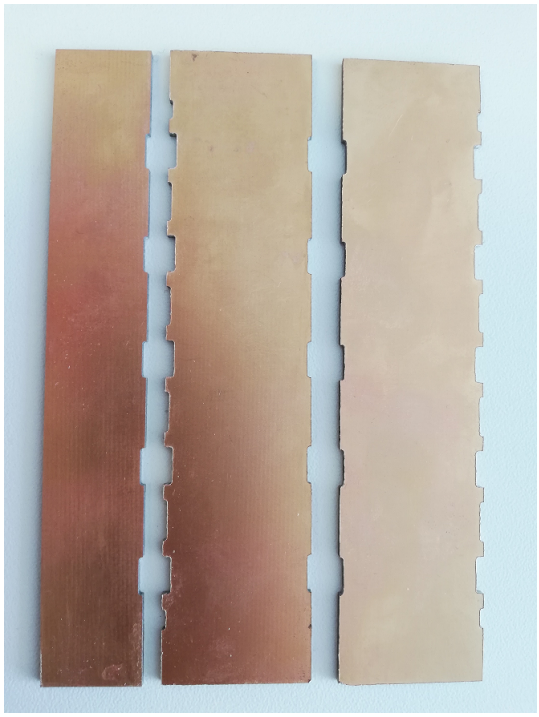

Figure 4.16: Ground Plane production process, small parts.

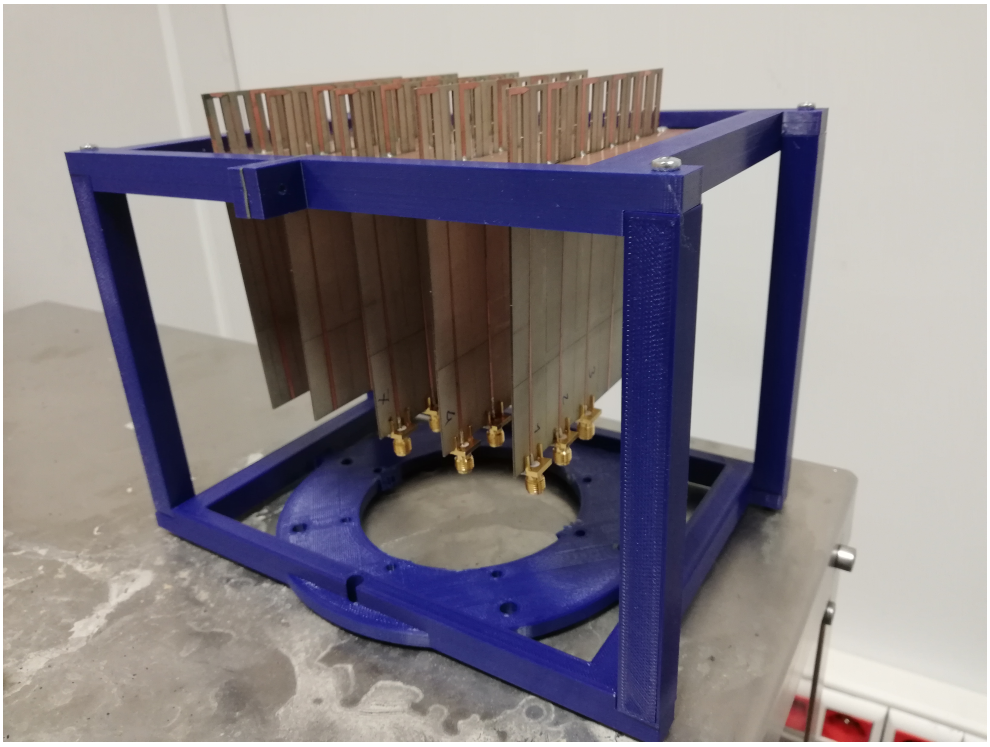

Figure 4.17: Fabricated 5×5 TCDA array, perspective view.

Figure 4.18: Fabricated 5×5 TCDA array, side view.

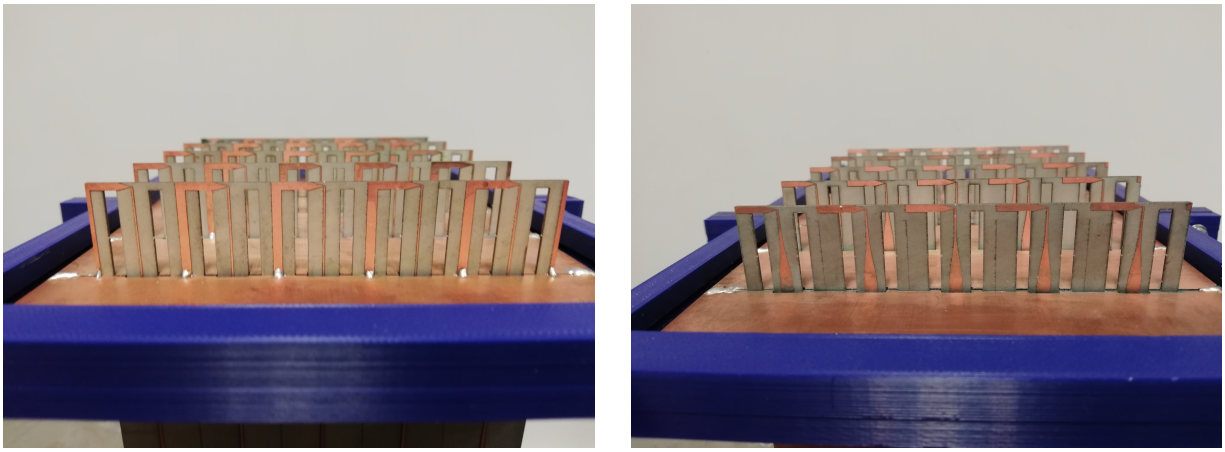

(a) (b)

Figure 4.19: (a) Front view of fabricated TCDA dipoles, (b) Back view of fabricated TCDA dipoles.

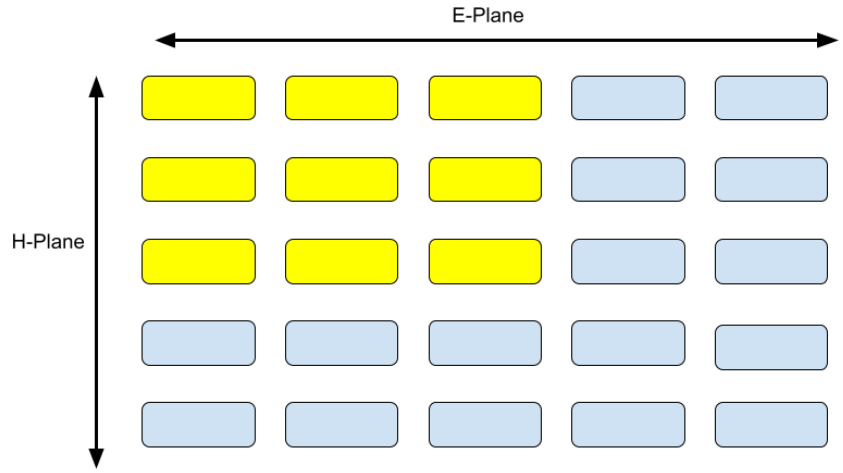

Figure 4.20: Connectorized elements shown in yellow.

4.3 Measurement Results and Comparison with Simulations

For the measurements of the fabricated array, only 9 out of 25 elements are connectorized. That is, all VSWR and pattern measurements are conducted via using those 9 elements, which could also be seen in Figure 4.20. For the VSWR and radiation pattern, gain measurements; all un-measured ports are kept as open-circuit and unterminated. The element measurements are active element pattern but with unterminated elements. The 9 measured patterns are duplicated and mirrored via the principles of symmetry along E and H planes of the array, in order to obtain the rest of the element patterns. For examining the array performance of the TCDA, the array patterns are synthesized via MATLAB. The creation of the total array pattern is made via planar array factor derivation method. In this study, all the measured 9 elements have different patterns, changes are small but still different. The array pattern is not synthesized in all planes, but for E-plane and H-plane, where ϕ is 90°and 0°respectively. The mathematical expression is provided in equations 5.1 and 5.2.

$$\mathrm{ArrayPattern_{G,E-Plane}} = \sum [\mathrm{G_n e^{jkd_{n,E-Plane}\sin(\theta)}}] \tag{5.1}$$

$$\mathrm{ArrayPattern_{G,H-Plane}} = \sum [\mathrm{G_n e^{jkd_{n,H-Plane}\sin(\theta)}}] \tag{5.2}$$

Where, G: gain, n: element number, d: spacing, θ: angle of gain pattern.

The patterns in the principle planes are obtained in MATLAB. The simulation result of array pattern in the same principle planes are displayed on the same graph. The comparisons and comments on the measurement results are presented after the figures of gain patterns which starts with Figure 4.25.

After the fabrication of the TCDA is finished, first measurement conducted is VSWR measurement by VNA. The measured VSWR is presented in comparison with the simulated VSWR at from Figure 4.21 to Figure 4.24. Characteristics of measurement and simulations are similar, noting the small variations at VSWR=3.1 frequencies.

5×5 TCDA array pattern is presented in from Figure 4.41 to Figure 4.44. As explained before, the measurement results are obtained for 9 elements only, the rest and the overall array response is sythesized digitally. Note that, simulation and measure-

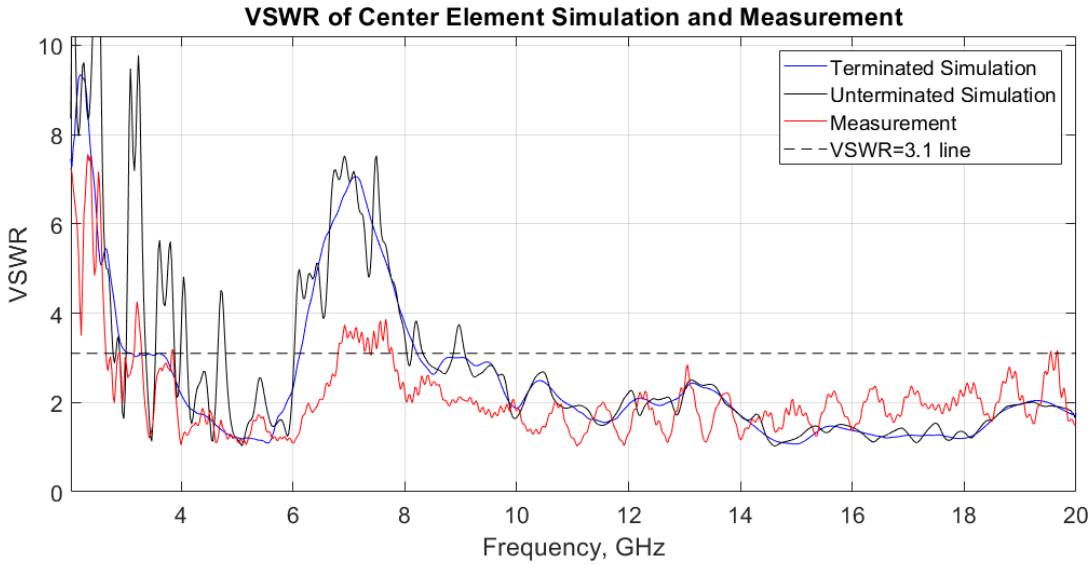

Figure 4.21: Measured and simulated VSWR of Center element.

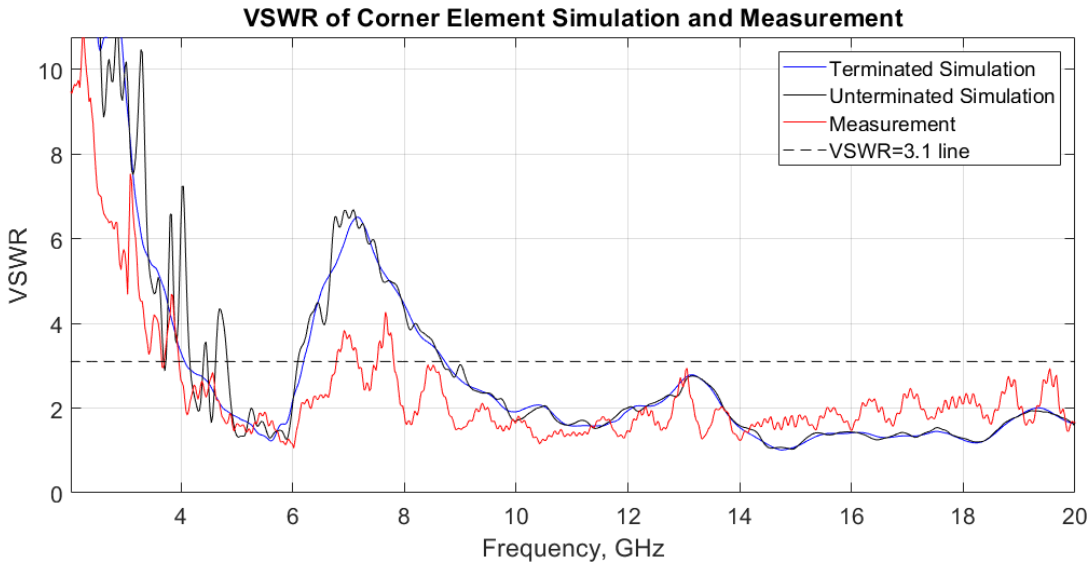

Figure 4.22: Measured and simulated VSWR of Corner element.

ment results have similar deep and peak frequencies but the magnitude is different. It should be stated that, the measurement results are gain values and the simulation results are the realized gain values in CST. Observing that, for the element patterns, simulation realized gain values are higher compared to measurement data. On the other hand, for the total array measurement gain is higher in average compared to simulation data. This probably is due to digitally synthesizing the array using only

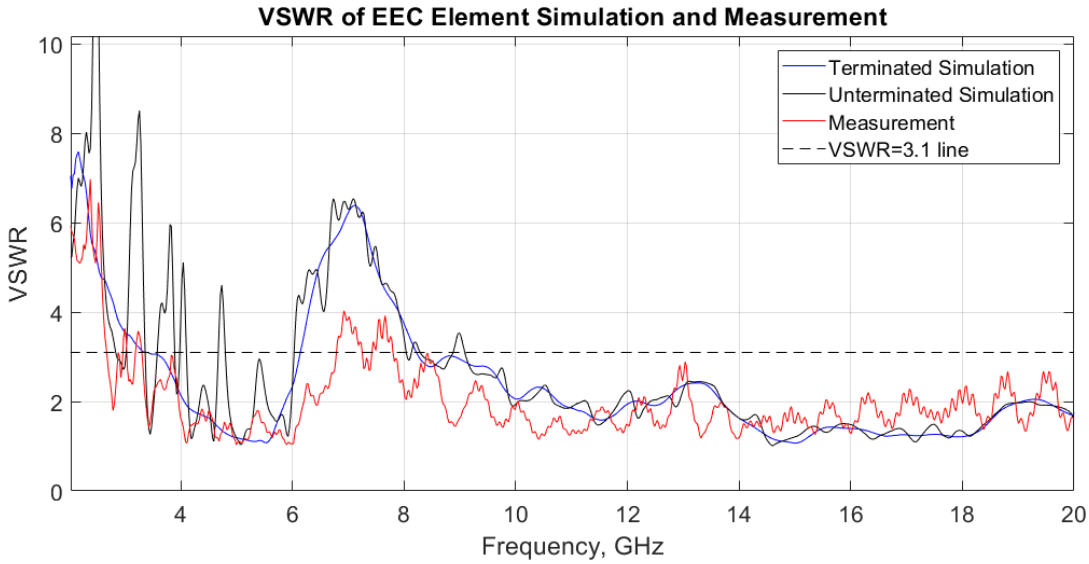

Figure 4.23: Measured and simulated VSWR of EEC element.

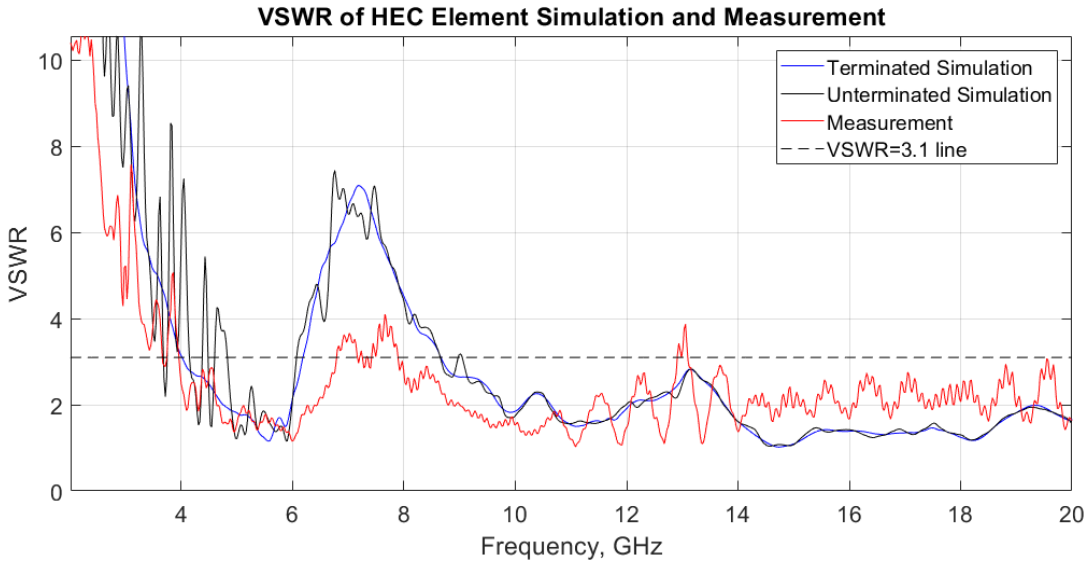

Figure 4.24: Measured and simulated VSWR of HEC element.

9 elements and taking all measurements with open-circuited elements. Array pattern synthesis and measurements should be in completely accordance with active element pattern measurements, terminating each and every element. Due to high cost and delivery problems not terminating the unmeasured elements can yield more inaccurate results. The pattern behaviour is similar in both simulation and in measurements.

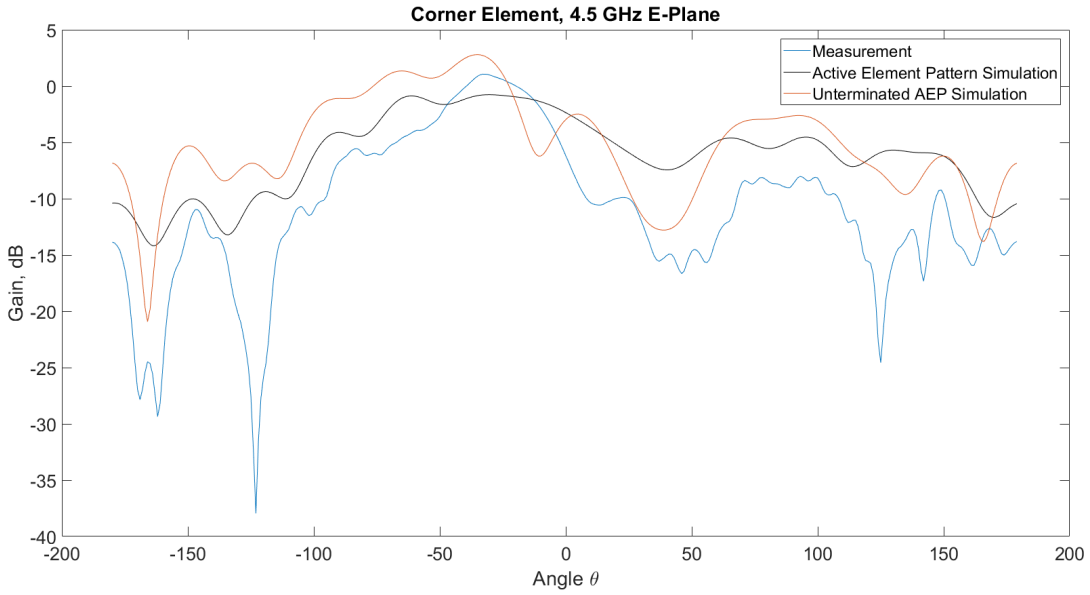

Figure 4.25: Corner Element E-plane gain pattern at 4.5 GHz, Measurement and simulation comparison.

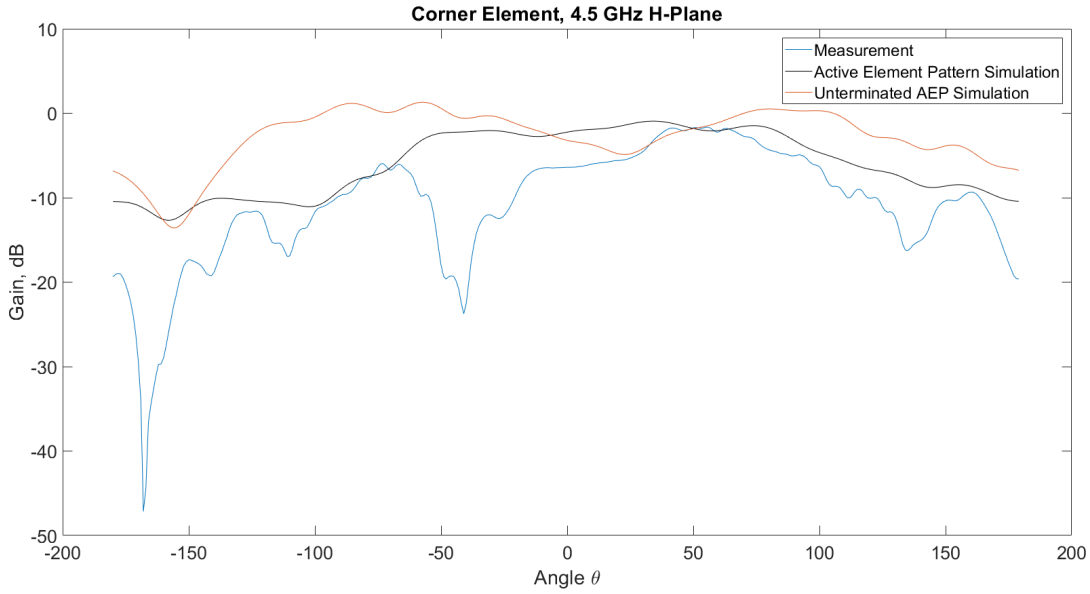

Figure 4.26: Corner Element H-plane gain pattern at 4.5 GHz, Measurement and simulation comparison.

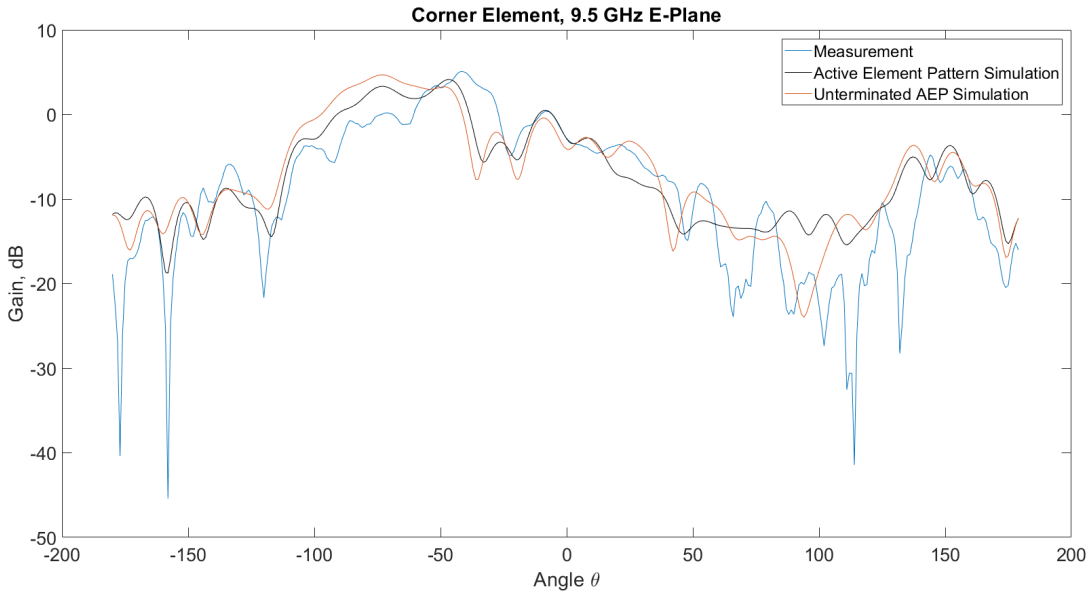

Figure 4.27: Corner Element E-plane gain pattern at 9.5 GHz, Measurement and simulation comparison.

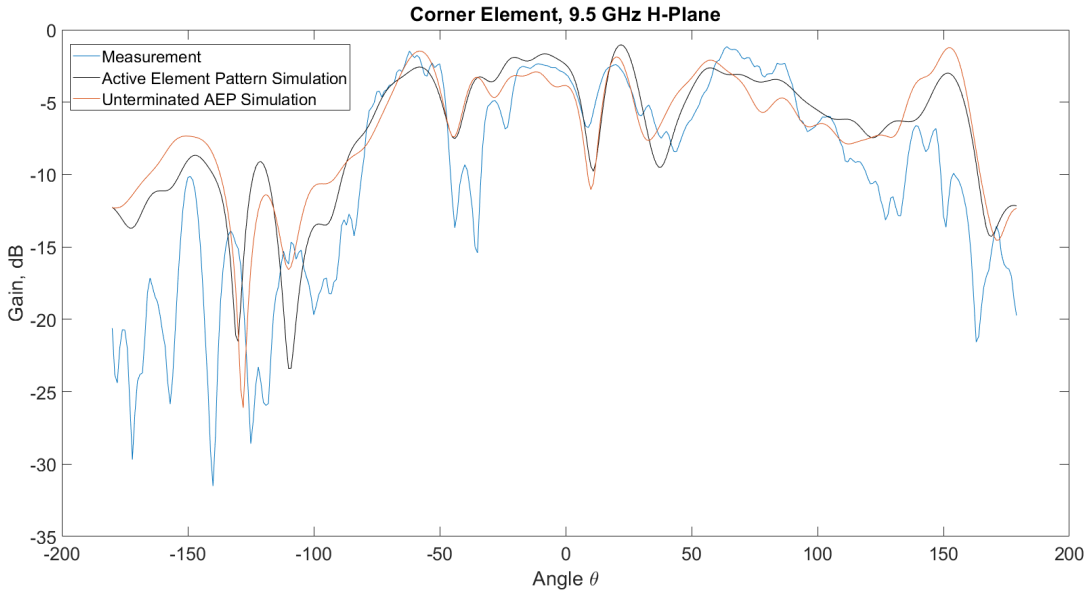

Figure 4.28: Corner Element H-plane gain pattern at 9.5 GHz, Measurement and simulation comparison.

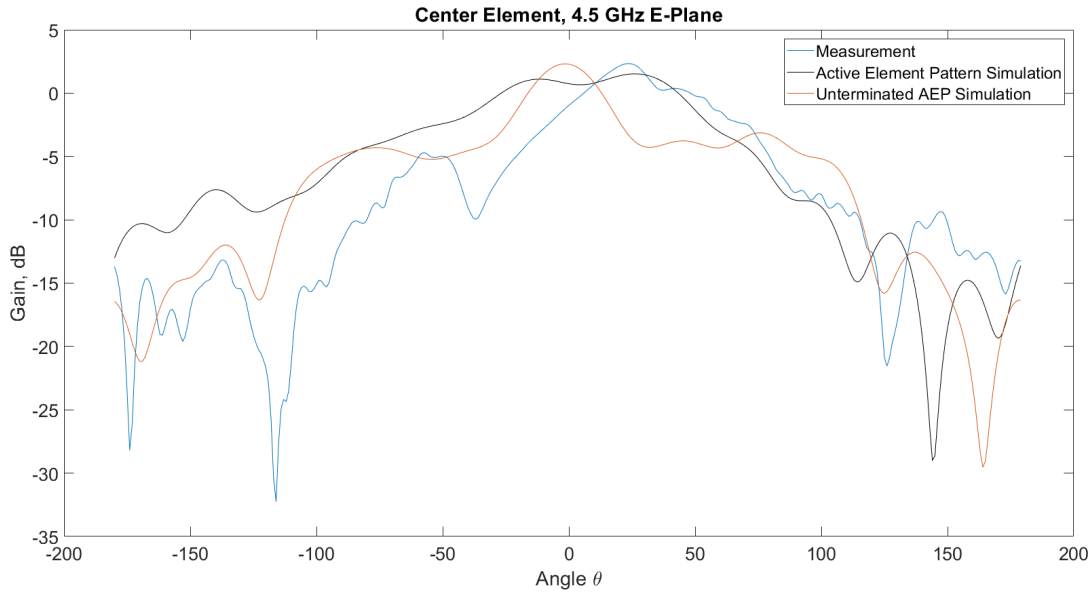

Figure 4.29: Center Element E-plane gain pattern at 4.5 GHz, Measurement and simulation comparison.

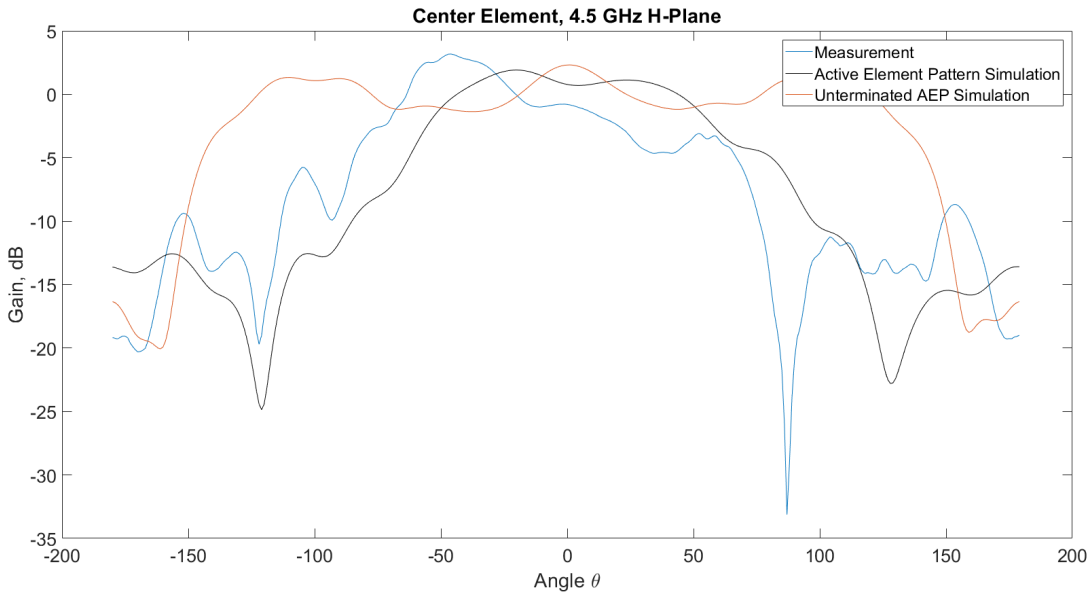

Figure 4.30: Center Element H-plane gain pattern at 4.5 GHz, Measurement and simulation comparison.

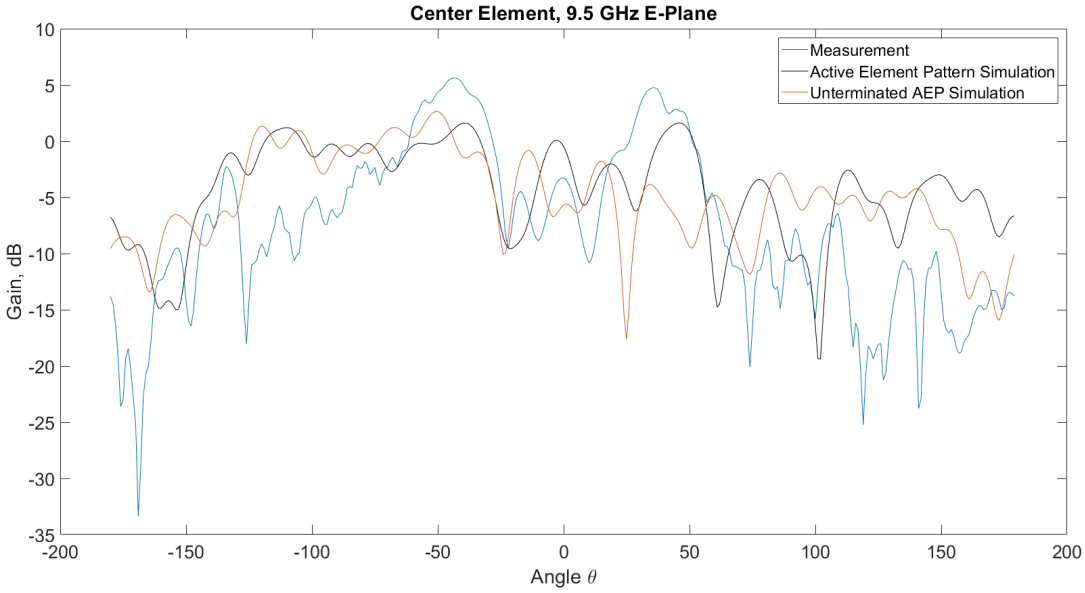

Figure 4.31: Center Element E-plane gain pattern at 9.5 GHz, Measurement and simulation comparison.

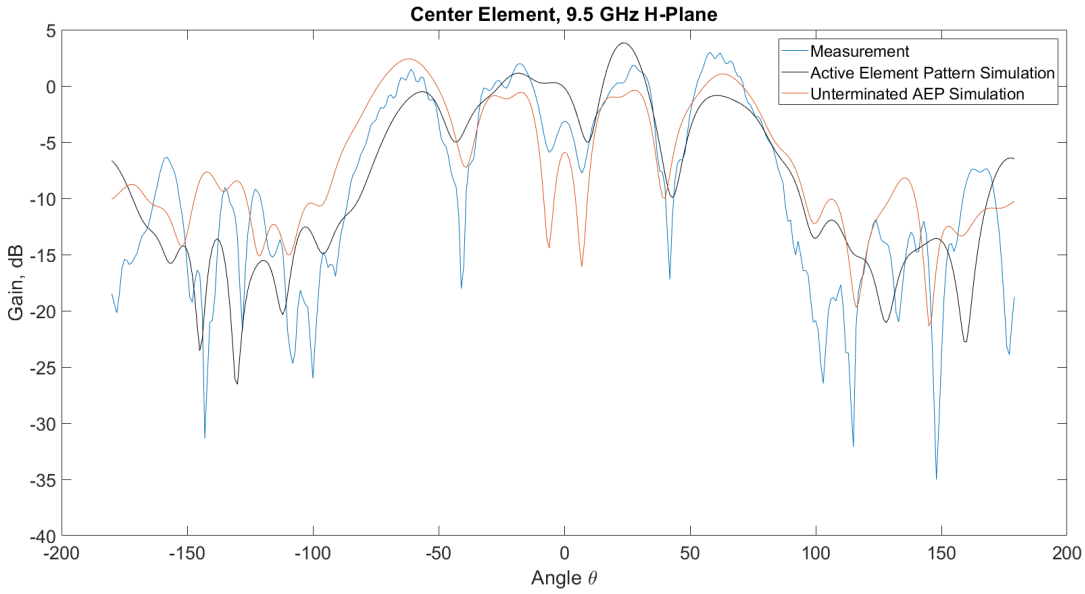

Figure 4.32: Center Element H-plane gain pattern at 9.5 GHz, Measurement and simulation comparison.

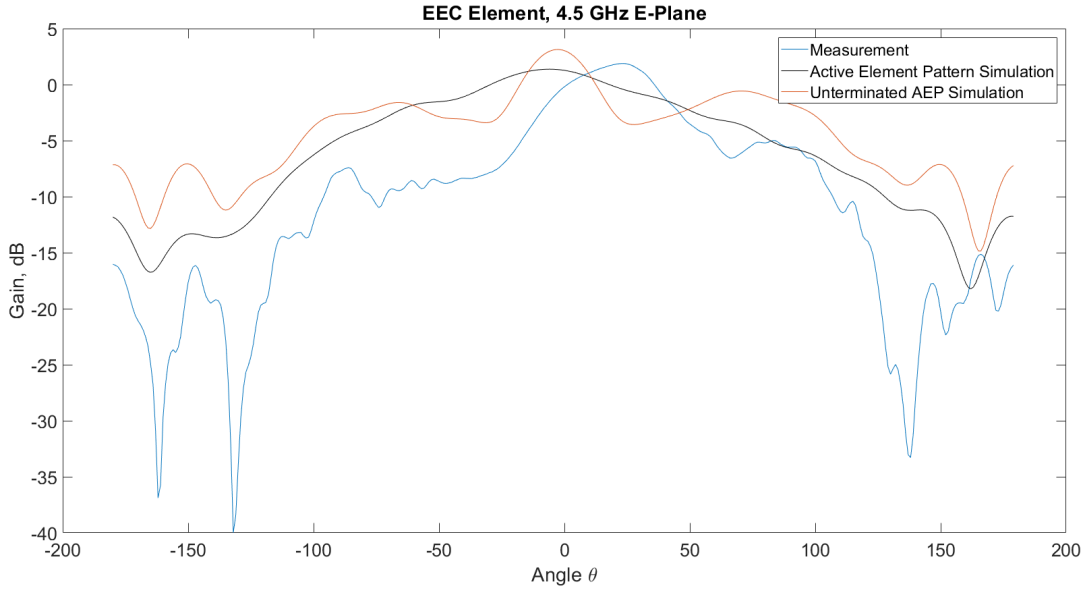

Figure 4.33: EEC Element E-plane gain pattern at 4.5 GHz, Measurement and simulation comparison.

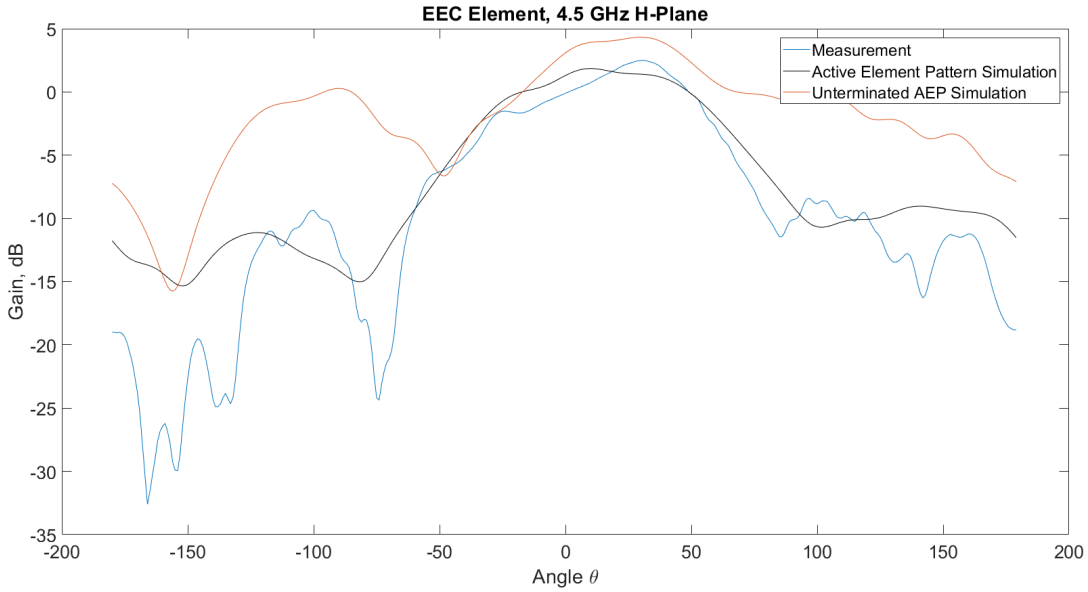

Figure 4.34: EEC Element H-plane gain pattern at 4.5 GHz, Measurement and simulation comparison.

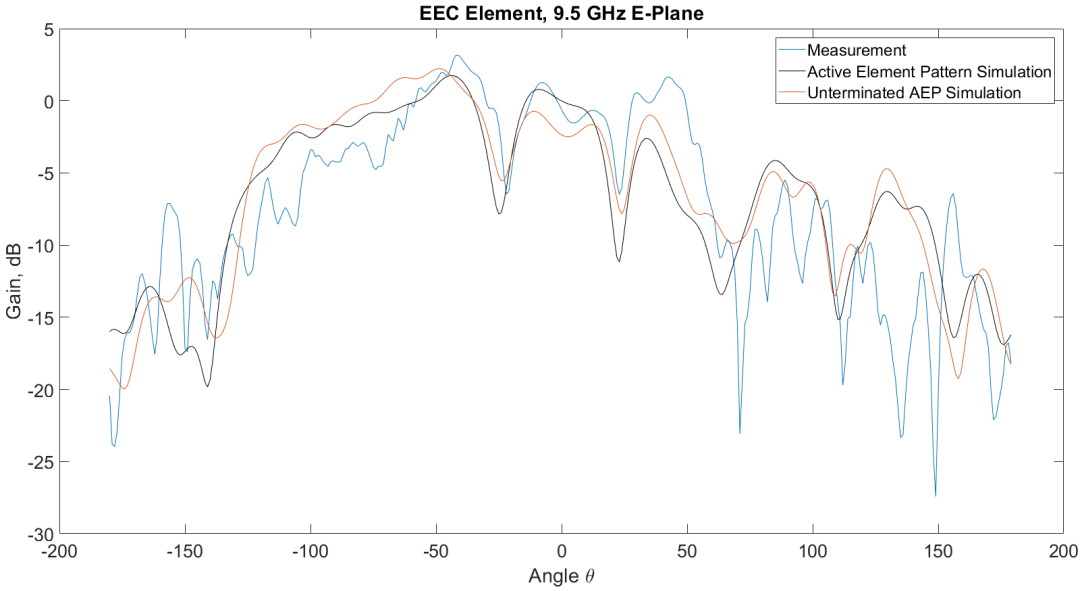

Figure 4.35: EEC Element E-plane gain pattern at 9.5 GHz, Measurement and simulation comparison.

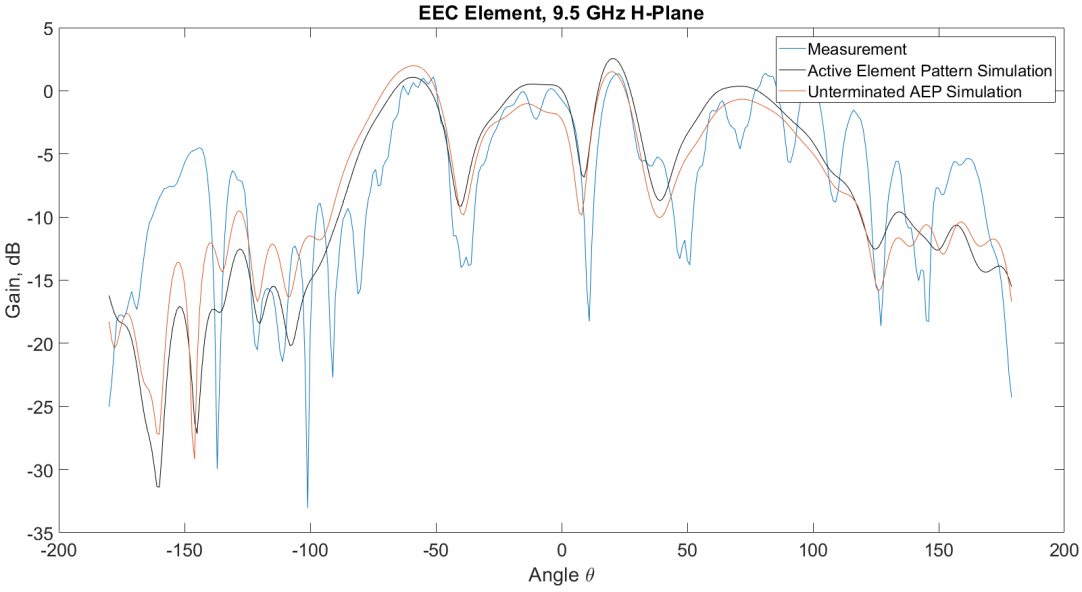

Figure 4.36: EEC Element H-plane gain pattern at 9.5 GHz, Measurement and simulation comparison.

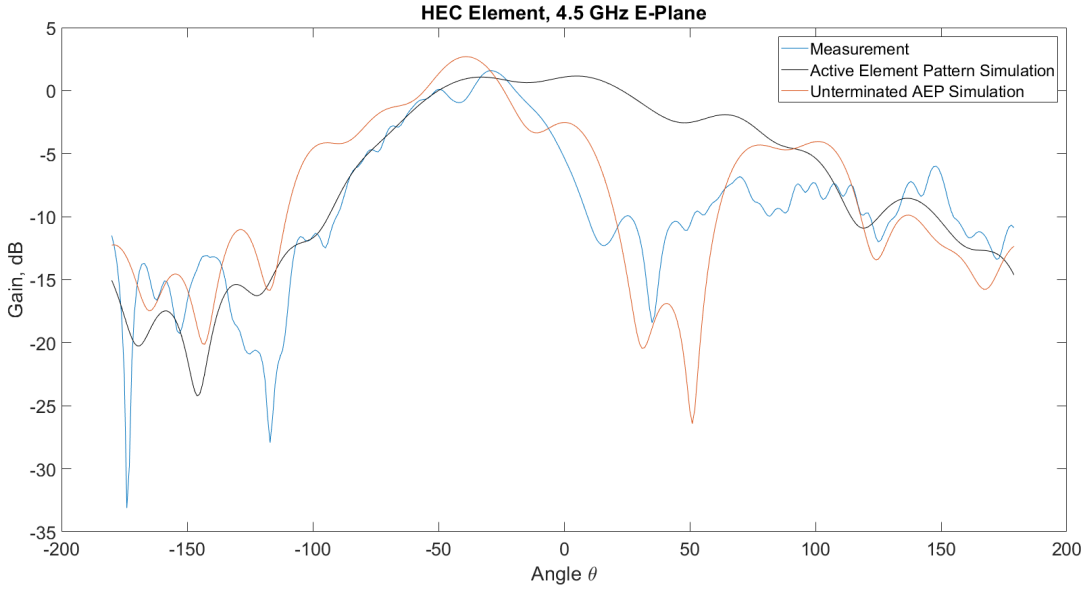

Figure 4.37: HEC Element E-plane gain pattern at 4.5 GHz, Measurement and simulation comparison.

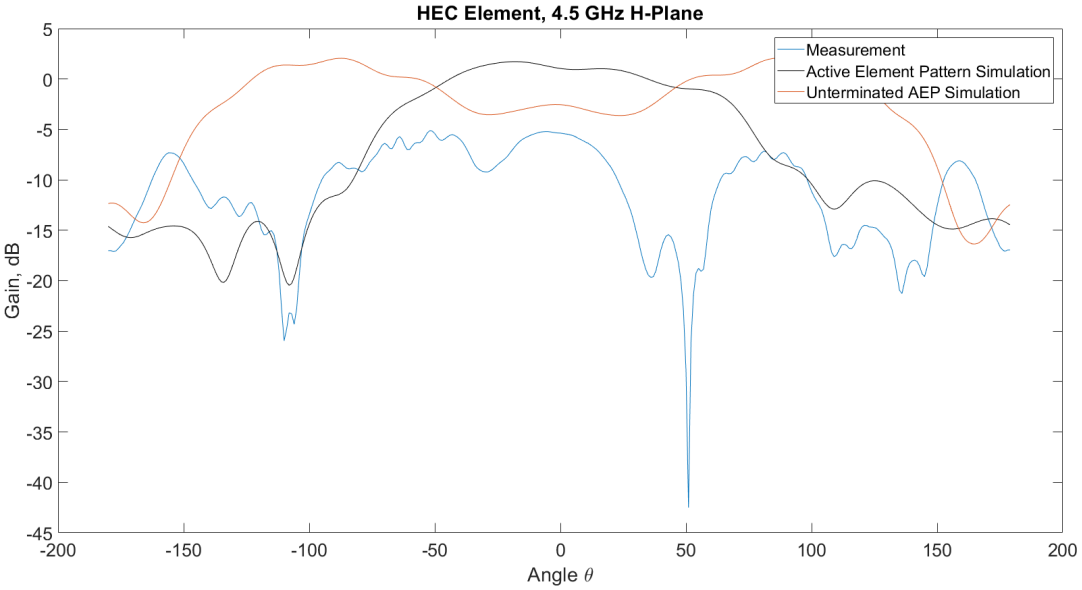

Figure 4.38: HEC Element H-plane gain pattern at 4.5 GHz, Measurement and simulation comparison.

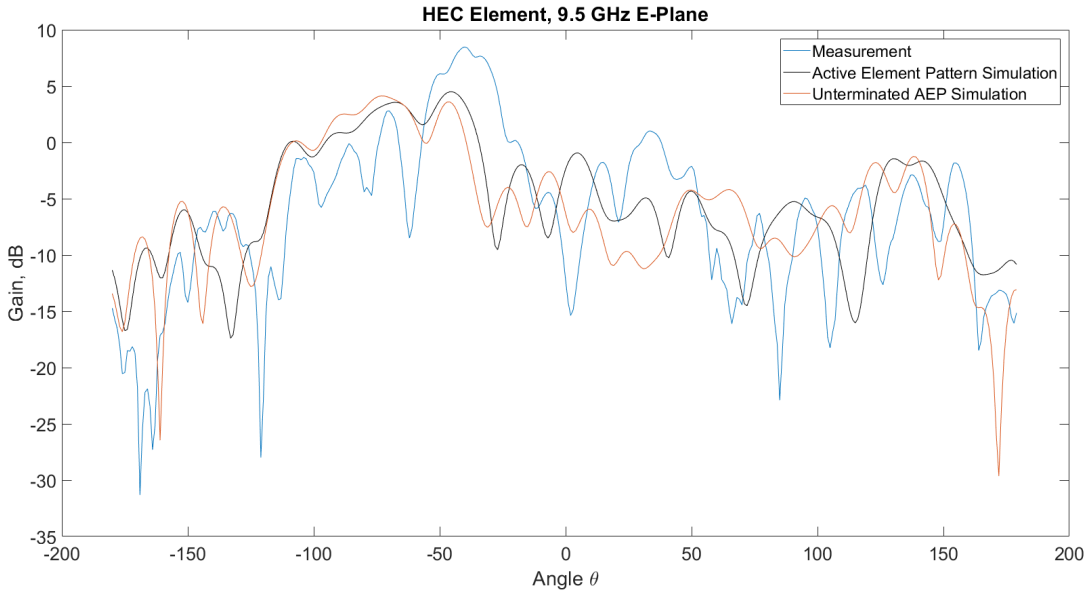

Figure 4.39: HEC Element E-plane gain pattern at 9.5 GHz, Measurement and simulation comparison.

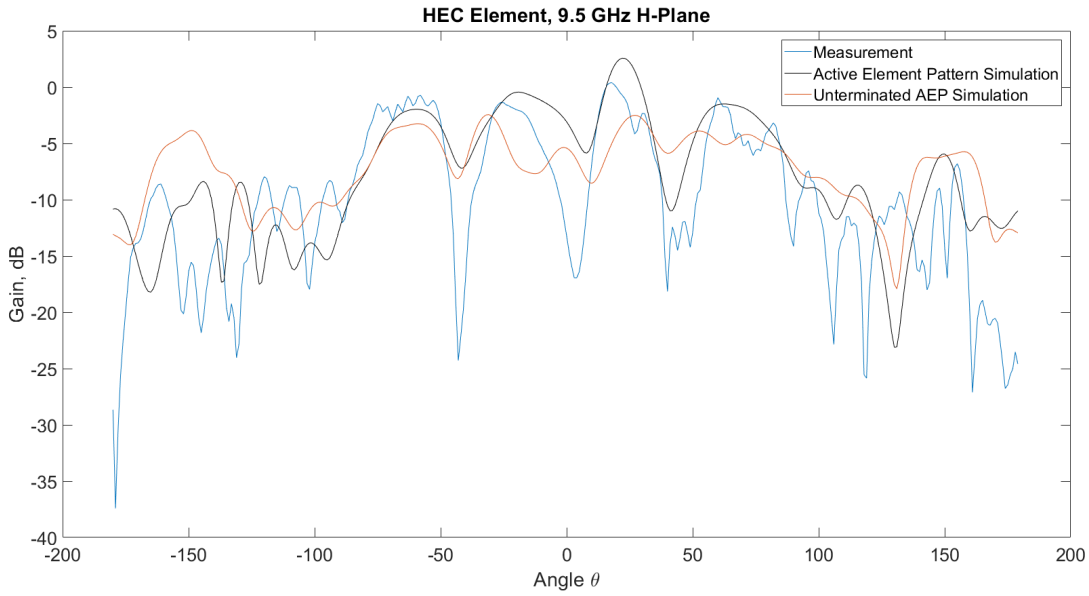

Figure 4.40: HEC Element H-plane gain pattern at 9.5 GHz, Measurement and simulation comparison.

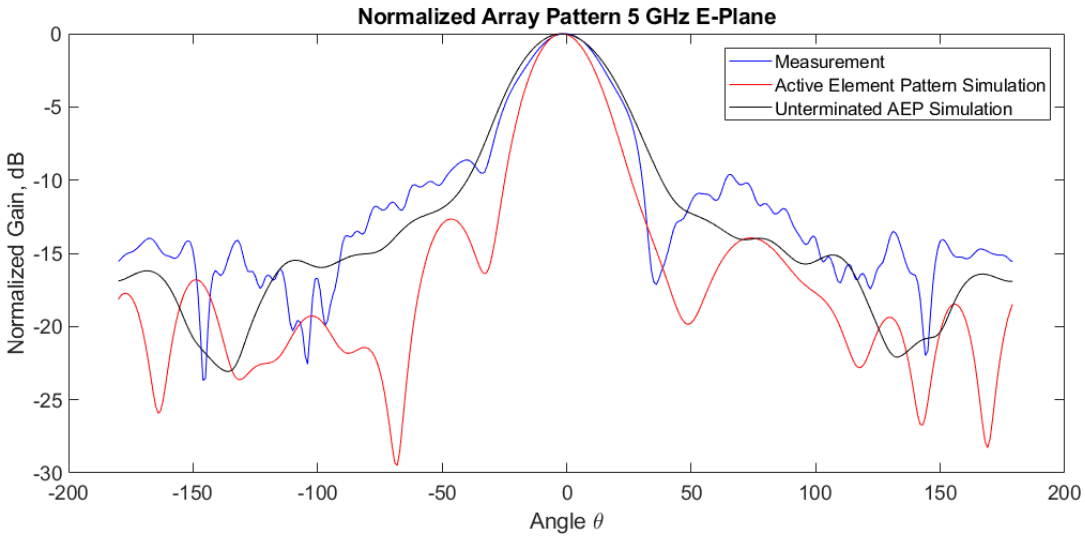

Figure 4.41: Normalized array pattern at 5 GHz, E-plane, Measurement and simulation comparison.

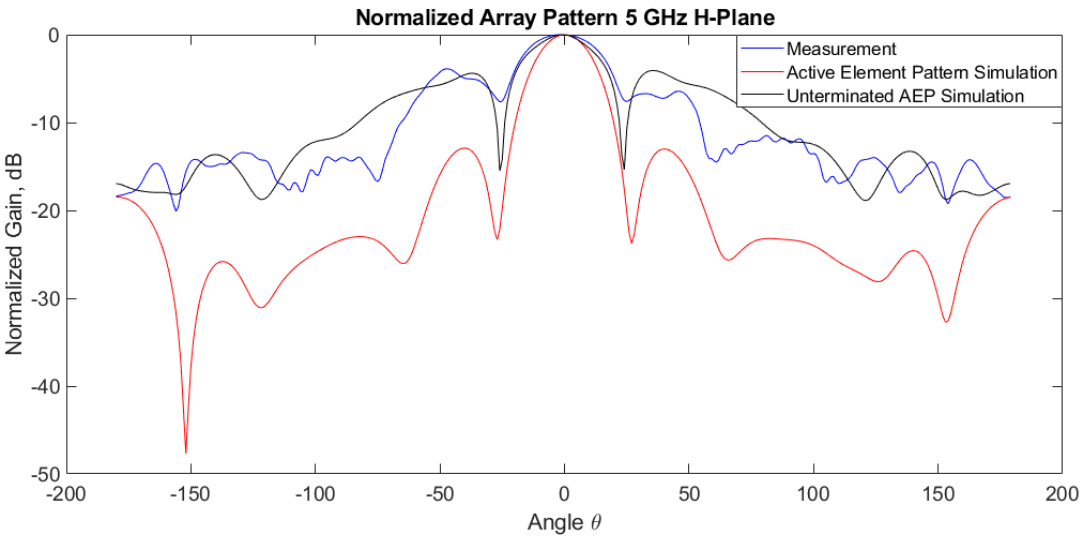

Figure 4.42: Normalized array pattern at 5 GHz, H-plane, Measurement and simulation comparison.

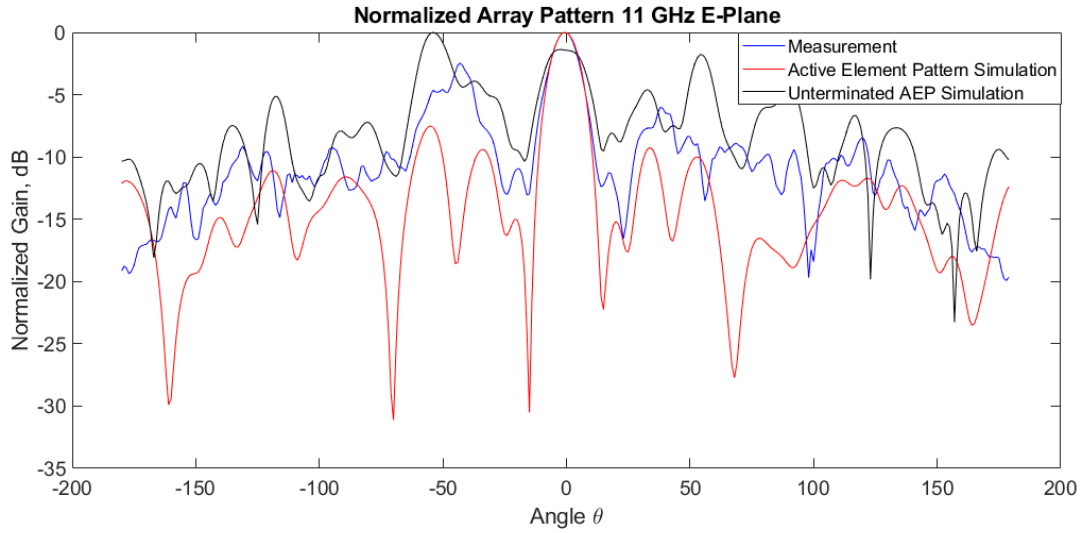

Figure 4.43: Normalized array pattern at 11 GHz, E-plane, Measurement and simulation comparison.

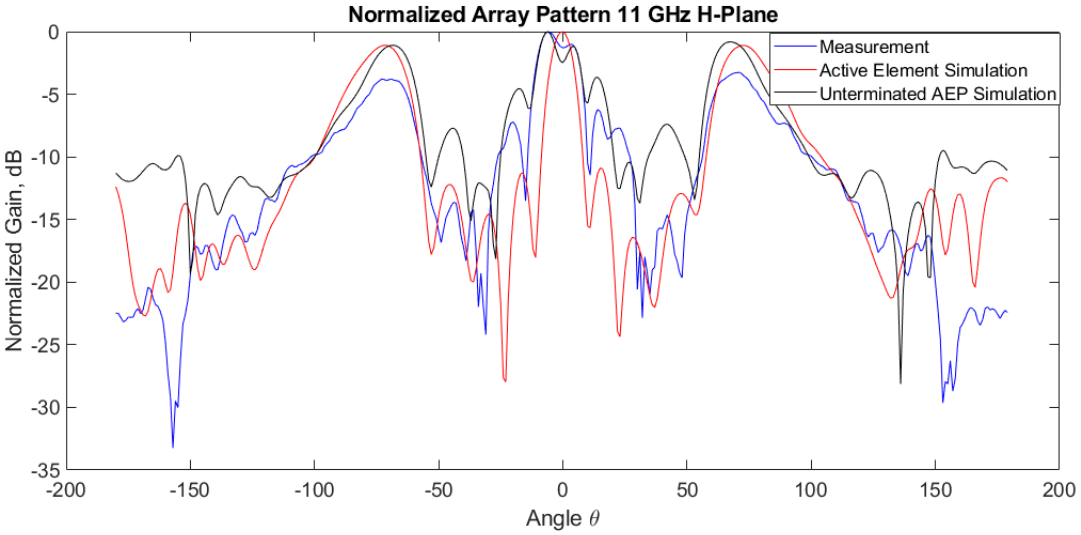

Figure 4.44: Normalized array pattern at 11 GHz, H-plane, Measurement and simulation comparison.

Table 4.1: Synthesized array gain from measurement

Measurement Plane	**4 GHz**	**5 GHz**	**6 GHz**	**9 GHz**	**10 GHz**	**11 GHz**
E-Plane	14.05 dB	14.23 dB	17.30 dB	11.90 dB	12.01 dB	13.00 dB
H-Plane	14.02 dB	14.14 dB	17.22 dB	6.95 dB	11.90 dB	14.50 dB

4.4 Future Work

The proposed TCDA in this study has the approach of Munk. However, the spacings of the elements in the tightly coupled array can be smaller indicating a meta-structure. As the element sizes can be decreased further in future to utilize the meta-material analysis and develop another, even much more compact TCDA.

In addition, note that the proposed TCDA has two operational bands in 5×5 version, and only one operational frequency is observed in infinite version (only lower half of half-wave cut-off). Investigating the mechanics behind this behaviour would enhance the grasp on the TCDA concept and may result in wider bandwidth designs in future. Also note that the half-wave cut-off frequency has significantly low VSWR compared to both theory and to literature. There are several works on "matching" the TCDA to this frequency using concepts like using a resistive sheet in between the dipoles and the ground plane [23]. By investigating the reasons behind decrease of VSWR in the cut-off region (assumed to be due to use of FR4 and penetration gaps on ground-plane), increasing the bandwidth further could also be an option.

As a different path from antenna design, tightly coupled arrays are relatively young area of phased arrays, and it is known that phased arrays are also used in RADAR applications. Using a TCDA in a RADAR application and developing a tightly coupled antenna RADAR, optimizing the patterns and characterizing the internal coupling to apply direction finding algorithms could be a future work to this study.

CHAPTER 5

CONCLUSION

In conventional UWB array design, elements of wideband characteristics are used and mutual coupling is avoided. In the UWB TCDA concept; elements of narrowband characteristic (i.e. dipoles) are placed under tight mutual coupling (in this study, with overlapping arms on top of adjacent dipoles). Utilizing narrowband elements to create an ultrawideband array is a novel approach in array antenna design. A tightly coupled array antenna with overlapping dipoles is designed, fabricated and measured.

Starting from the transmission line circuit model for the TCDA, first an infinite array of dipoles are iteratively generated. Sweeping parameters, using built-in optimizers of CST (genetic algorithm based) and manual tuning, an initial form of TCDA unit cell is created and simulated. After satisfactory results achieved, impedance transformers and balun structures are introduced to the unit cell. Both of which are based on Klopfenstein tapered lines. Then, dipole dimensions, overlapping edge dimensions and element spacings are once again optimized. In order to validate the TCDA, a prototype of finite version is developed. Finite version of the array was chosen as 5×5 array, simulation results demonstrated a promising VSWR vs frequency performance. Even though the lower cut-off frequency becomes higher, the array showed another pass-band behavior after the frequency stop-band corresponding to ground plane height being half-wavelength, centered around $f = c/2h$. Meaning that the overall operational frequency increases.

Lower cut-off frequency (f_L) is increased in fabricated finite array in comparison with the infinite version. Recall that the infinite array unit cell has no spikes in VSWR response when excited with ideal lumped port. When balun and impedance transformer is introduced, some spikes at VSWR at certain frequencies are observed. Tightly

spaced Klopfenstein tapered lines have similar behaviour in VSWR, shown in simulations. Balun fed infinite TCDA has the VSWR spikes, thought to be the common modes induced at the balun and impedance transformer lines. Usage of balun and impedance transformer of Klopfenstein tapered lines caused the fabricated array to have higher f_L since common modes arising in lower frequencies are thought to change the impedance and mismatch the antennas for the interval of common modes.

Antenna array is fabricated using LPKF U4 laser prototype machine, on RO4350b 0.762mm substrate with 0.035 mm copper thickness, the ground plane is made of FR4 core material of thickness 1.5 mm. The antenna casing for the interface and support unit during the anechoic chamber tests, created via 3D printer using ABS plastic material. Used connectors are 2.92 edge-mount connectors of up to 18 GHz. Only 9 out of 25 elements are connectorized, active element patterns with unterminated elements are measured and the rest of the array is created on MATLAB environment based on 9 measurement results via the principles of symmetry and array theory. Then, the array pattern is synthesized in MATLAB environment via planar array formulations, all 25 obtained element patterns are kept as variables during the calculations, instead of assuming identical patterns for the elements. Measured results are similar to the ones obtained by simulations.

The center element operates in between 2.67 to 6.8 GHz yielding 2.5 BW and having a secondary operational BW from 7.73 GHz to 20 GHz yielding 2.58 BW as well. Most of the studies provided in Table 1.1 have wider bandwidth comparing to the proposed antenna of the thesis, on the other hand they have a single bandwidth while the proposed antenna having two operational bandwidths. Considering the frequency range in both bandwidths, the poposed antenna can be proclaimed as competitive in terms of impedance bandwidth. In surveyed studies in Table 1.1, popular balun types are Marchand baluns and integrated baluns. These balun types are complex and harder to fabricate in comparison with Klopfenstein tapered lines. Moreover in surveyed studies, many designs have superstrates or resistive sheets or FSS structures while our proposed design has none. Overall complexity of the proposed TCDA is significantly low and low-cost, claiming to be suitable for fast and low budget prototyping in TCDA designs. On the other hand, fabricated TCDA is semi-connectorized and partially measured with unterminated elements, this aspect can be noted as a dis-

advantage comparing with the studies presented in Table 1.1 but supports the idea of fast and low budget prototyping as the initial design step of a much refined TCDA array antenna.

As suggestions on improvements, first of all balun and impedance transformer section could be improved so that the lower frequency response can be improved. Suppression methods on common modes arising in the balun and feed structure can be studied further. As well, the stop-band resulting from the presence of ground plane can be mitigated, there are several examples of mitigation such as using resistive sheets but with the cost of ohmic loss or using polarization converter layers but with the cost of polarization changes at certain frequencies. Moreover, the array patterns of high frequecy response of the TCDA, on the second operational band, are not smooth as isolated element patterns. This disadvantage is thought to be improved by altering element design parameters or adding additional layers on top of the antenna layer such as frequency selective surfaces (FSS) or superstrates, etc. Finally, the measurement setup can be further improved as connectorizing all 25 elements, terminating the unmeasured elements (active element pattern) and utilizing phase shifters together with wideband RF power combiners to obtain the array patterns for various scan angles.

REFERENCES

[1] C. A. Balanis, *Antenna theory: analysis and design*. John wiley & sons, 2015.

[2] G. Adamiuk, T. Zwick, and W. Wiesbeck, "Uwb antennas for communication systems," *Proceedings of the IEEE*, vol. 100, no. 7, pp. 2308–2321, 2012.

[3] J.-B. Yan, S. Gogineni, B. Camps-Raga, and J. Brozena, "A dual-polarized 2–18-ghz vivaldi array for airborne radar measurements of snow," *IEEE transactions on antennas and propagation*, vol. 64, no. 2, pp. 781–785, 2015.

[4] J. P. Doane, K. Sertel, and J. L. Volakis, "A wideband, wide scanning tightly coupled dipole array with integrated balun (tcda-ib)," *IEEE Transactions on Antennas and Propagation*, vol. 61, no. 9, pp. 4538–4548, 2013.

[5] S. S. Holland and M. N. Vouvakis, "The planar ultrawideband modular antenna (puma) array," *IEEE Transactions on Antennas and Propagation*, vol. 60, no. 1, pp. 130–140, 2011.

[6] S. Camacho-Lara, S. Madry, and J. N. Pelton, "United states meteorological satellite program," *Handbook of Satellite Applications, 2nd edn. Springer Press, Basel*, p. 1185, 2017.

[7] V. Pavlikov, V. Volosyuk, and S. Zhyla, "Ultra-wideband passive radars fundamental theory and applications," in *2018 IEEE 17th International Conference on Mathematical Methods in Electromagnetic Theory (MMET)*, pp. 1–6, IEEE, 2018.

[8] H. A. Khan, W. Q. Malik, D. J. Edwards, and C. J. Stevens, "Ultra wideband multiple-input multiple-output radar," in *IEEE International Radar Conference, 2005.*, pp. 900–904, IEEE, 2005.

[9] M. Huang, K. Zhang, L. Wang, and W. Qiao, "An ultrawideband tightly coupled antipodal vivaldi antenna array for uhf-ku band applications," in *2017 IEEE In-*

ternational Symposium on Antennas and Propagation & USNC/URSI National Radio Science Meeting, pp. 1323–1324, IEEE, 2017.

[10] M. H. Novak and J. L. Volakis, "Ultrawideband antennas for multiband satellite communications at uhf–ku frequencies," *IEEE Transactions on Antennas and Propagation*, vol. 63, no. 4, pp. 1334–1341, 2015.

[11] H. Wheeler, "Simple relations derived fom a phased-array antenna made of an infinite current sheet," *IEEE Transactions on Antennas and Propagation*, vol. 13, no. 4, pp. 506–514, 1965.

[12] I. Tzanidis, J. P. Doane, K. Sertel, and J. L. Volakis, "Wheeler's current sheet concept and munk's wideband arrays," in *Proceedings of the 2012 IEEE International Symposium on Antennas and Propagation*, pp. 1–2, IEEE, 2012.

[13] B. A. Munk, *Finite antenna arrays and FSS*. John Wiley & Sons, 2003.

[14] M. Jones and J. Rawnick, "A new approach to broadband array design using tightly coupled elements," in *MILCOM 2007-IEEE Military Communications Conference*, pp. 1–7, IEEE, 2007.

[15] I. Tzanidis, *Ultrawideband low-profile arrays of tightly coupled antenna elements: Excitation, termination and feeding methods*. The Ohio State University, 2011.

[16] M. Novak, E. Alwan, F. Miranda, and J. Volakis, "Conformal and spectrally agile ultra wideband phased array antenna for communication and sensing," *NASA Glenn Research Center*, 2015.

[17] A. D. Johnson, J. Zhong, M. Livadaru, E. A. Alwan, and J. L. Volakis, "Tightly coupled dipole array with wideband differential feeding network," in *2018 IEEE International Symposium on Antennas and Propagation & USNC/URSI National Radio Science Meeting*, pp. 1987–1988, IEEE, 2018.

[18] N. Marchand, "Transmission line conversion transformers," *Electron*, vol. 17, no. 12, pp. 142–145, 1944.

[19] A. O. Bah, P.-Y. Qin, R. W. Ziolkowski, Y. J. Guo, and T. S. Bird, "A wideband low-profile tightly coupled antenna array with a very high figure of merit,"

IEEE Transactions on Antennas and Propagation, vol. 67, no. 4, pp. 2332–2343, 2019.

[20] J. A. Kasemodel, C.-C. Chen, and J. L. Volakis, "Broadband planar wide-scan array employing tightly coupled elements and integrated balun," in *2010 IEEE International Symposium on Phased Array Systems and Technology*, pp. 467–472, IEEE, 2010.

[21] W. Zhou, Y. Chen, and S. Yang, "Dual-polarized tightly coupled dipole array for uhf–x-band satellite applications," *IEEE Antennas and Wireless Propagation Letters*, vol. 18, no. 3, pp. 467–471, 2019.

[22] I. Tzanidis, K. Sertel, and J. L. Volakis, "Uwb low-profile tightly coupled dipole array with integrated balun and edge terminations," *IEEE Transactions on Antennas and Propagation*, vol. 61, no. 6, pp. 3017–3025, 2013.

[23] W. F. Moulder, K. Sertel, and J. L. Volakis, "Superstrate-enhanced ultrawideband tightly coupled array with resistive fss," *IEEE Transactions on Antennas and Propagation*, vol. 60, no. 9, pp. 4166–4172, 2012.

[24] Y. Zhou, F. Zhu, S. Gao, Q. Luo, L.-H. Wen, Q. Wang, X. Yang, Y. Geng, and Z. Cheng, "Tightly coupled array antennas for ultra-wideband wireless systems," *IEEE Access*, vol. 6, pp. 61851–61866, 2018.

[25] I. Tzanidis, K. Sertel, and J. L. Volakis, "Interwoven spiral array (ispa) with a 10: 1 bandwidth on a ground plane," *IEEE Antennas and Wireless Propagation Letters*, vol. 10, pp. 115–118, 2010.

[26] J. A. Kasemodel, C.-C. Chen, and J. L. Volakis, "Wideband planar array with integrated feed and matching network for wide-angle scanning," *IEEE Transactions on Antennas and Propagation*, vol. 61, no. 9, pp. 4528–4537, 2013.

[27] E. Yetisir, N. Ghalichechian, and J. L. Volakis, "Ultrawideband array with 70° scanning using fss superstrate," *IEEE Transactions on Antennas and Propagation*, vol. 64, no. 10, pp. 4256–4265, 2016.

[28] D. K. Papantonis and J. L. Volakis, "Dual-polarized tightly coupled array with substrate loading," *IEEE Antennas and Wireless Propagation Letters*, vol. 15, pp. 325–328, 2015.

[29] T. R. Vogler, *Analysis of the radiation mechanisms in and design of tightly-coupled antenna arrays*. PhD thesis, Virginia Tech, 2010.

[30] S. S. Holland, D. H. Schaubert, and M. N. Vouvakis, "A 7–21 ghz dual-polarized planar ultrawideband modular antenna (puma) array," *IEEE Transactions on Antennas and Propagation*, vol. 60, no. 10, pp. 4589–4600, 2012.

[31] H. H. Vo, C.-C. Chen, P. Hagan, and Y. Bayram, "A very low-profile uwb phased array antenna design for supporting wide angle beam steering," in *2016 IEEE International Symposium on Phased Array Systems and Technology (PAST)*, pp. 1–8, IEEE, 2016.

[32] E. A. Alwan, K. Sertel, and J. L. Volakis, "A simple equivalent circuit model for ultrawideband coupled arrays," *IEEE Antennas and Wireless Propagation Letters*, vol. 11, pp. 117–120, 2012.

[33] R. W. Klopfenstein, "A transmission line taper of improved design," *Proceedings of the IRE*, vol. 44, no. 1, pp. 31–35, 1956.